EFFECT OF CARBON FILLER CHARACTERISTICS ON THE ELECTRICAL PROPERTIES OF CONDUCTIVE POLYMER COMPOSITES POSSESSING SEGREGATED NETWORK MICROSTRUCTURES

A Thesis
Presented to
The Academic Faculty

by

Laurissa Alia Prystaj

In Partial Fulfillment
of the Requirements for the Degree
Masters of Materials Science and Engineering

Georgia Institute of Technology
December 2008

EFFECT OF CARBON FILLER CHARACTERISTICS ON THE ELECTRICAL PROPERTIES OF CONDUCTIVE POLYMER COMPOSITES POSSESSING SEGREGATED NETWORK MICROSTRUCTURES

Approved by:

Dr. Rosario A. Gerhardt, Advisor
School of Materials Science and Engineering
Georgia Institute of Technology

Dr. Hamid Garmestani
School of Materials Science and Engineering
Georgia Institute of Technology

Dr. Gleb Yushin
School of Materials Science and Engineering
Georgia Institute of Technology

Date Approved: July 23, 2008

I dedicate this work to my family, especially my Mom for her support, and Nana and Gigi who watch over me everyday

ACKNOWLEDGEMENTS

I would like to start by thanking everyone who has helped me through my journey. A special thanks to my advisor Dr. Rosario A. Gerhardt for her guidance and support. She gave me the opportunity to continue my learning at a fine institute. Working with her was a great experience in an environment that was both challenging and fun. Thank you to my committee members, Dr. Hamid Garmestani and Dr. Gleb Yushin, for taking the time to help me in the final step in this chapter of my life.

I would like to thank, NEI Corp., Dr. Runqing Ou and NSF grant DMR-0604211, for the financial support during the completion of my research. Thanks to Ilia Ivanov at Oak Ridge National Laboratories for his guidance along with allowing me to use the optical absorbance equipment to complete my studies.

I want to thank the Georgia Tech Athletic Association, who made it financially possible for me to attend Georgia Tech. Special thanks to John Ames for his guidance and faith in me through my undergrad years. Not only was he a great coach, but he was a friend and a mentor. Thank you to all of my group and lab members for their support. A special thanks to Cantwell Carson for answering my technical questions, Charlie Capozzi for helping me with SEM, Salil Joshi for helping me with TEM, and Siva Kumar for teaching me how to use some of the equipment.

To my family, thank you Mom and Dad for your support and tolerating all of my stressful moments at Tech, Loreal for being not only a great sister, but my best friend, and Stephen for showing me that no matter what, your family is always there to support you. I would like to thank the Silver family for being my family away from home and

welcoming me into their home as a family member. Finally, thank you to all of my friends who have always been there for me, I will never forget you guys.

TABLE OF CONTENTS

LIST OF TABLES

LIST OF FIGURES

LIST OF SYMBOLS AND ABBREVIATIONS

CB	Carbon black
CNT	Carbon nano-tubes
Z^*	Complex impedance (ohms)
Z'	Real part of impedance (ohms)
Z''	Imaginary part of impedance (ohms)
I	Current (ampere)
V	Voltage (Volts)
θ	Phase angle
f	Frequency (Hz)
ω	Angular frequency (radians/sec)
i	The imaginary unit
ε^*	Complex dielectric permittivity (F/m)
ε_r'	Real part of dielectric constant
ε_r''	Imaginary part of dielectric constant
Y^*	Complex admittance (siemens)
Y'	Real part of admittance (siemens)
Y''	Imaginary part of admittance (siemens)
M^*	Complex electric modulus (m/F)
M'	Real part of electric modulus (m/F)
M''	Imaginary part of electric modulus (m/F)
C_o	Geometric capacitance (F)
C	Measured capacitance (F)
ε_o	$8.854*10^{-12}$ F/m permittivity in vacuum
A	Area of samples (cm^2)
t	Thickness of samples (cm)
R	Resistance (ohms)
CPE	Constant phase element
C_v	Critical volume fraction
ρ_m	Resistivity of composite (ohm-m)
ρ_p	Resistivity of insulating material (ohm-m)
ρ_c	Resistivity of conducting material(ohm-m)
V_c	Volume fraction of conducting material
p	Dipole moment
Q	Charge (Coulombs)
α_e	Polarizability
PMMA	Polymethyl methacrylate
N-550	Carbon black N-550
N-772	Carbon black N-772
PB	Pureblack carbon black
MWCN	Short multi-wall CNT
CF	Carbon filler
σ	Conductivity (S/m) (1/(ohm-m))

SUMMARY

The work for this thesis focused on making composites consisting of a polymethylmethacrylate matrix, with various carbon fillers added. The fillers that were examined were 3 different carbon blacks: N-550, N-772 and pureblack, and short multi-wall carbon nano-tubes. The method of producing these composites was consistent throughout the study. The carbon fillers were coated onto the polymethylmethacrylate, and they were subsequently compression molded in order to form a segregated microstructure. The goal of this thesis is to compare the electrical and optical properties of the composites consisting of a segregated microstructure, containing various carbon fillers.

Through the use of scanning electron microscopy the fracture surface of the composites were determined. Impedance Spectroscopy was used to measure the electrical response of the material, over a frequency range with a set current and voltage. These were used to determine the conductivity and dielectric properties of the composites and estimate the percolation threshold. The multi-wall carbon nano-tubes were found to have the lowest percolation threshold, due to their rod like structure. All of the carbon black fillers displayed similar characteristics in their conductivity and dielectric properties. As the filler content increased, the conductivity and the dielectric constant of the composites increased.

Optical absorption measurements were used to determine the amount of light that travel through the specimen. With these measurements, it was observed that the

absorbances for the carbon black samples were lower than the multi-wall carbon nano-tubes at filler contents below a phr of 0.1. The absorption of the carbon black samples was then higher than multi-wall carbon nano-tubes at phrs higher than 0.1. This was found to be due to the structure of the carbon nano-tubes which allow them to start forming a segregated microstructure at lower filler contents than the sphere-like carbon black nano-particles.

CHAPTER 1

INTRODUCTION

1.1 INTRODUCTION

This thesis will evaluate the electrical and optical properties of conductive polymer composites possessing a segregated network microstructure. To fully understand the results obtained during the study of these composites, some background information is offered. The thesis will begin by discussing conductive polymer composites, what they are and their advantages. Subsequently, an overview of the materials used to produce these composites and some of the applications of conductive polymer composites will be discussed.

To interpret and understand the results, this thesis will give an overview of impedance spectroscopy, percolation and dielectric properties. Impedance spectroscopy was the method used to collect the data. Percolation is used to describe the conductivity of the composites. The dielectric constant will express the ability for the composites to hold a charge.

To fully examine the capabilities of these composites, optical absorption measurements will be made to determine how much light is absorbed by the sample at various wavelengths. Optical transmittance can determine the amount of light transmitted through the sample and give further information about the type of microstructure that has been formed within the composite.

1.1.1 Conductive Polymer Composites

Polymers are one of the most widely used materials, due to their versatile properties. Polymers contain properties which make them unique and virtually irreplaceable for some applications. For example, elastomers have the ability to deform by a thousand percent with an applied force and, after the force is removed, they can restore their initial shape. In general, polymers are known for their low density with intermediate stiffness and strength.

Although polymers have ideal properties for a wide range of applications, they were unable to be used for applications requiring electrical conductivity. When there was the addition of a conductive filler particle, it was discovered that a polymer would allow the flow of current through its system. This increased the number of industrial applications for polymers [1]. Materials that contain a polymer matrix with conductive filler are known as conductive polymer composites [2-16].

These composites are known for having high dielectric constants and for being extremely conductive. This is achieved by the conductive filler forming a network throughout the composite which allows for the flow of current through the composite. The conductivity of these composites can increase by several orders of magnitude. Since the matrix consists of a polymer, these composites have the potential of increasing in flexibility, if the polymer used in the matrix is flexible. The composite can be brittle and weak due to the amount of filler that is needed to produce a highly conducting material. The main advantage of conductive polymer composites is that they display characteristics of both a metal and of a polymer [2, 3].

Conductive polymer composites can consist of two types of microstructures. The system can either have a random microstructure or a segregated microstructure. A random microstructure consists of a polymer matrix with filler particles that are sporadically placed throughout the matrix. These composites have isotropic characteristics and the filler shows no bias to its location. A segregated microstructure consists of filler particles that show bias to their location. These composites have filler-rich regions along with polymer rich regions [4-16]. Figure 1.1 shows a cartoon of a segregated versus a random microstructure. Later in the thesis, the advantages of a segregated microstructure will be discussed.

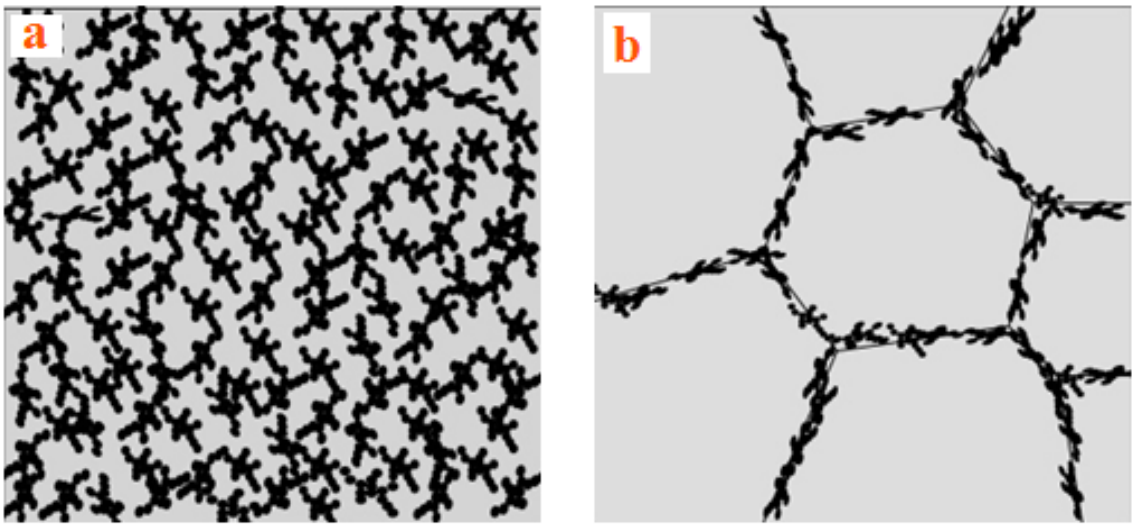

Figure 1.1 Illustrates a cartoon of (a) randomly oriented microstructure and (b) segregated microstructure [4]

1.1.2 Materials that can be used to make the composites

Conductive polymer composites use a wide range of fillers. Inorganic materials are often used; common fillers are ceramics and metals [3, 4, 17,18]. Organics can also be used as fillers; the most common organic filler is carbon based. The types of carbon fillers that have been heavily researched are carbon blacks (CB) and carbon nano-tubes (CNT) [2, 4, 19-21]. CB is one of the most desirable fillers to use due to its relatively low cost; it has a chain like aggregate structure and can easily be obtained in a wide variety of particle sizes [2, 4]. Many different polymer matrices have been examined. Some of the more common polymers used are acrylonitrile butadiene styrene (ABS) [10, 15], polymethylmethacrylate (PMMA) [7-8, 11-14], epoxy, polystyrene (PS) [16], polyimide and polyethylene (PE) [2-16]. In order to decrease the amount of agglomeration that occurs within the composite, a polymer/filler interaction has to be examined. If the affinity for filler/filler interaction is greater than filler/polymer interaction, the agglomeration of filler particles will occur. On the other hand, if the affinity for polymer/polymer is greater than polymer/filler interaction, it will be difficult for a continuous network to form while some agglomeration will still occur [19].

1.1.3 Applications

Conductive polymer composites can be fabricated to obtain the desired properties for specific applications. One of the most useful applications for conductive polymer composites is as electromagnetic interference shields (EMI) [3, 17, 19, 23]. Since

electronic devices play a large role in everyday life, EMI regulators will allow electronics to work in the intended fashion without any loss of performance. The intent of EMI shields is to protect electronic devices and circuits against interference from external electromagnetic fields of different frequencies. The main requirements for EMI devices are that they should be light weight, contain high-quality mechanical properties, are easy to process and most importantly, cost efficient. Meeting all of these requirements is what makes conductive polymer composites ideal for these applications [23].

The composites are geared towards containing a conductive network that can be interrupted with an outside source. Applications that require this phenomenon are self regulating heaters, over-current protectors and chemical sensors [24-26]. M.B. Heaney studied carbon black polymer composites. In his studies, he observed in a sample with the same filler content that the resistance of the sample increased by over eight decades when the temperature went from 25^{o}C to 180^{o}C [25]. This large change in resistance is known as the positive temperature coefficient of resistance. Ralf Strumpler studied temperature sensors and observed the same effect in epoxy composites containing Ni, Ni coated Ag, and TiB_2 [24]. Chemical sensors work in the same fashion; instead of the change in temperature, the vapors from the chemical causes the polymers to swell [26].

Z.-M Dang's group has done a further investigation of the use of polymer composites containing carbon nano-tubes [27]. They are looking at using the composites as actuators for artificial muscles. These composites must contain a high dielectric constant and a large elastic energy density [27]. To be used as actuators, the material has to contain as low of a percolation threshold as possible in order to contain the desired elastic modulus values. These are only a few of the useful applications for conductive

polymer composites. It is important to fully understand the electrical and optical properties of the composites and see how the filler actually affects the microstructure and the properties of the composites.

1.2 IMPEDANCE SPECTROSCOPY

1.2.1 Introduction

Impedance spectroscopy is performed by applying an alternating current (AC) to a material and measuring the resistance through that material. Impedance is a more general term than resistance since impedance is a complex quantity. Complex impedance is represented by $Z^* = Z' - iZ''$, where Z' is the real part of impedance representing the energy that is passed through the material and Z'' is the imaginary part of impedance representing the energy lost or stored in the material. Since resistance is measured in terms of voltage over current, resistance is constant over a wide range of voltages. Complex impedance is more general than resistance since it can be expressed in terms of current ($I(\omega)$), voltage ($V(\omega)$), and a phase angle (θ) over a range of applied frequencies (f), where the angular frequency ω is equivalent to $2\pi f$. The expression for complex impedance is shown in equation 1, while equation 2 shows the calculation for voltage and equation 3 shows the calculation for current. The sinusoidal response for the current and voltage has the same frequency, but vary by a phase shift; this is represented in figure 1.2 [28-30].

$$Z^* = \frac{V(\omega)}{I(\omega)} \qquad \text{Equation 1}$$

$$V(\omega) = V_0 \sin(\omega t) \qquad \text{Equation 2}$$

$$I(\omega) = I_0 \sin(\omega t + \Theta) \qquad \text{Equation 3}$$

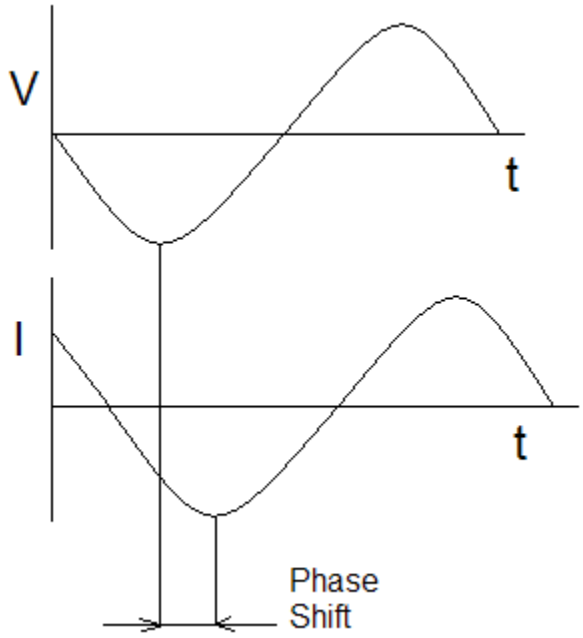

Figure 1.2 A graphical representation of the sinusoidal response for the voltage and current data, and represents the phase shift that is undergone by the current.

There are several other parameters of a material that are frequency dependent that can be determined with the use of impedance spectroscopy. Those parameters are the

complex admittance (Y*), the complex dielectric constant (ε*) and the complex electric modulus (M*). Through the use of mathematical transformation, all four parameters can be related. This is shown in equations 4, 5, 6, and 7, where $i = (-1)^{1/2}$, C_o is the geometric capacitance, and ω is the angular frequency [28-30].

$$Z^* = Z' - iZ''$$ Equation 4

$$\varepsilon^* = \varepsilon_r^{'} - i\varepsilon_r^{''} = \frac{1}{\left(i\omega C_0 Z^*\right)}$$ Equation 5

$$Y^* = Y^{'} + iY^{''} = i\omega C_0 \varepsilon^* = \frac{1}{Z^*}$$ Equation 6

$$M^* = M^{'} + iM^{''} = \frac{1}{\varepsilon^*}$$ Equation 7

When dealing with a pair of parallel plates or disks, the real part of the dielectric constant can be calculated using the equations 8 and 9. In these equations, A is the area of the thin plate or disk, t is the thickness or distance between the electrodes, ε_0 is the permittivity in vacuum ($8.854*10^{-12}$ F/m) and C is the actual capacitance that is measured [4, 28-30].

$$C_0 = \varepsilon_0 \frac{A}{t}$$ Equation 8

$$\varepsilon_r^{'} = \frac{C}{C_0}$$ Equation 9

All four properties can once more be related by evaluating the dielectric loss, dissipation or tan delta of the material. The tan delta is the tangent of the phase shift

between the current and the voltage. The tan delta for a material is shown in the equation below, equation 10. Since all parameters that calculate the tan delta are frequency dependent, the tan delta is also frequency dependent.

$$Tan(delta) = \frac{\varepsilon_r^{''}}{\varepsilon_r^{'}} = \frac{Z^{'}}{Z^{''}} = \frac{M^{''}}{M^{'}} = \frac{Y^{'}}{Y^{''}} \qquad \text{Equation 10}$$

1.2.2 Representation of Impedance Data

There are two styles that are used to represent impedance data, Complex plane plots and Spectrum plane plots.

1.2.2.1 Complex Plane Plots

Complex plane plots are known as Nyquist plots and plot the real part versus the imaginary part of the component. When graphing the Z" vs. Z', the display results in a semicircle below the x-axis and the graphs are displayed in the form of –Z" vs. Z', as shown in figure 1.3. These plots do not explicitly show the frequency, but the frequency increases as it approaches the origin, as shown in figure 1.3. The resistance (R) is represented by the real part of the impedance and is the value that is found when the semicircle crosses the x-axis. The capacitance of the system can be found on these plots by using the maximum of the curve where the maximum is expressed as $C = 1/(\omega_{max} R)$ [4, 28-30].

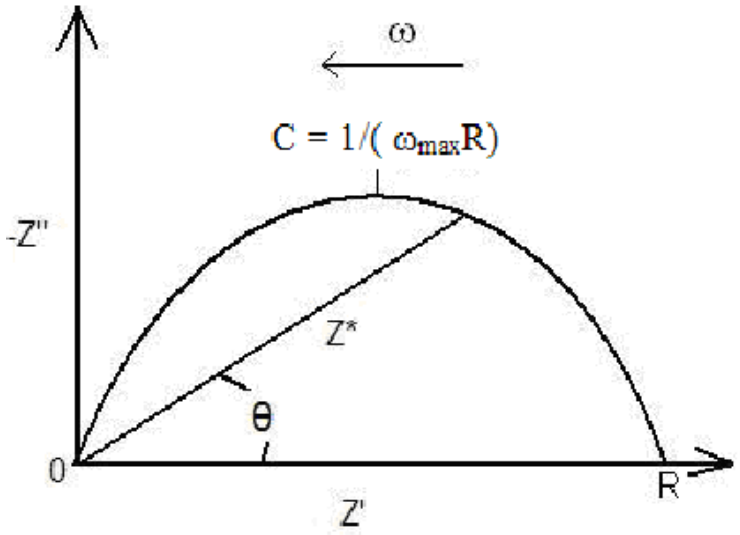

Figure 1.3 Complex impedance plot of –Z" vs. Z'. The figure highlights the main information that can be obtained from the plot.

1.2.2.1 Spectrum Plane Plots

When using spectrum plane plots, also known as Bode plots, the graphs consist of one real or imaginary component of the parameters versus the log(ω) or log(f). In figure 1.4, both the real component and the imaginary component of impedance are graphed versus frequency on a logarithmic scale. The real part of impedance levels off and remains constant in the low frequency ranges. This trend is valid for the real parts of Y, M and ε, as well. When the real component either decreases or increases, a relaxation from one mechanism to another is occurring. This relaxation is more clearly shown when the imaginary component is graphed versus the frequency when a peak appears. When a relaxation peak occurs, the value of the peak represents either the maximum or minimum of the parameter. The location of the peak is an important parameter and is used to calculate the relaxation time, based on the frequency at which the peak occurs. The parameter is shown in figure 1.4 [4, 28-30].

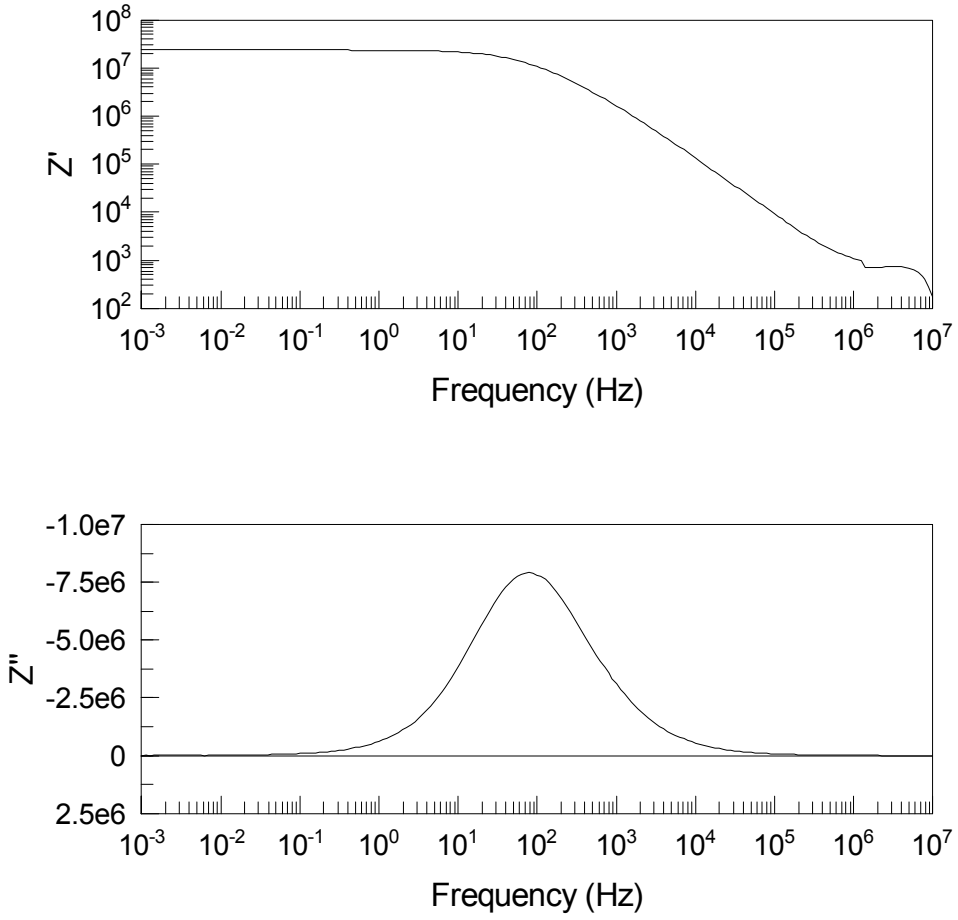

Figure 1.4 Represents a Bode plot of Z vs. the applied frequency. The top image shows real impedance Z' vs. frequency. The bottom image shows imaginary impedance Z" vs. frequency. A relaxation peak occurs around 100 Hz in this case.

1.2.3 Equivalent Circuits

When the data is analyzed and a Nyquist plot is produced, the data needs to be matched with an equivalent circuit to enable the data to be extrapolated and form a best-fit semicircle to properly analyze the data. Figure 1.5 shows the equivalent circuit, consisting of a resistor and a constant phase element (CPE) in parallel, which is used to analyze insulating samples [4, 6, 31].

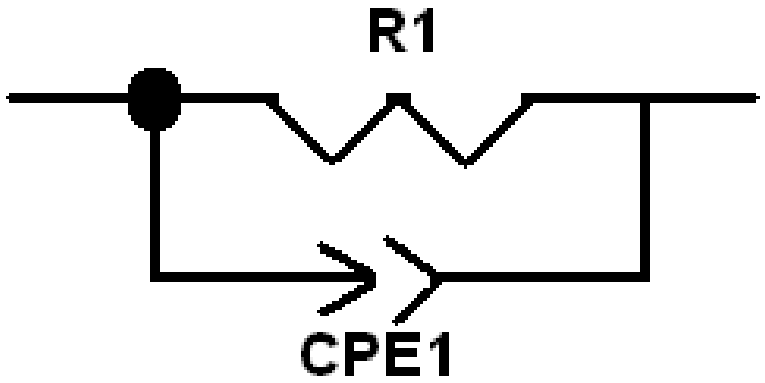

Figure 1.5 Simulated equivalent circuit used by Z-view used to extrapolate data

The CPE is a non-intuitive element used when analyzing circuits to compensate for any abnormalities in the circuit, such as surface roughness, varying thickness or composition throughout the sample, and non-uniform current distribution. CPE is

defined by the equation below, where Y_o is a constant and is numerically equal to the admittance (1/ Z*) at ω=1 rad/s, α is a value ranging from 0 to 1 [4, 31].

$$Z = \frac{1}{\left(Y_0 (i\omega)^{\alpha}\right)} \qquad \text{Equation 11}$$

Since Y_o has units of s^{α}/Ω and the unit for C is s/Ω, Y_o is being used in the same fashion as C. If the properties of a material have a low dielectric constant, using Y_o results in a higher ε value than actually present in the sample [31]**.** To relate C to Y_o, equation 12 can be used, where ω_{max} is the frequency at which the imaginary part of the impedance has a maximum. If α =1, then the system is identical to that of an ideal capacitor. When combining equations 11 and 12, capacitance can be related to the impedance, and this provides the relationship for the Nyquist plot [31].

$$C = Y_0 (\omega_{\max})^{\alpha - 1} \qquad \text{Equation 12}$$

$$Z = \frac{1}{(i\omega C)} \qquad \text{Equation 13}$$

The CPE is frequently used with impedance spectroscopy since it is common to have somewhat skewed semicircles. The result produces the semicircle shown in the previous section that can be used to further evaluate a material. Figure 1.6 shows the complex admittance and impedance plots, for data that has been fit to an equivalent circuit, with a CPE present [31, 32].

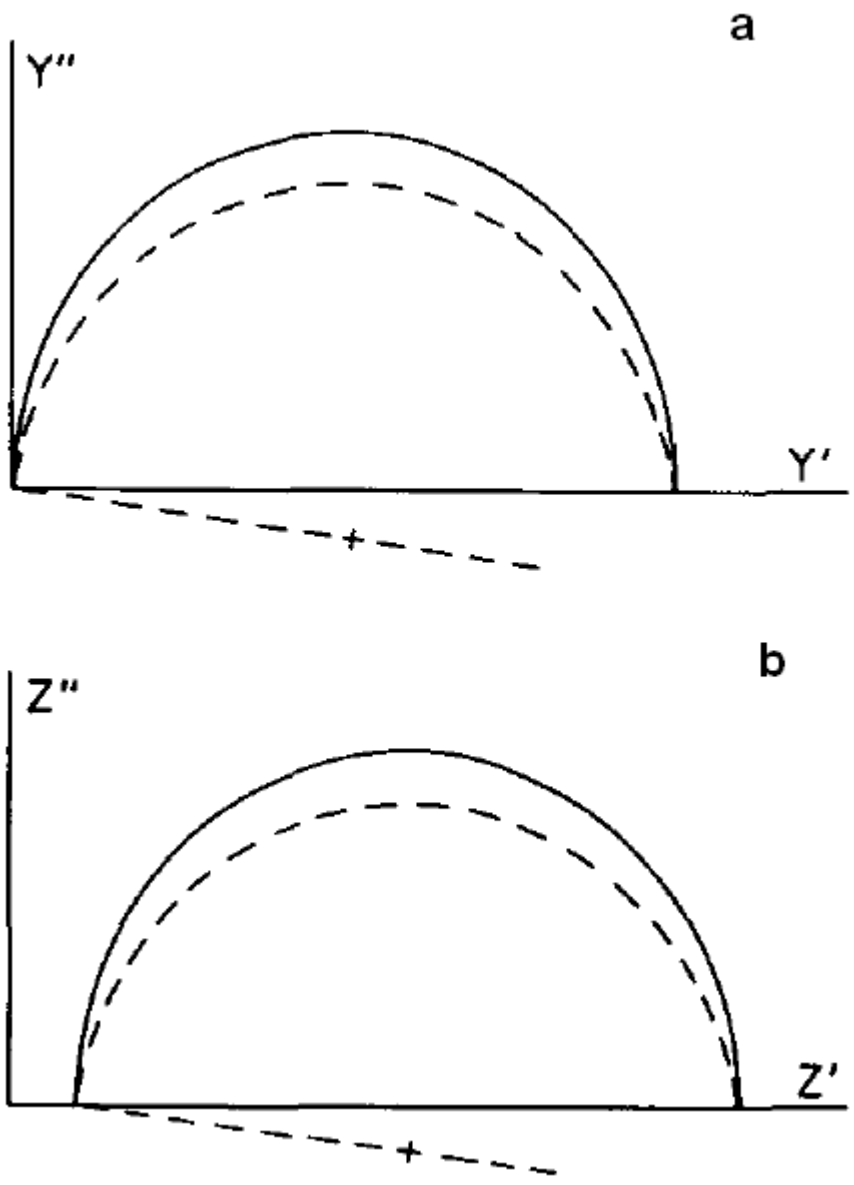

Figure 1.6 Impedance and admittance plot, with an equivalent circuit applied, varying α, the dash line represents α= 0.1 and the solid line α=0 [32].

1.3 PERCOLATION

Percolation describes the movement of a substance or signal through a system. It is most often used to describe the movement of a liquid through a porous material, such as the passage of water, first through coffee grounds and finally through the filter. The idea of percolation is common in many aspects of science and technology. Civil engineers refer to percolation as the passage of water through soil; computer scientists and programmers use the term to describe the transferring of data from a secondary storage device back to the main storage device; others use it to determine which trees to remove in a forest to decrease the spread of forest fires [6, 33]. In recent years, the study of percolation in a two phase composite has caught the attention of many researchers in the technical community. Percolation is used to describe the mechanism of conduction within a composite. When the concentration of filler (the minor phase/conductive phase in the composite) is low, the formation of a continuous network - which allows for conduction to penetrate or percolate through the composite - is not formed, leaving the resistivity of the composite extremely high. After increasing the filler content, a network starts to form throughout the major phase in the composite. The point at which the first conductive pathway is formed throughout the composite is known as the percolation threshold. As the filler content increases, more connective pathways form, leading to a decrease in the resistivity of the composite [1-16]. Figure 1.7 shows the formation of a percolated system. The image on the left shows the isolated particles, forming an unpercolated system (no continuous path). The image in the middle shows the particles

starting to connect, forming a network throughout the matrix. The image on the right shows a percolated system where a continuous network has been formed.

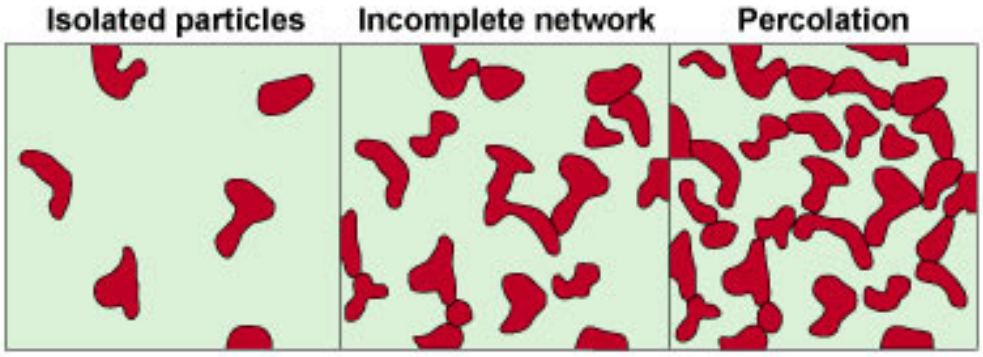

Figure 1.7 Displays how the unpercolated network becomes percolated with the addition of filler to form a continuous network throughout the polymer matrix.

The critical volume fraction (C_v) is the value which defines the minimum amount of filler needed for the formation of an interconnected network throughout the matrix, known as the percolation threshold. Above or below the C_v, the addition of filler to the system does not affect the resistivity of the sample substantially. Figure 1.8 represents an ideal graph, showing the percolation threshold. The onset of percolation is labeled on the figure as C_v, where it is shown how adding a small amount of filler can significantly lower the resistivity of the sample [1-17, 33, 34].

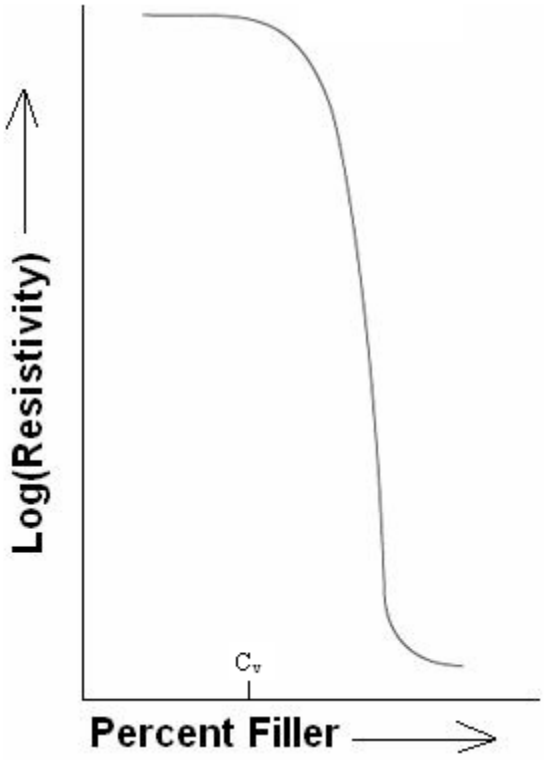

Figure 1.8 Represents the ideal resistivity vs. content of filler curve

In a percolation model, the resistivity of a conductive polymer composite can be calculated using equation 14, where ρ_m is the resistivity of the composite, ρ_p is the resistivity of the more resistive materials, ρ_c is the resistivity of the more conductive material, z is the coordination number of the filler, V_c is the volume fraction of the more conductive material, and C_v is the critical volume fraction [33, 34].

$$\rho_m = \frac{(z-2)\rho_c\rho_p}{\sqrt{(A+B+(A+B)^2+2(z-2)\rho_c\rho_p)}} \qquad \text{Equation 14}$$

A and B are described in equations 15 and 16.

$$A = \rho_c\left(-1+\left(\frac{z}{2}\right)\right)\left(1-\left(\frac{C_v}{V_c}\right)\right) \qquad \text{Equation 15}$$

$$\mathrm{B} = \rho_m\left(\left(\frac{2C_v}{2V_c}\right)-1\right) \qquad \text{Equation 16}$$

The percolation threshold of a material can be affected by many factors, such as the size and shape of the conducting filler and the method used to process the composites [34-37]. This thesis will investigate the effects of varying parameters of the filler particles, but will maintain the same processing procedure and the same matrix polymer for all of the samples.

1.3.1 Influence of Processing on Percolation Threshold

The filler can be added to a single polymer matrix by various methods to form the composite; some methods that have been studied are: (1) pressing the dry mixed CB and polymer powder together [4-8, 19], (2) using toluene dissolved polymer and mixing the mixture with CB, then drying out the mixture, followed by ball milling and finally pressing [19], or by dissolving the polymer in a solution and adding desired amounts of

filler [18], and (3) calendering a mixture of CB and polymer; in the calendering process, the mixture was ground and then the material passed through a set of heated rollers [19, 26]. The processing technique will affect the type of network that forms throughout the composite and the amount of agglomeration that is present throughout the system. There are two main microstructures that can be obtained by conductive polymer composites, randomly oriented and segregated microstructures, which were discussed in the introduction [1, 4-6, 17, 19, 20].

When using solution mixing, agglomerates of filler are formed throughout the matrix due to the lack of shear forces that can be applied during processing. The agglomeration of filler particles may be due to the filler particles being exposed to forces that cause the filler particles to have a higher affinity to be near each other leading to clustering throughout the composite. When the filler particles are added to the polymer in the melt, the filler particles may interact with the polymer differently due to the change in the viscosity of the system. This has been explained by the DLVO theory, which was developed in the 1940s and named after, Derjaguin, Landau, Verwey and Overbeek. This can be demonstrated in figure 1.9, where it is shown that if the filler particles can attract opposite charged ions, the ions will align can form a double layer. The DLVO theory is used to describe the interaction of charged surfaces through a liquid medium, taking into account the van der Waals attraction and the electrostatic repulsion [39]. This is believed to play a role in the clustering of the filler particles as well. When adding the filler during polymerization, it is observed that the filler is generally evenly distributed throughout the matrix, not showing a bias to this position. All of these methods described here lead to the formation of a random microstructure.

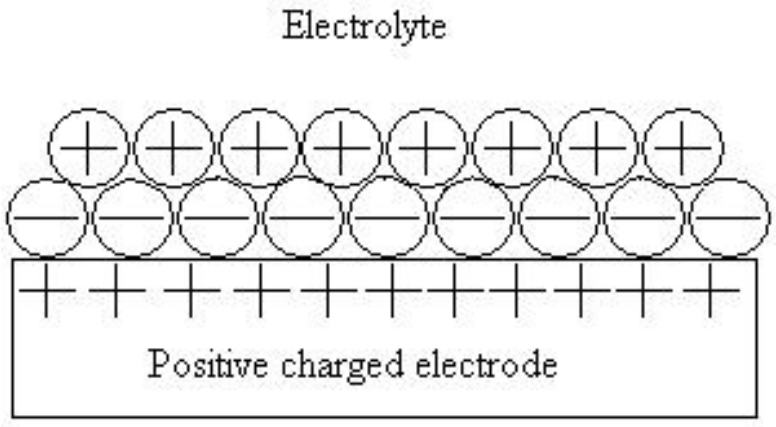

Figure 1.9 Shows the formation of a double layer on a positively charged electrode

Studies have shown that a lower percolation threshold can be obtained if the composite consists of a segregated microstructure [4, 5]. Since the filler is preferentially forced to stay in certain locations, a path can be made through the composite with lower amounts of filler. Figure 1.10 (a) shows filler particles forming a connective path in a random microstructure, while figure 1.10 (b) shows a conductive path formed in a segregated network microstructure. This figure demonstrates that less filler is needed in order to form a pathway through the sample with a segregated microstructure. Various studies have been done using different methods to obtain a segregated microstructure [2-17, 40, 41]. These composites can be synthesized using semi-crystalline polymers, block copolymers [4], and immiscible polymer blends [41].

Heterogeneous matrix consisting of two immiscible polymers is usually used to produce a segregated microstructure. In most of these systems, the filler particles are added to one of the polymers, leaving the other polymer as the pure insulating matrix.

These systems lead to a lower percolation threshold, but often display double or two-step percolation [4, 41]. This is caused by the formation of a network throughout the filler rich region and then the formation of the network throughout the bulk of the composite. Figure 1.11 shows double percolation occurring in CB filled ethylene-vinyl acetate copolymer/ low density polyethylene (EVA/LDPE) [41]. The first percolation occurs due to the network forming in the LPDE, while the second percolation occurs at the EVA/LDPE interfaces [41].

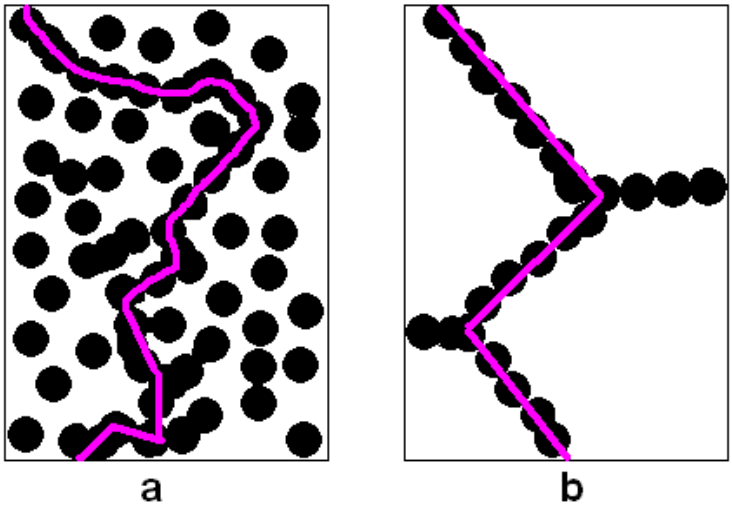

Figure 1.10 Represents filler particles forming a connective path throughout a (a) random microstructure and (b) segregated microstructure

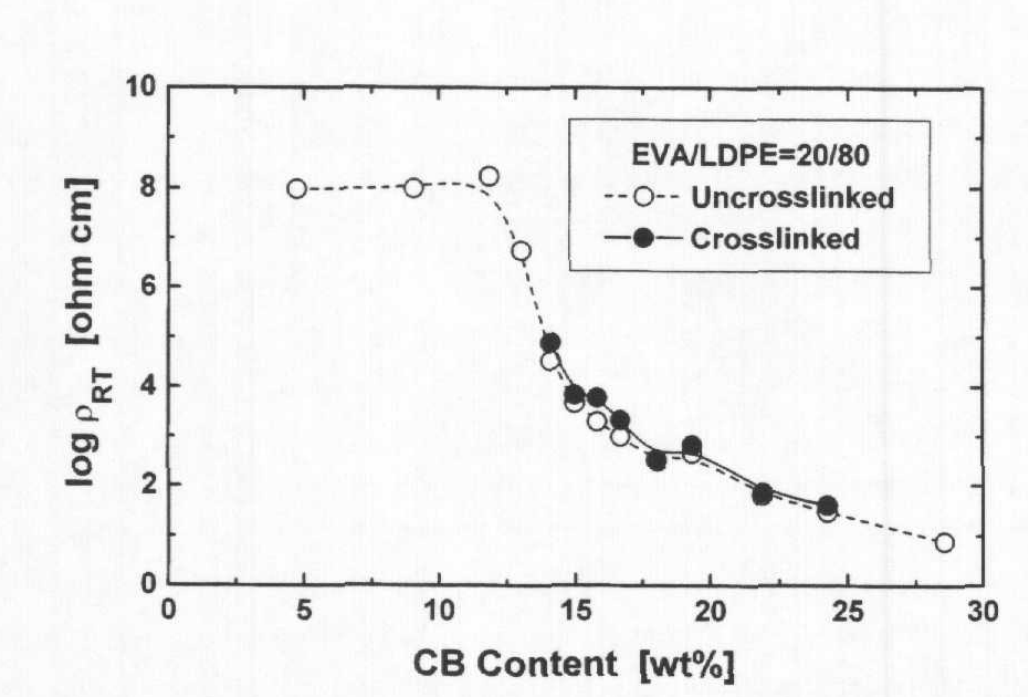

Figure 1.11 Illustrates two-step or double percolation occurring. One at about 11 wt% CB and another at about 20 wt% CB [41]

In 1970, D.T. Turner was the first to synthesize a polymer composite which consisted of a segregated microstructure where there were filler-rich regions throughout the microstructure [5]. The filler-rich regions led to a lower content of filler needed to form a continuous network throughout the composite. In his experiments, he fabricated composites consisting of high-density polyethylene powder and nickel. The samples were prepared by tumbling and then pressed at 1000 kg/cm^2. He noticed that the smaller particles of nickel stuck to the larger polyethylene particles and formed a segregated microstructure throughout the composite. His group looked at various particle sizes of nickel and concluded that if the ratio of the radius of the polymer to filler was high, such

as 16, the filler particles surrounded the polymer particles [5]. When the ratio was equal to 1, a more uniform distribution of filler particles throughout the polymer occurred. When he tested his samples, he noticed that the samples' percolation threshold decreased as the ratio between the radius of the polymer particles to nickel particles increased since the segregated microstructure was present [5]. Studies done by, R.P. Kusy, J. Li, D. He and N. Lebovka have all witnessed the effect that a smaller particle size or larger aspect ratio leads to a lower percolation threshold [8, 42-46]. It has also been seen that when CB contains a high structure, it has the highest ability to form a continuous network, leading to lower percolation thresholds as well [35]. These studies all support Turner's findings.

A method has recently been developed at Georgia Institute of Technology in Dr. Gerhardt's lab [4, 6-16] that produces a segregated microstructure with a lower percolation threshold and without displaying double percolation since it consists of using a single polymer matrix. With this method, composites are made by mechanically mixing together the polymer and filler particles and hot pressing the powder at a temperature above the glass transition temperature and within the processing range for compression molding of the polymer. This processing technique has shown that a segregated network is formed throughout the composite, and the resistance obtained at various filler levels is reproducible. This method has been used to investigate: PMMA/indium tin oxide (ITO) [6, 8, 11-14], PS/CB [16], and ABS/CB [10, 15] composites.

An in-depth study was performed to see the influence of the random versus segregated microstructure for composites consisting of PMMA/CB; the CB used was

CDX-975 [4, 7, 9]. In the paper, two methods were used to make the composites; the solution method was used to form a random microstructure, and the mixing method was used to form a segregated network. All other parameters were held constant and the resistivity at various filler contents was calculated.

When mechanically mixing the polymer and filler together, the filler particles do not tend to agglomerate throughout the system, but they do show bias to their location [4-8]. The SEM images in figure 1.12, displays examples of a randomly oriented microstructure (figure 1.12 (a)), along with a segregated microstructure (figure 1.12 (b)) for PMMA/CB composites consisting of the same composition [4]. It can be observed that in the segregated microstructure network (figure 1.12 (b)), the polyhedra shaped PMMA particles can be seen with the filler particles surrounding the surface of the polymer matrix particles. In a random microstructure, the filler is evenly distributed throughout the matrix, resulting in the composite having homogeneous properties and a much higher percolation threshold [4, 7, 9].

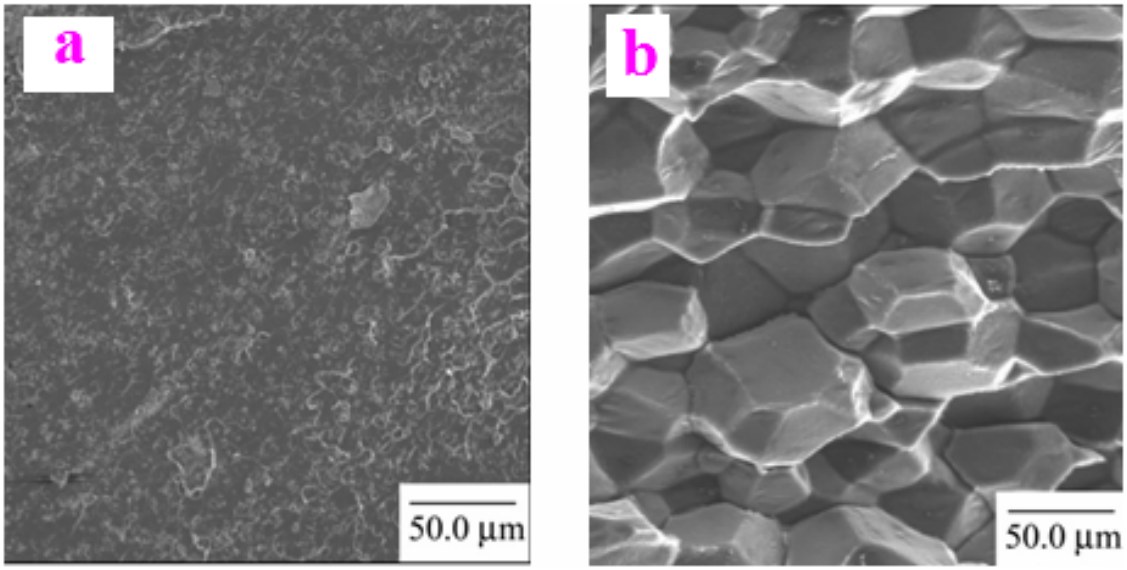

Figure 1.12 SEM images comparing the microstructure of (a) solution mixing, leading to a randomly oriented microstructure and (b) mechanical mixing, leading to a segregated microstructure [4].

Figure 1.13 shows a comparison for the percolation threshold of the two microstructures, and supports Turner's findings. The percolation threshold for the random microstructure occurs at about 2.7 vol% CB while in a segregated microstructure, percolation occurs as low as 0.26 vol% [4].

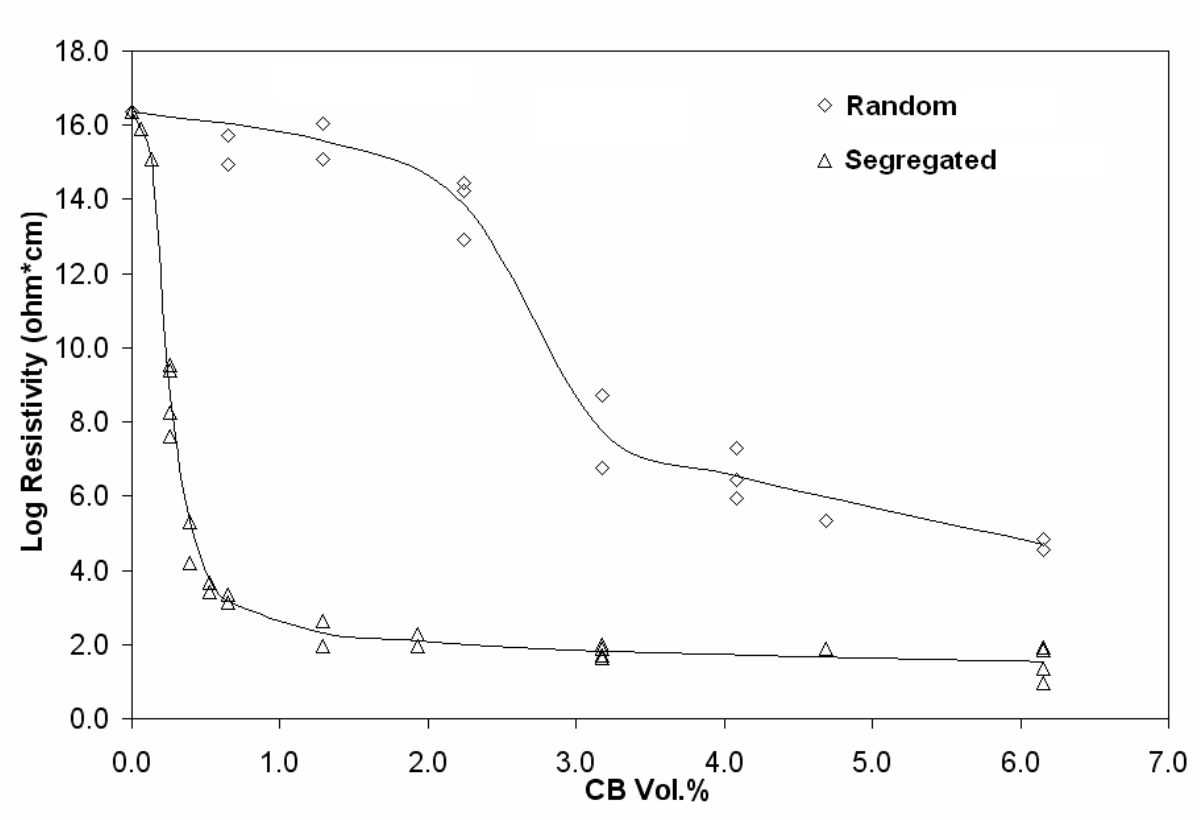

Figure 1.13 Displays that the percolation threshold for a segregated microstructure is substantially lower than that for a random microstructure [4]

1.4 DIELECTRIC CONSTANT

1.4.1 Cause of Dielectric Properties

As discussed in the impedance section, the dielectric constant of a material is directly related to the capacitance of the material. The capacitance is a measure of the capability for a material to store a charge and this value depends on the polarizability of the material. Polarizability is a term used to relate to the induced dipole moment caused by an applied field.

One type of dipole is an electric dipole moment (p) and it is the product of a pair of opposite charges (Q) in an electric dipole with distance separating them. If the positive and negative charged centers coincide, the material will not contain a dipole, as shown in figure 1.14. The positively charged nucleus is surrounded by a spherical electron cloud with equal and opposite charges without an electric field being applied. Electrons are much lighter than the positively charged centers. When an electric field is applied to the system**,** the electrons become displaced by the electric field and the centers of the positive and negative charges do not coincide, resulting in an induced dipole moment. An atom is polarized when there is a separation between the positive and negative charged centers. Figure 1.15 shows an electric dipole moment within an atom. Polarizability can be defined in equation 17, where α is the polarizability, p_{induced} is the induced dipole moment, and E is the electric field causing the dipole moment [47-49].

$$p_{induced} = \alpha \, \mathrm{E} \qquad \text{Equation 17}$$

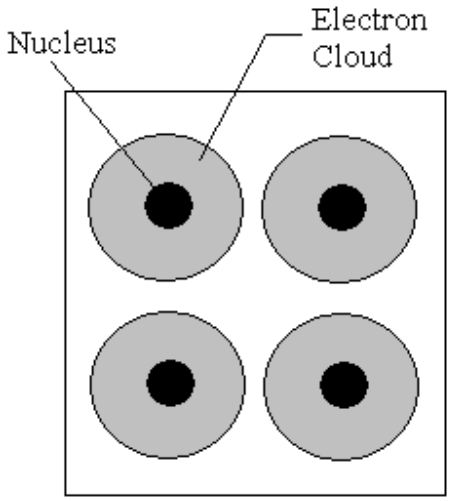

Figure 1.14 Schematic representing a neutral system with no dipoles present

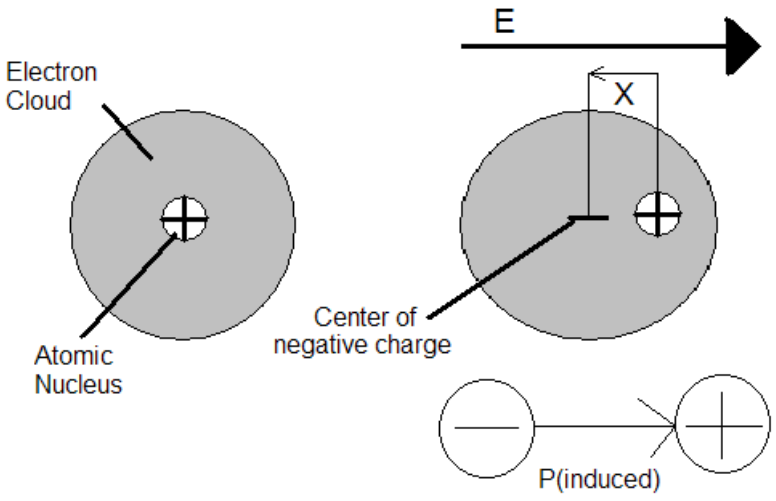

Figure 1.15 Schematic representing electronic polarization

There are four types of polarization that occur and are frequency dependent: electronic polarization, ionic polarization, dipolar or orientation polarization, and interfacial polarization. Electronic polarization occurs when a field is applied to a solid substance and the electron clouds within each atom become shifted by the field, as recently discussed in this section. Ionic polarization occurs in ionic crystals when an applied field causes the cations to move in the positive x-direction and the anions to move in the negative x-direction from their equilibrium position; this is shown in figure 1.16. Orientation polarization occurs in molecules that have a permanent dipole. This occurs when an electric field is applied and causes the dipoles to align parallel to the field; this is shown in figure 1-17. Interfacial polarization happens when there is an accumulation of charges at an interface between two materials or a build up of a charge within a region of a material, as shown in figure 1.18 [47-49].

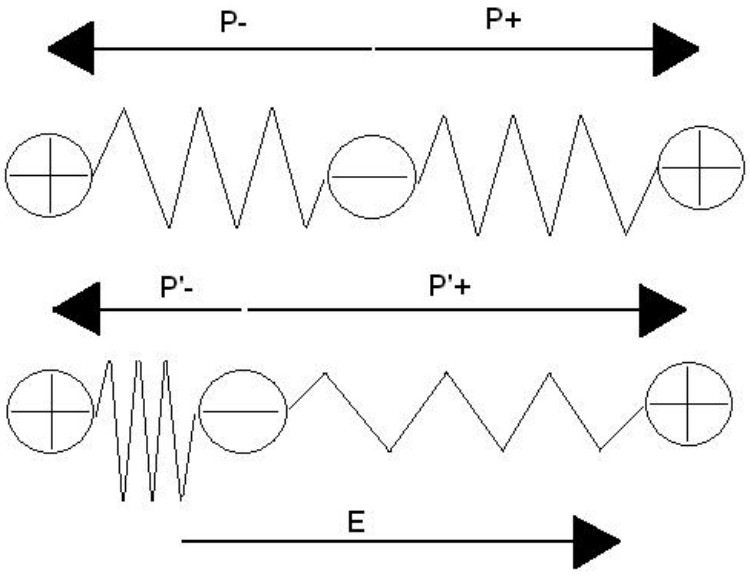

Figure 1.16 Schematic representing ionic polarization

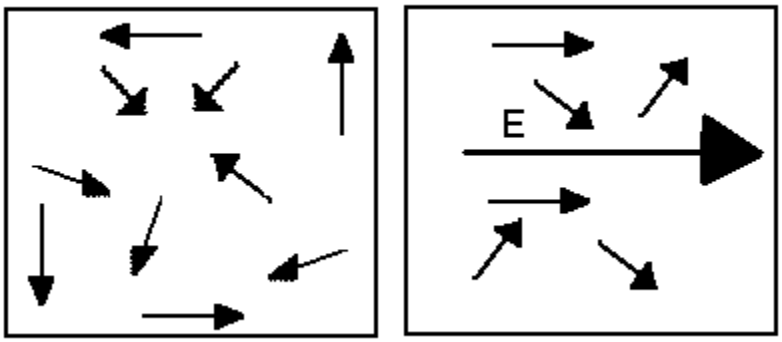

Figure 1.17 Schematic representing dipole polarization

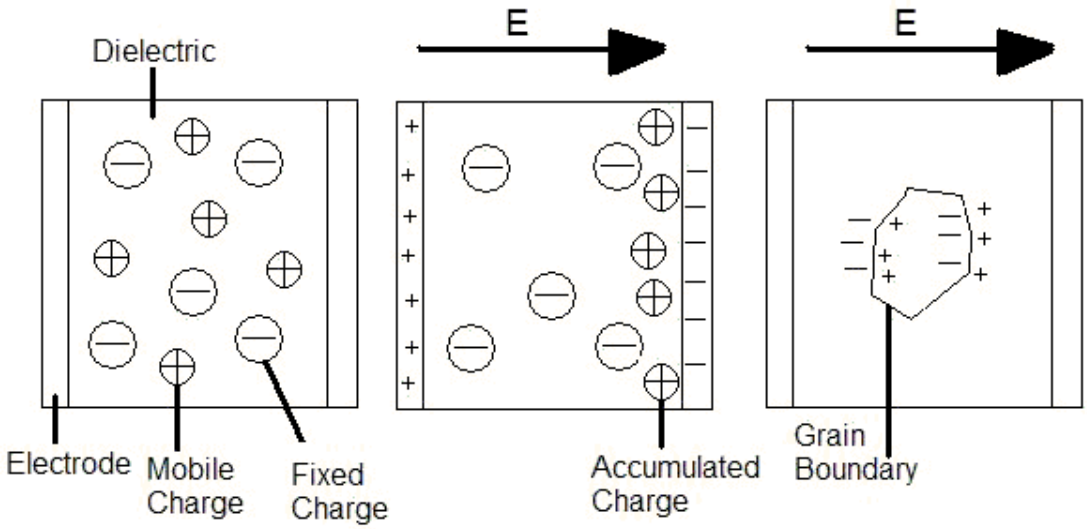

Figure 1.18 Schematic representing interfacial polarization

Each of these factors influence the total polarizability of a dielectric material and equation 18 represents the calculation to find the total polarizability by summing up, α_e, α_i, α_o, α_{int}; electronic, ionic, dipolar and interfacial polarization respectively [47-49].

$$\alpha = \alpha_e + \alpha_i + \alpha_0 + \alpha_{\text{int}} \qquad \text{Equation 18}$$

The Clausius-Mosotti equation is used to relate the material's polarizability, a microscopic property, to the complex dielectric constant that is a macroscopic property, as shown in equation 19. N_i represents the number of polarizable species and i represents the type of polarization, either electronic, ionic, dipolar and interfacial.

$$\frac{\varepsilon^* - 1}{\varepsilon^* + 2} = \left(\frac{1}{3\varepsilon_0}\right)\sum_i \left(N_i^* \alpha_i\right) \qquad \text{Equation 19}$$

This relationship shows that as the polarizability of the material increases, the dielectric constant increases. The dielectric properties of a material are frequency dependent, due to being related to the types of polarization present in a material. Polarization occurs when there is electron movement or the inertia of charge; therefore, a material's polarizability does not occur immediately when the external field is applied. Instead, there is a delay between the time the field is applied and the time when the system is stably polarized. An example of this is the time required to align a dipole due to the applied field, known as the relaxation time. When there is an increase in frequency, there may be a decrease in the dielectric constants because fewer mechanisms

are active at the higher frequencies, see figure 1.19. The decrease takes place because a dipole is unable to reverse direction at an equivalent rate to the applied electric field. This reversing of the dipole is known as the reverse rate. If the reverse rate occurs with no relaxation time in between, then the system will have a constant dielectric response since the material remains in phase with the applied field [47-49]. Figure 1.19 represents a plot showing the frequencies at which a particular polarization dictates the calculation of the dielectric properties. When the frequency range is greater than 10^{14} Hz, electronic polarization, movement of free electrons, is the only polarization that can respond to the electric field and is the only contributor to the dielectric properties of the material. Dipole polarization is the main contributor to the dielectric constant for polymers and occurs in the microwave region. Ionic polarization has the highest relaxation time and the lowest relaxation frequency up to about 10^3 Hz. The interfacial polarization dominates in the medium to low frequency range and is the main cause for the maximum in the tan delta versus frequency plot. The change in the dielectric constant due to frequency is given by Debye's equation. Equation 20 shows the frequency effect for the real part of the dielectric ($\varepsilon_r'(\omega)$) and equation 21 shows the change for the imaginary part of the dielectric ($\varepsilon_r''(\omega)$), where τ is the relaxation time [47, 50].

$$\varepsilon_r'(\omega) = 1 + \left(\frac{\varepsilon_r(0) - 1}{(1 + \omega\tau)^2} \right) \qquad \text{Equation 20}$$

$$\varepsilon_r''(\omega) = \frac{((\varepsilon_r(0) - 1)\omega\tau)}{(1 + \omega\tau)^2} \qquad \text{Equation 21}$$

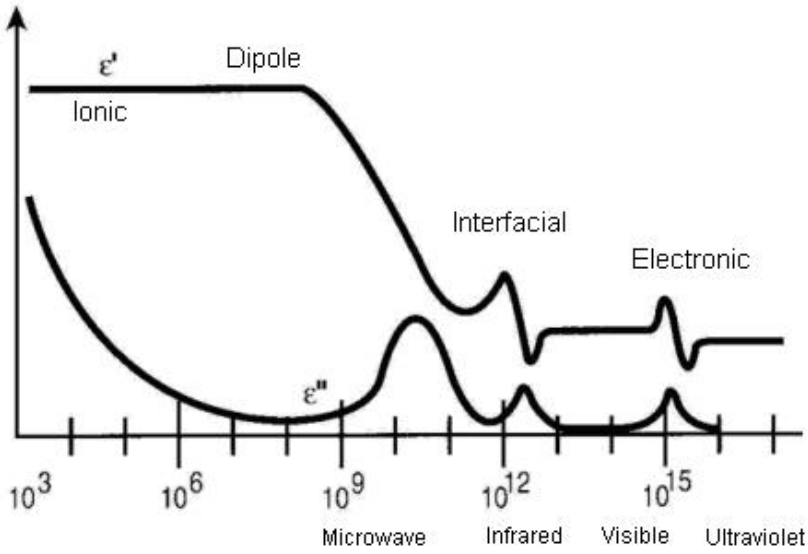

Figure 1.19 Frequency dependence of polarizability [51]

1.4.2 Trends of the Dielectric Constant in Conductive Polymer Composites

The dielectric constant of conducting polymer composites is investigated due to their technical applications. In conductive polymer composites, the percolation threshold has a direct relationship with the dielectric constant. When the system is below the percolation threshold, a connected network has not formed; it is predicted that the dielectric constant should increase since there is an increase in filler concentration [27, 52, 53]. Above the percolation threshold, the dielectric constant is expected to decrease dramatically, similar to the dramatic increase prior to percolation. The dielectric constant and conductivity of the composite containing insulating and conducting material should follow the universal scaling laws, shown in equations 22, where ($V<V_c$) and in equation

23 where ($V>V_c$), where V is the concentration of CB and V_c is the percolation threshold. The critical exponents t and s are influenced by the dimensions of the structure for randomly oriented 3-D microstructures; s is roughly 0.75 and t is about 2.0 [2-4, 37, 52, 54].

$$\varepsilon_r^{'} \propto (V_c - V)^{-s} \qquad \text{Equation 22}$$

$$\sigma_{dc} \propto (V - V_c)^{t} \qquad \text{Equation 23}$$

This idea has carried over to the models that predict how the concentration of filler will affect the dielectric constant of a composite [46]. It showed that the dielectric constant should reach a maximum at the percolation threshold concentration which is how most colloidal structures behave. This was shown not to be true for CB composites, but instead the dielectric constant continues to increase with an increase in filler concentration [46]. The percolation model predicts that after the percolation threshold is reached, the dielectric constant should decrease with increasing filler content. This is because beyond the percolation threshold, the model considers the presence of conducting links and does not consider electrons tunneling, capacitance gaps being present in the composite. With the increasing in filler concentration leading to a constant increase in the dielectric constant, it leads to the conclusion that tunneling plays a large roll in transporting the current through the composite [55].

Other papers examine how the dielectric constant is influenced by frequency and by the weight percentage of filler. As the frequency increases, the real and imaginary part of the dielectric constant decreases. Z.-M. Dang and his group investigated multi-

wall CNT in a polyvinylindene fluoride, and observed that as the filler content increased, there was an increase in the dielectric constant [1, 27, 18]. At frequencies around the 0.2 THz range, the real part of the dielectric constant in PMMA/Graphite composites with 35.7 wt% of graphite head to zero and then continue to negative values for the real part of the dielectric; this is shown in figure 1.20 [22]. Since the negative values are achieved, PMMA/Graphite composites are capable of behaving as poor metals [22]. On the other hand, as the concentration of graphite increases, there is an increase in the imaginary portion of the dielectric. Polypropylene (PP)/CB composites, consisting of Vulcan XC-72R as the CB filler, displayed different behavior than the PMMA/graphite composites. As the percentage of CB increased, both the real and imaginary part of the dielectric increased [1].

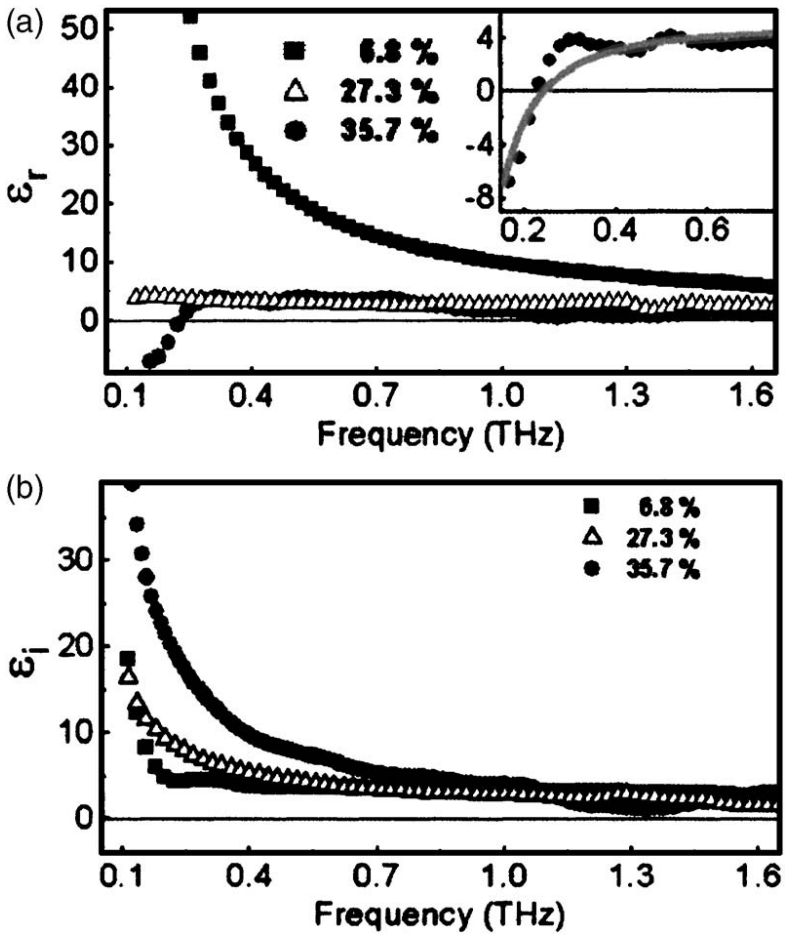

Figure 1.20 Real and imaginary parts of the dielectric constants as a function of frequency are shown in (a) and (b), respectively, displaying that at frequencies below 0.2 THz the real component of the dielectric constant is negative at higher filler contents [22].

Q. Chen and P. Du's group [44] looked at the dielectric constant of thin films. Previous work had been done on the dielectric constant for materials in the bulk; Chen and Du observed that the dielectric constant for the materials could be high, but this resulted in a high dielectric loss. They noticed that at higher frequencies, in the range of 10^5-10^6 Hz, the dielectric constants for composites around the percolation threshold reduced rapidly with frequency; this is shown in figure 1.21 [53]. This shows how the dielectric constant displayed a plateau region with the sharp decrease for Polyvinylindene fluoride (PVDF)/ acetylene black (AB) composites. This was also seen by Dang's group in polymer composites containing Ni, Cu and carbon fiber dependence of dielectric behavior [18]. The percolation theory states that $\varepsilon_r' \approx \omega^{n-1}$, where n is the critical exponent, and as n approaches 1, the dielectric constant is less dependent on the frequency [18] since the exponent the frequency is raised to is approaching zero. Therefore, when the exponent is zero the frequency has no influence on the dielectric constant.

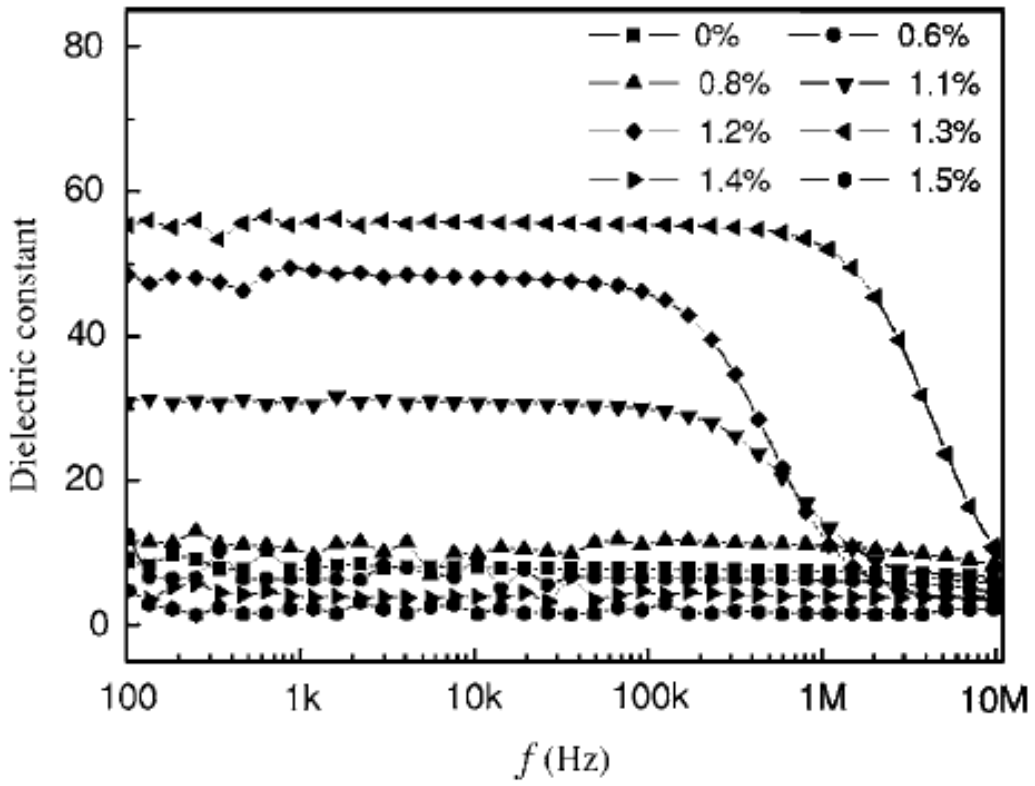

Figure 1.21 Dielectric constant of the PVDF/AB composite film as a function of composition, showing that a sharp decrease in the dielectric constant occurs at high frequencies for composites with a high filler concentration [18].

1.5 Optical Properties

Optical properties are used to determine the material's interaction with light/ various wavelengths. One of the most common measurements of materials' optical properties is the refractive index (n). The refractive index is used to determine the speed of light through the material, as shown in equation 24, where c is the speed of light in free space (299,792,458 m / s) and S is the speed of light through the material. n is directly related to the wavelength (λ) and the dielectric properties of the material. Knowing the wavelength of light and refractive index, the materials n-λ behavior can be calculated and is known as the dispersion relation.

$$S = \frac{c}{n} \qquad \text{Equation 24}$$

There are four key aspects to optical properties, absorption, refraction, diffraction and dispersion. Absorption occurs when light passes through a material and the intensity is reduced based on the colors that are absorbed. Refraction takes place when light travels from one medium to another medium with a different optical density. Diffraction is when the wave that is traveling through an object bends, due to obstacles that it encounters. Dispersion is the separation of light into its constituent wavelengths when entering a medium. In this thesis, the main optical aspects examined were optical absorption and transmittance. Absorbance and transmittance are directly related to each other and this relationship is shown in equations 25 and 26, where T is transmittance, I_0 is

the intensity of the light entering the sample, I is the intensity of the light leaving the sample and $\hat{A}$ is the absorbance.

$$T = \frac{I}{I_0} \qquad \text{Equation 25}$$

$$\hat{A} = -\log(T) \qquad \text{Equation 26}$$

When light travels through a material, the amplitude of the wavelength decreases; therefore, the intensity decreases in the direction of propagation. This is due to molecules being polarized. If there are no losses in the polarization process, relative permittivity, known as the dielectric constant, is related to the refractive index, $n=(\varepsilon_r')^{1/2}$. In polarization, as discussed in the previous section, there is a decrease in the energy due to losses; this makes the relative permittivity a complex number. The decrease in the amplitude of wave can be due to the complex propagation factor, as shown in equation 27. The real component of the propagation factor describes the propagation characteristics, where the speed of the wavelength traveling through a sample is know ($S=\omega/k'$), and the imaginary component is related to the decrease in the amplitude. These relationships build the foundation to determine the complex refractive index.

$$k^* = k' - ik'' \qquad \text{Equation 27}$$

The complex refractive index is equal to N and is directly related to the complex propagation, as shown in equation 28 where k_0 is the propagation constant in a vacuum.

In this case, the complex refractive index can be related to the complex dielectric constant by $N=(\varepsilon^*)^{1/2}$.

$$N = \frac{1}{k_0}(k' - ik'') \qquad \text{Equation 28}$$

When light travels through a sample, some of the wave's energy is converted to other forms of energy. This conversion can be related to the type of polarization that occurs within the material as the wave travels through. For example, ionic polarization occurs when the wave that propagates through the sample causes the opposite charged ions to move in the opposite direction, which leads to the ions vibrating at the same frequency as the wave. This is known as lattice absorption and energy from the wave is lost by transferring to heat energy.

Another form of absorption is photon absorption that results in the creation of an electron-hole pair. For example, when an incident photon with a wavelength shorter than the upper cut off wavelength (λ_g) is penetrated through a sample, it becomes absorbed. Therefore, the intensity of the beam leaving the sample exponentially decreases, as shown in equation 29, where t is the thickness/distance the wavelength travels and α is the absorption coefficient. The absorption coefficient is a material property. This process of absorption leads to a decrease in the intensity of the incident beam that is observed when it leaves a sample.

$$I(t) = I_0 \exp(-\alpha t) \qquad \text{Equation 29}$$

The absorption coeficcent can be related to the imaginary component of the complex refractive index, K =k''/k_0. K is known as the extinction coefficient. Equation 30 shows the relationship between the extinction coefficient and the absorption coefficient , where λ is the vacuum wavelength.

$$K = \frac{\lambda}{4\pi}(\alpha) \qquad \text{Equation 30}$$

CHAPTER 2

MOTIVATION

Polymers are known for their versatility in properties; plastics such as polystyrene, polymethyl methacrylate or polycarbonate are known for their strength and flexible plastics, such as propylene and polyethylene, are known for their toughness. Polymers are not known for their electrical properties. When adding conductive fillers to the polymer, conductive polymer composites are formed and they have many advantages, including an increase in their electrical conductivity and/or their dielectric properties. For many applications, the unique properties of the composites make them technologically superior and cheaper than alternative materials.

To keep costs down in the production of conductive polymer composites, one wants to use the least amount of filler particles possible. One reason is because the filler is the more costly material and with increasing the filler particles, the cost of the composites increases. With greater amounts of filler, processing of the composites becomes difficult and the mechanical properties of the composite deteriorate, such as the strength and toughness. The main objective to producing conductive polymer composites is to decrease the amount of filler needed to form a continuous network. Studies have been done on different processing techniques along with various polymer filler combinations. In recent years, a new method to produce a segregated microstructure for conductive polymer composites has been introduced by our group at the Georgia Institute of Technology. To produce a segregated network, the filler particle and the polymer are

mechanically mixed, causing the filler to coat the outside of the polymer particles and form a continuous network throughout the composite.

The properties of the filler used in the composites directly correlate to the amount of filler needed. It has been observed that as the aspect ratio of the filler increases or the surface area increases, there is a decrease in the amount of filler needed to form a conductive composite. Turner noted that the larger the difference in the radius of the filler particles to polymer particles, the lower the percolation threshold. While many studies have investigated the use of carbon black as filler, none have evaluated the effect of various types of carbon fillers using the same polymer matrix and fabrication method. This thesis will look at various carbon fillers (CF) and how their properties affect the electrical and optical properties of conductive polymer composites fabricated using of a polymethyl methacrylate (PMMA) as the matrix.

The properties that will be examined are the electrical resistivity of the composites to determine the percolation threshold, the dielectric properties of the composites, the influence that frequency has on the conductivity, the optical transmittance and the absorbance of the composites.

CHAPTER 3

EXPERIMENTAL SECTION

3.1 PREPARATION OF THE SAMPLES

The samples being examined for this work were all produced with the same method and consisted of the same polymer matrix, Buehler©; PMMA, a transoptic powder with a size distribution of 25-100 μm [4, 6]. Mechanical mixing was used to allow for the coating of the PMMA by the carbon nano-particles. To mix these powders, 20 grams of PMMA was measured out and various amounts of filler were added based on the desired filler content (phr). The phr stands for parts per hundred and is another way to express a percentage based on weight. The powders were blended in a mixer for 10 minutes, alternating between 5 seconds on, 5 seconds off. This procedure prevented the over heating of the PMMA. Various amounts of carbon filler were added to the PMMA to produce compositions of powder ranging from phrs of 0.01 to 5 in order to compare the different carbon fillers.

To form the test discs, roughly 2 grams of the mechanically blended mixture was measured out and hot pressed at 170^{o}C using the Struers ProntoPress-2 . The samples were pressed for 2 minutes at 8 kN, directly followed by 13 minutes at 20 kN, and concluded with a 5 minute cool down. The resulting discs had a diameter of roughly 31.6 mm and a thickness of approximately 2.2 mm.

3.2 VARIOUS FILLERS

3.2.1 Carbon Blacks

Carbon Blacks were supplied by Columbian Chemicals Company (CCC) or by Superior Graphite (SG). The CB's examined from CCC were N-550 and N-772; the average particle size of these two CB's was around 50 nm [56]. Pureblack (PB) was supplied by SG. Even though there was not an average diameter stated on the material data sheet, the aggregate size was listed as having 10% of the aggregates less than 0.1 microns, 50% less than 0.3 microns and 85% less than 0.85 microns [57]. With the PB having a more uniform size distribution, this should lead to a more defined percolation threshold value. Table 3-1 shows the characteristics, such as oil absorption, iodine number and static thick surface area (STSA), highlighted for each of the fillers used. When comparing the N-550 and N-772, it can be seen that the oil absorption for the N-550 is greater. Since oil absorption has a direct correlation to the amount of branching that is present [56], the higher the oil absorption, the more branching the CB has, and therefore, a lower the percolation threshold is expected.

Table 3-1 Various CB types that are being investigated and their different properties as reported by manufacturers

Type of CB	**Oil absorption (cc/100g)**	**Iodine number (mg/g)**	**STSA (static thick surface area) (m^2/g)**	**Pore Density (kg/m^3)**	**Average Particle Size**	
N-550	121	43	38	360	~50 nm	[56]
N-772	65	30	30	520	~50 nm	[56]
Pureblack	Acetone Absorption 290		45	70	Aggregate Size Distribution D10 0.1 μm D50 0.3 μm D90 0.85 μm	[57]

3.2.2 Short Multi-wall Carbon Nano-tubes

Short multi-wall carbon nano-tubes (MWCN) were purchased from Cheap Tubes Inc. The MWCN have an outside diameter ranging from 8-15 nm, an inside diameter ranging from 3-5 nm, and a length between 0.5-2.0 μm. The batch purchased had purity greater than 95 wt% and ash content of less than 1.5 wt%. The surface area of the MWCN is 233 m^2/g, which is much larger than any of the CBs' surface area [58].

3.3 Experimental measurements

3.3.1 Powder Analysis

The JEOL 100CX transmission electron microscope (TEM) was used to analyze the various fillers. The powders were mixed with acetone and placed in the sonicator to break up the agglomerated particles. A small amount of the mixture was placed on a Lacey Formvar/Carbon 200 mesh copper grid that was purchased from Ted Pella, Inc. The acetone evaporated away and the dry powder was left on the grid allowing the sample to be tested in the TEM. The applied voltage was 100kV when examining the powders.

3.3.2 Impedance Spectroscopy

In order to perform these measurements, each composite had to be coated with SEM high-purity silver paint, which acted as a current collector. The samples were tested initially using the Solartron© Impedance-Grain Phase Analyzer. The frequency range for the machine is 0.1 mHz to 10 MHz. The conductive samples were run in a range of 0.01 Hz to 10 MHz, while the extremely insulating samples needed to go to frequencies as low as 0.1 mHz. The machine was set up to take readings at 10 points per decade, with the input ac voltage being 0.1 and no dc voltage applied.

The samples were run through the machine and the values that were measured were the real and imaginary parts of impedance, Z' and Z", as a function of frequency. The experimental setup is shown in figure 3.1. An image of the screen display for the complex and spectrum impedance plot is shown in figure 3.2. Conductivity, dielectric properties and resistivity were all calculated based on the impedance data.

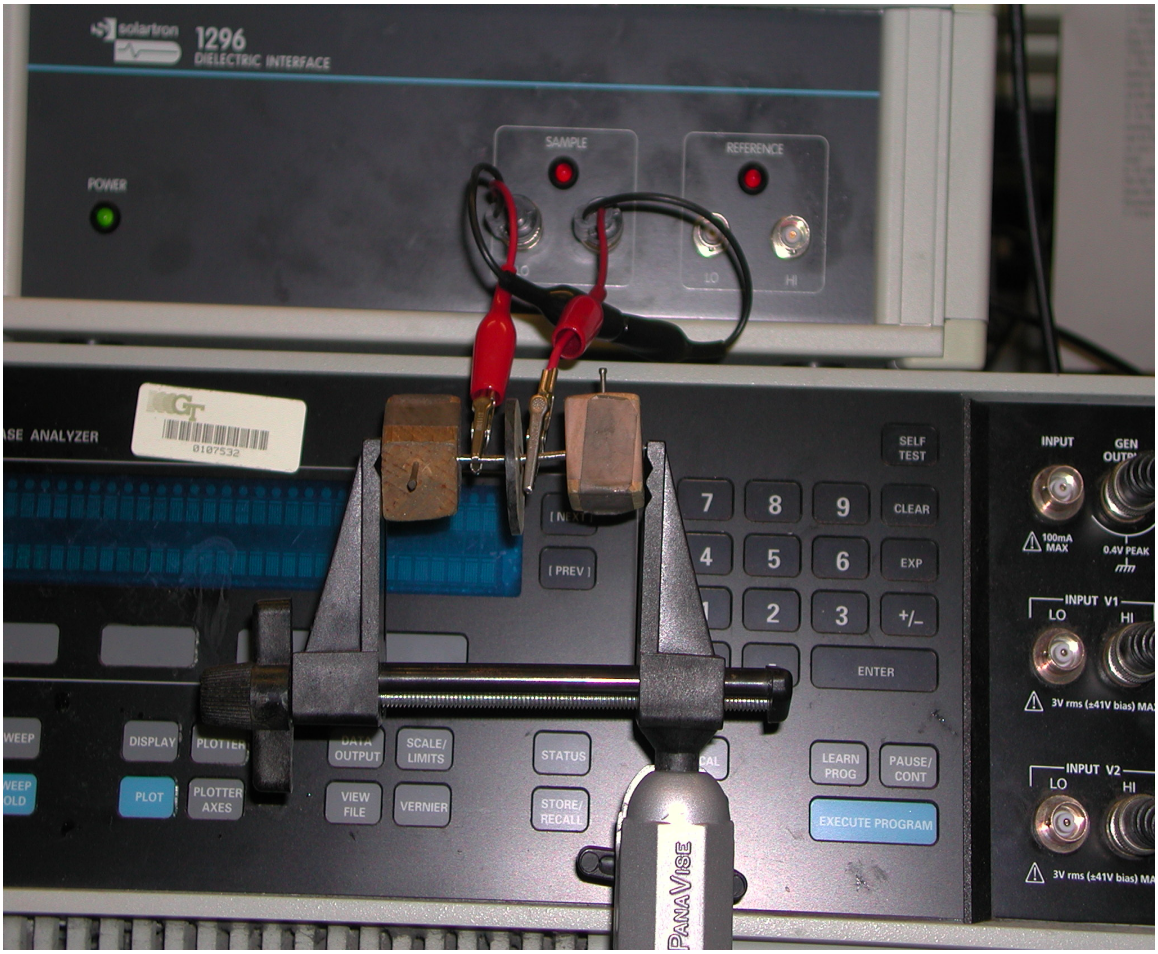

Figure 3.1 Shows the setup and fixture that was used to test the samples

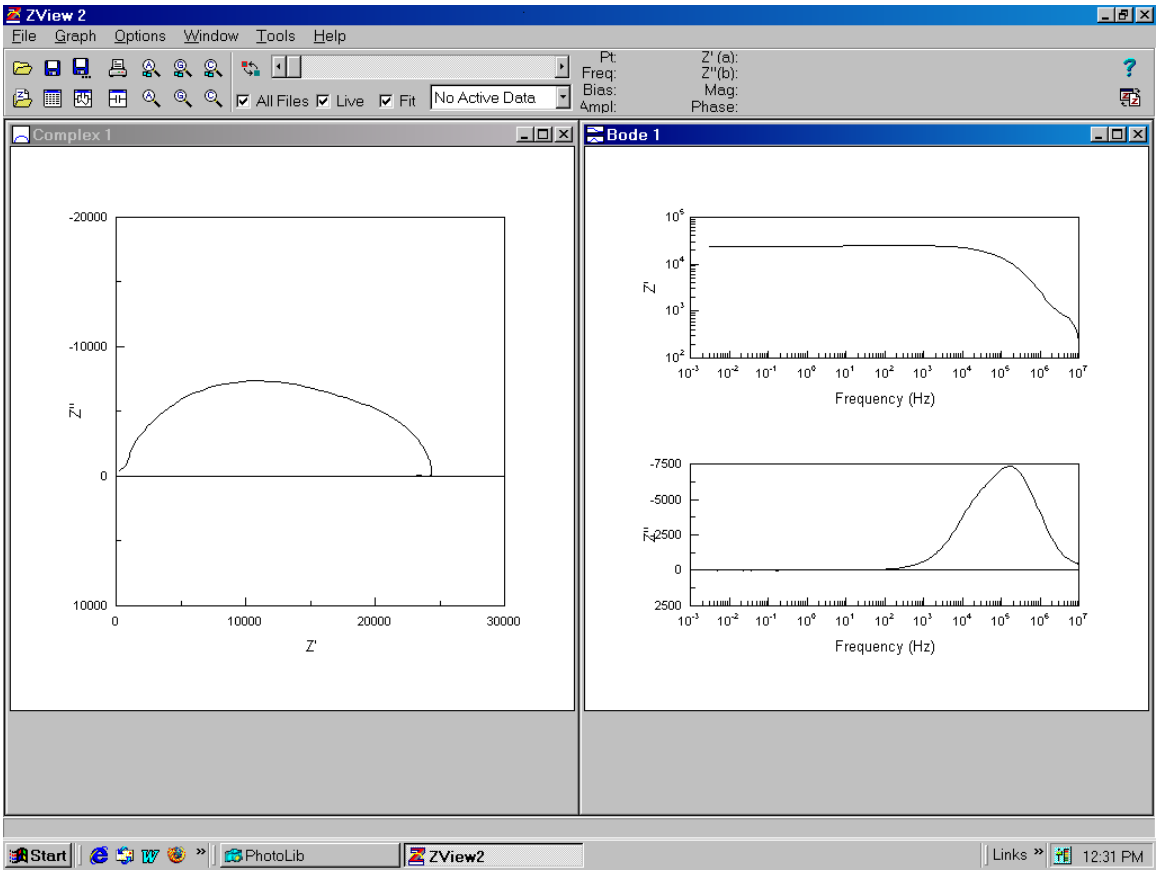

Figure 3.2 Screen display, containing the complex and spectrum plane plots for impedance measurements, that was used to evaluate the data

Since the Solartron does not give reliable data in the frequency range above 100 kHz, for the more conducting samples, the QuadTech 1910 Inductance Analyzer was used for samples with a resistivity on the order of 10^3 ohms. The sample setup was the same, except the tests were run starting at 10 MHz and running down to 10 Hz. Readings were taken at a rate of 20 points per decade with a one second delay for each reading. The values measured by the QuadTech are the complex impedance and the phase as a

function of frequency. This data was used to calculate the conductivity of the higher conducting samples.

For extremely insulating samples at high frequencies, the Solartron does not give accurate data. The Hewlett Packard 4192A LF Impedance Analyzer (HP) was used for the samples with resistivity above 10^{13} ohms. The frequency range of this machine is 5 Hz to 13 MHz, but measurements were made in the frequency range between 5 Hz and 10MHz. With the HP, the frequency step is in a logarithmic scale. Again, the sample setup was the same as for the Solartron and the QuadTech. The HP measured the real and imaginary parts of impedance, Z' and Z", as a function of frequency and the conductivity of the samples was calculated. This is shown in equations 31 and 32, where Y' is the real part of the admittance, t is the thickness of the sample and A is the area of the sample.

$$Y' = (Z')/(Z'^2 + Z"^2) \qquad \text{Equation 31}$$

$$\sigma = (Y'*t)/A \qquad \text{Equation 32}$$

3.3.3 Microstructure Analysis

The LEO 1530 scanning electron microscope (SEM) was used to examine the fracture surface of sample composites containing N-550 and MWCN. The samples were initially fractured and placed on test stands. To fully evaluate the samples, the fracture surface needed to have a conductive paint on it and the samples were sputter coated with gold. The images were acquired at an accelerating voltage of 10kV. The images show if

the fracture surface was representative of intra or inter granular fracture along the segregated microstructure region [4, 6, 8]. Transmission optical images were also taken, which allowed viewing of the segregated microstructure present in the composites.

3.3.4 Optical Measurements

Absorbance measurements were made on composites containing N-550 and MWCN with the use of a Cary 5000, located at Oak Ridge National Laboratory. Samples were specifically made for the optical measurements in the same manner as stated above, but the weights of these samples were ~0.5g. This was to allow for the optimal number of readings to be made since the 2g samples are mostly opaque in color. Wavelengths ranging from 180-850 nm were sent through the sample to assure reliable data was obtained for the visible light spectrum. The percent of absorbance was measured as a function of wavelength. Absorbance above 4.5% was considered unreliable.

CHAPTER 4

RESULTS

4.1 TEM IMAGES

Figure 4.1 shows the TEM images of all four powders being examined. The image in Figure 4.1 (a) is MWCN, which has distinctively different characteristics than the other images. The MWCN display rod-like characteristics, with minimal agglomeration. The CB N-550, N-772 and PB are shown in figure 4.1 (b), (c), (d) respectively. N-550 and N-772 have a similar behavior of agglomerating together and show a wider size range distribution than the PB. The PB particles also appear to have a smaller average particle size than both the N-550 and N-772.

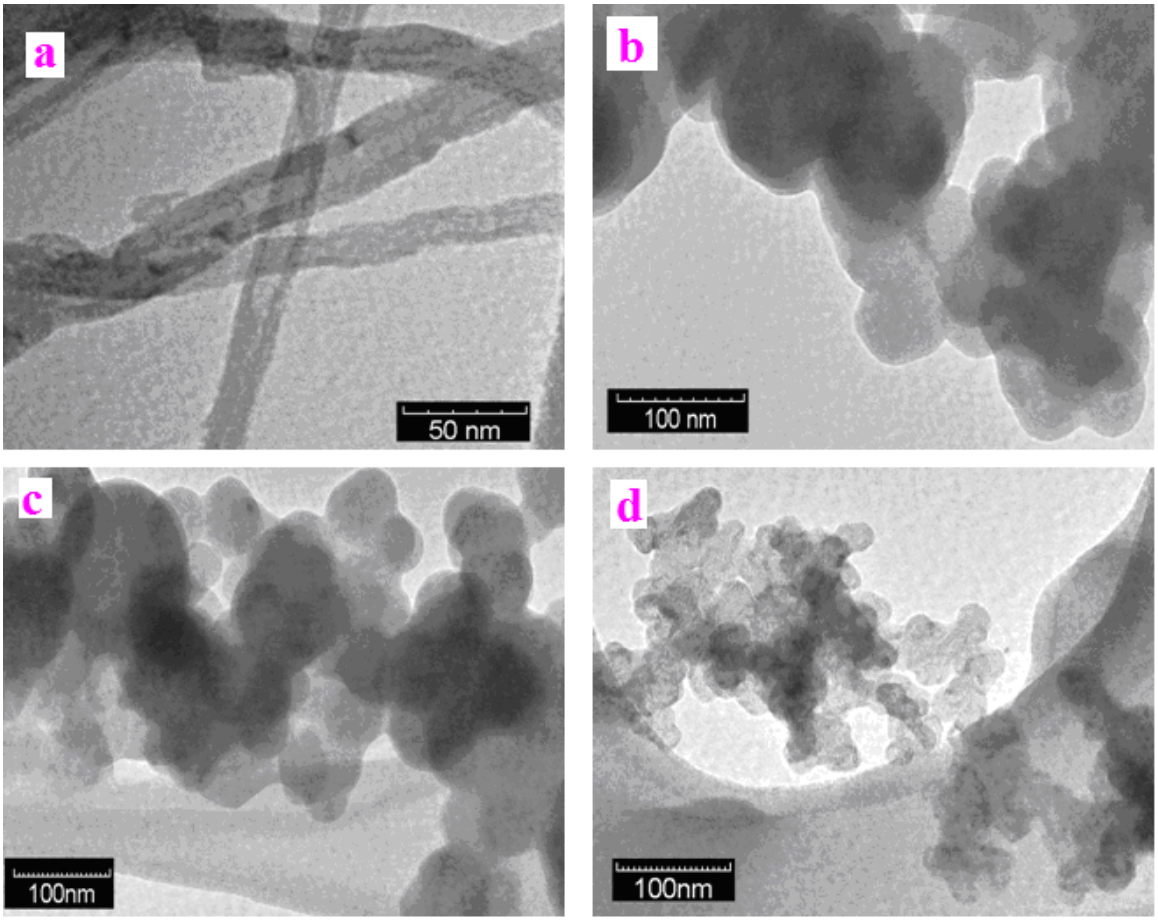

Figure 4.1 TEM images of powders: (a) MWCN, (b) N-550, (c) N-772, and (d) Pureblack.

4.2 IMPEDANCE MEASUREMENTS

Impedance measurements were taken to determine the percolation threshold, conductivity, and dielectric constants of the composites. The interpretation of the data and formulas used to obtain these properties is discussed in sections 4.2.1- 4.2.3.

4.2.1 Percolation Threshold

The resistance of the samples were calculated using the Nyquist plots (-Z' vs. Z"), as discussed in section 1.2.2.1. Figure 4.2 shows the complex impedance plots for N-550 samples with varying phr. For the sample with a phr of 0.4, figure 4.2 has an arrow pointing to the resistance of the sample where the semicircle intersects the real axis. As the amount of filler decreases, the size of the semicircle increases. In the figure, the full semicircle for samples with a phr of 0.4 and 0.5 can be seen. The semicircle for a sample with a phr of 0.6 is too small and appears as a dot; the semicircles for samples with a phr of 0.3 and 0.2 are larger and only the initial portion of the semicircle can be viewed at that scale.

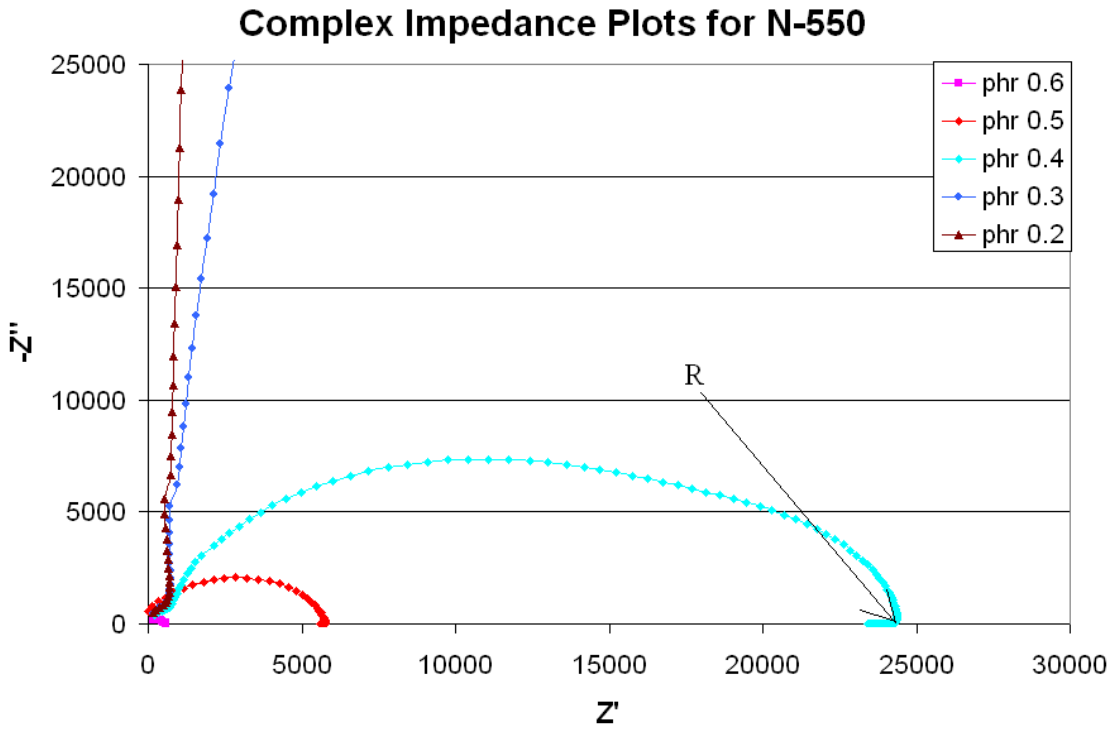

Figure 4.2 Shows the complex impedance plot for PMMA/CB N-550 samples as a function of phr and demonstrates how the resistances of the samples were found.

Once the resistance can be determined, conductivity (σ) can be calculated, as shown in equation 33 [48, 49]. The resistivity of the sample is the inverse of the conductivity and is shown in equation 34 [48, 41]. The percolation threshold curve can be formed with this data [1-13].

$$\sigma = \frac{t}{A^* R} \qquad \text{Equation 33}$$

$$\rho = \frac{1}{\sigma} \qquad \text{Equation 34}$$

Once the resistivities of the samples were found, the percolation threshold curves for all of the samples could be obtained. Figure 4.3 shows a comparison between all four of the filler's percolation thresholds in the form of log(ρ) versus phr. Each data point shown represents the average of at least three different samples. In some cases the standard deviation was so small that error bars can barely be seen; this occurs most often in the region after the sample is fully percolated. At lower phrs, the error bars can be greater; this is due to the samples being extremely insulating and the data obtained was noisy. The equivalent circuit had to be applied to calculate a best fit semicircle to determine the resistance of the sample. Notice, MWCN has the lowest percolation threshold, while the N-772 composites have the highest percolation threshold.

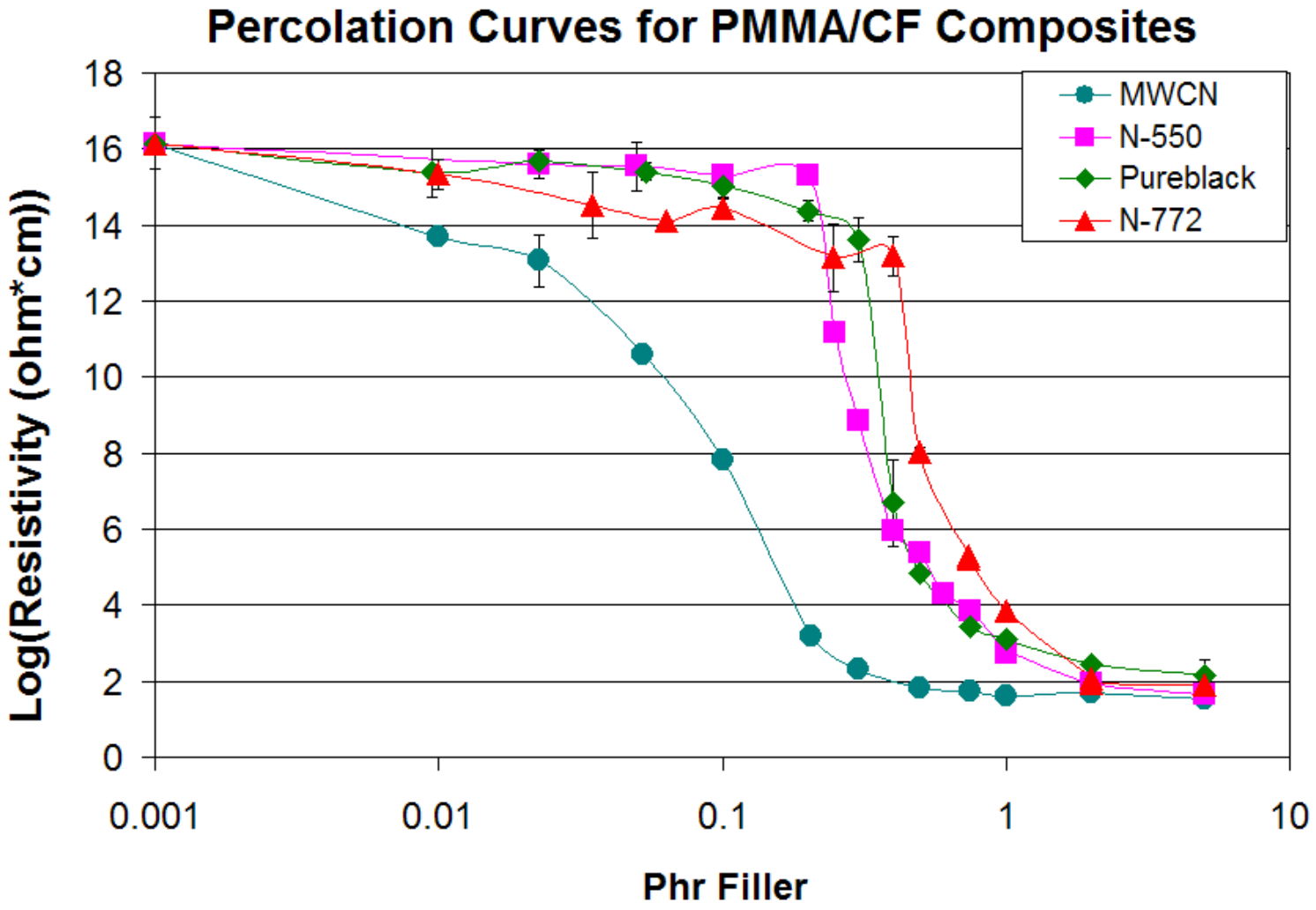

Figure 4.3 Comparison of resistivity vs. phr for composites containing MWCN, N-550, PB and N-772 all made by the same method

To further understand how to interpret the data obtained from the Solartron, there are trends that conductive and insulating samples follow. Figure 4.4 shows the complex impedance and admittance plots for a sample of N-550 containing 2 phr, which is above the percolation threshold. Both the N-550 and the N-772 had a sample which displayed both conductive and insulating behaviors in its complex impedance and admittance plot. Figure 4.5 shows the complex plots for N-550 with a phr of 0.74, which displays this behavior. The insulating and conductive behavior for N-772 occurred at a phr of 0.75, which is roughly the same phr as for the N-550. When dealing with the more insulating samples, especially samples before the onset of percolation, the machine did not go to low enough frequencies to produce a whole semicircle in the complex impedance plot. This is shown in figure 4.6 (a) for the N-550 composite with a phr of 0.2 where the formation of the semicircle is occurring. Figure 4.6 (b) shows the corresponding complex admittance plot [28].

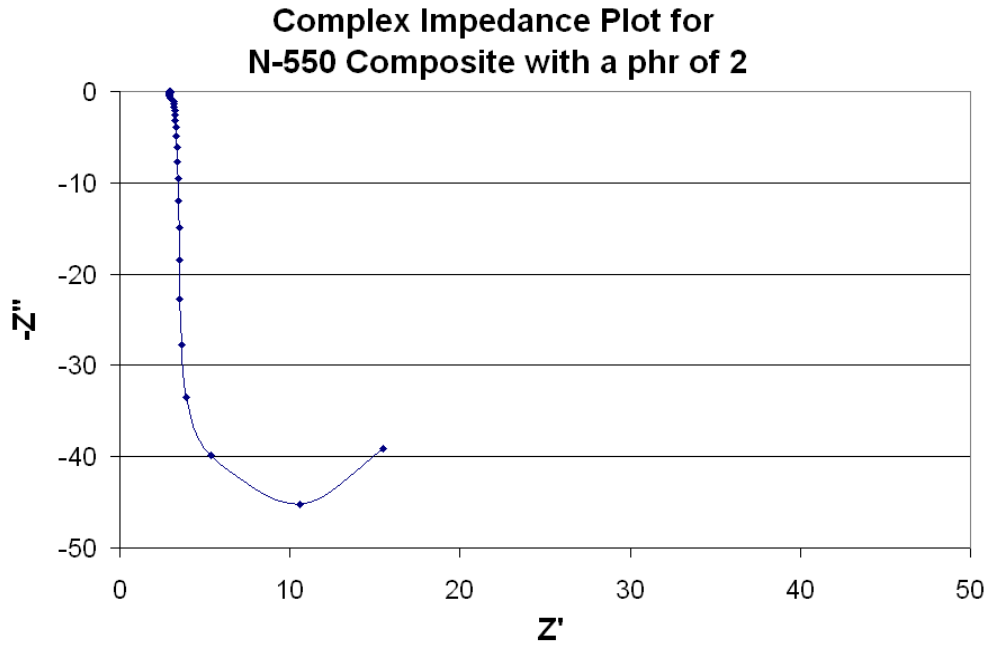

(a)

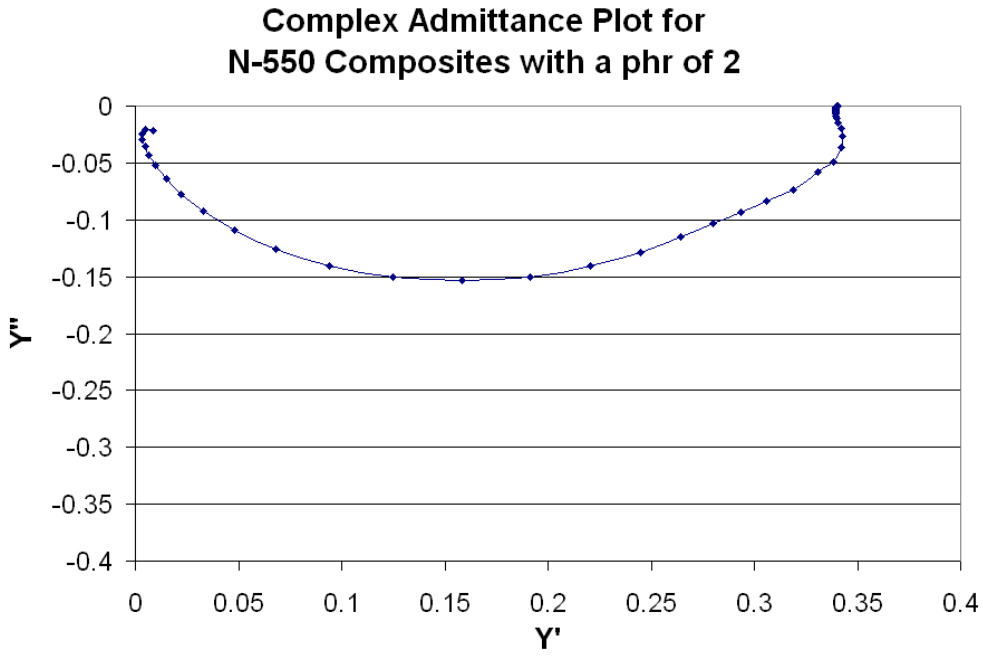

(b)

Figure 4.4 Represents complex plots for a conducting sample of PMMA/CB N-550 composites with a phr of 2 (a) Complex impedance, (b) Complex admittance

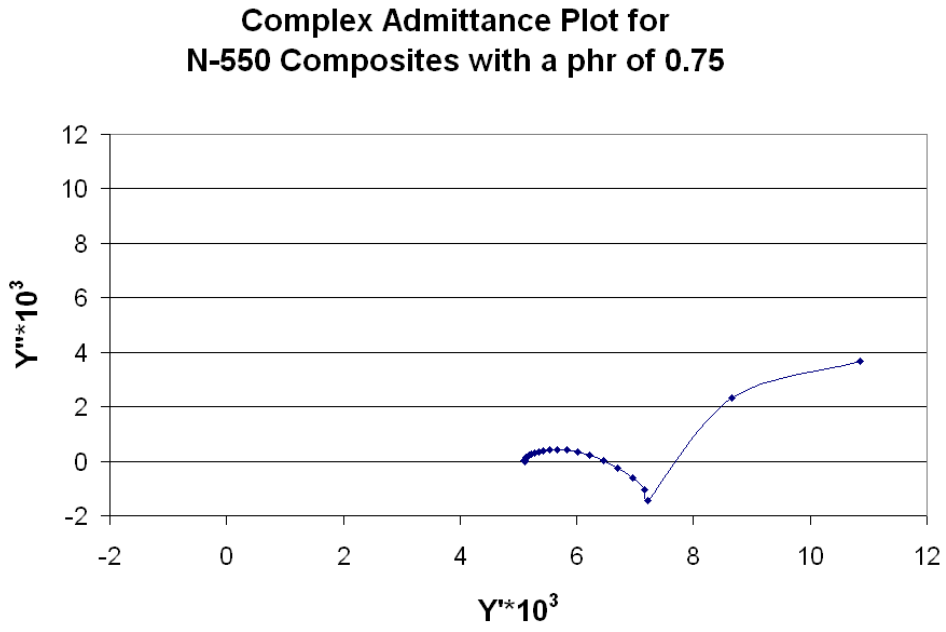

(a)

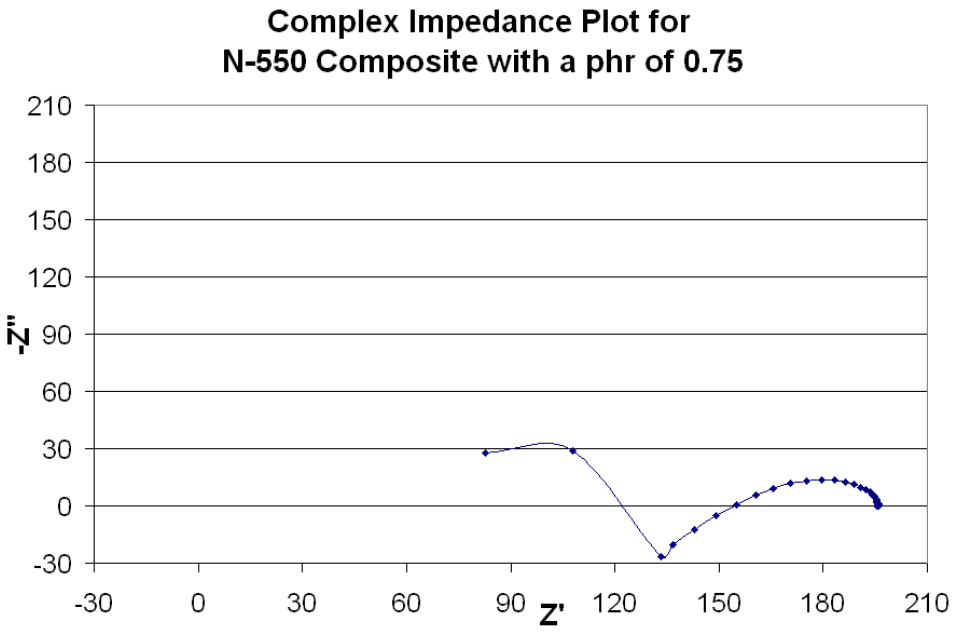

(b)

Figure 4.5 Represents complex plots for PMMA/CB N-550 sample with a phr of 0.75 (a) Complex impedance, (b) Complex admittance.

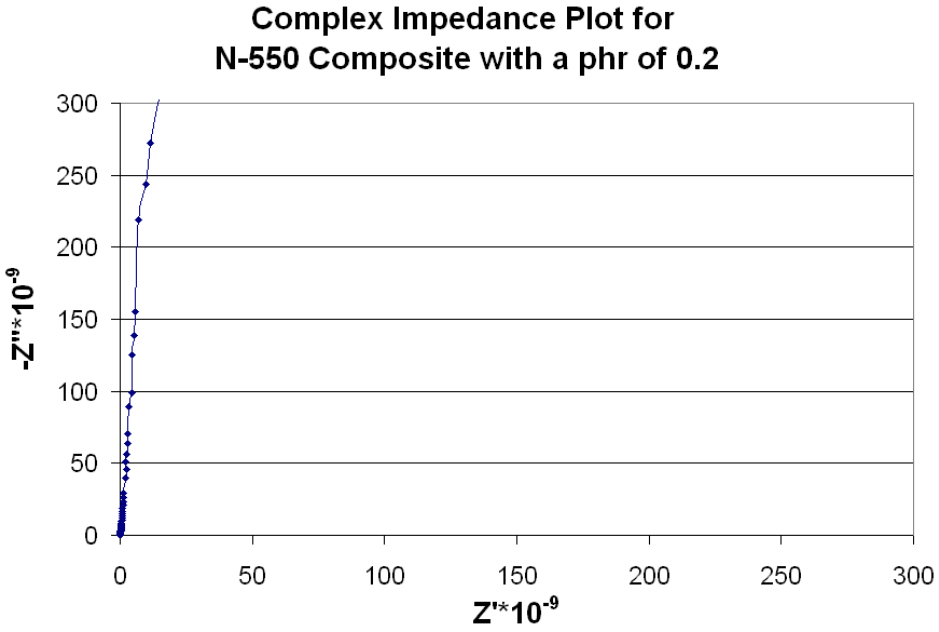

(a)

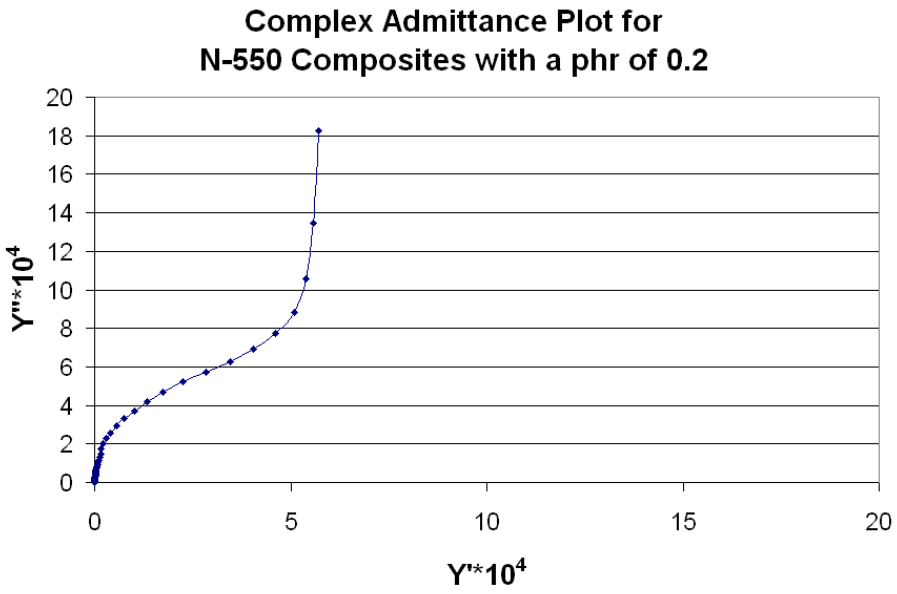

(b)

Figure 4.6 Represents complex plots for an insulating sample of N-550 (a) Complex impedance, (b) Complex admittance containing 0.2 phr.

4.2.2 AC Conductivity

The AC conductivity of a material is found through the use of impedance measurements. The conductivity is directly related to the admittance of the sample and was discussed in previous sections. The AC conductivity versus frequency plot for all N-550 samples measured is shown in figure 4.7. For highly conductive samples, the conductivity is constant over a large range of frequencies. As the samples become more insulating, initially the conductivity of the sample displays a plateau region at low frequencies until the critical frequency is reached. Afterwards, the sample's conductivity increases with increasing frequency. For the highly insulating samples, there was not a plateau region, just an increase in the conductivity with increasing frequency [4].

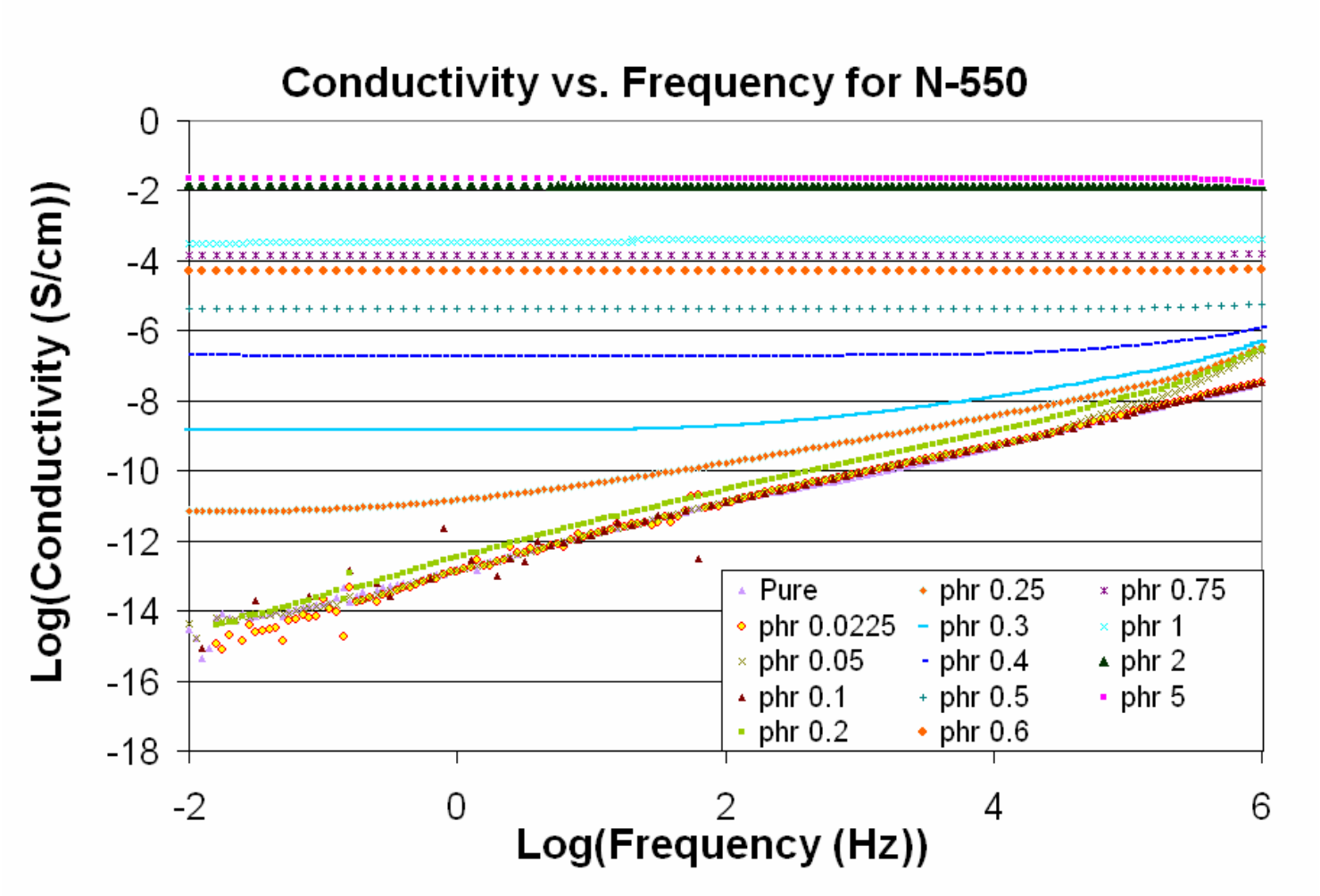

Figure 4.7 Conductivity vs. frequency for PMMA filled with CB N-550

The conductivities for all of the fillers displayed the same behavior as the N-550 filler shown in the previous graphs, and showed a slight difference in conductivities when the data was obtained from different machines. The combined conductivity vs. frequency graphs for the composites containing N-772, PB and MWCN are shown in figures 4.8, 4.9 and 4.10 respectively. For the more conductive samples, the Solartron did not give accurate data, and a drop in the conductivity was seen at higher frequencies. The HP or the Quadtech was used to gather further information about the composites (refer back to experimental section) and get more accurate measurements of the ac conductivity as a function of frequency. The slight differences in conductivities for a given phr for a sample can be accounted for in the use of different machines.

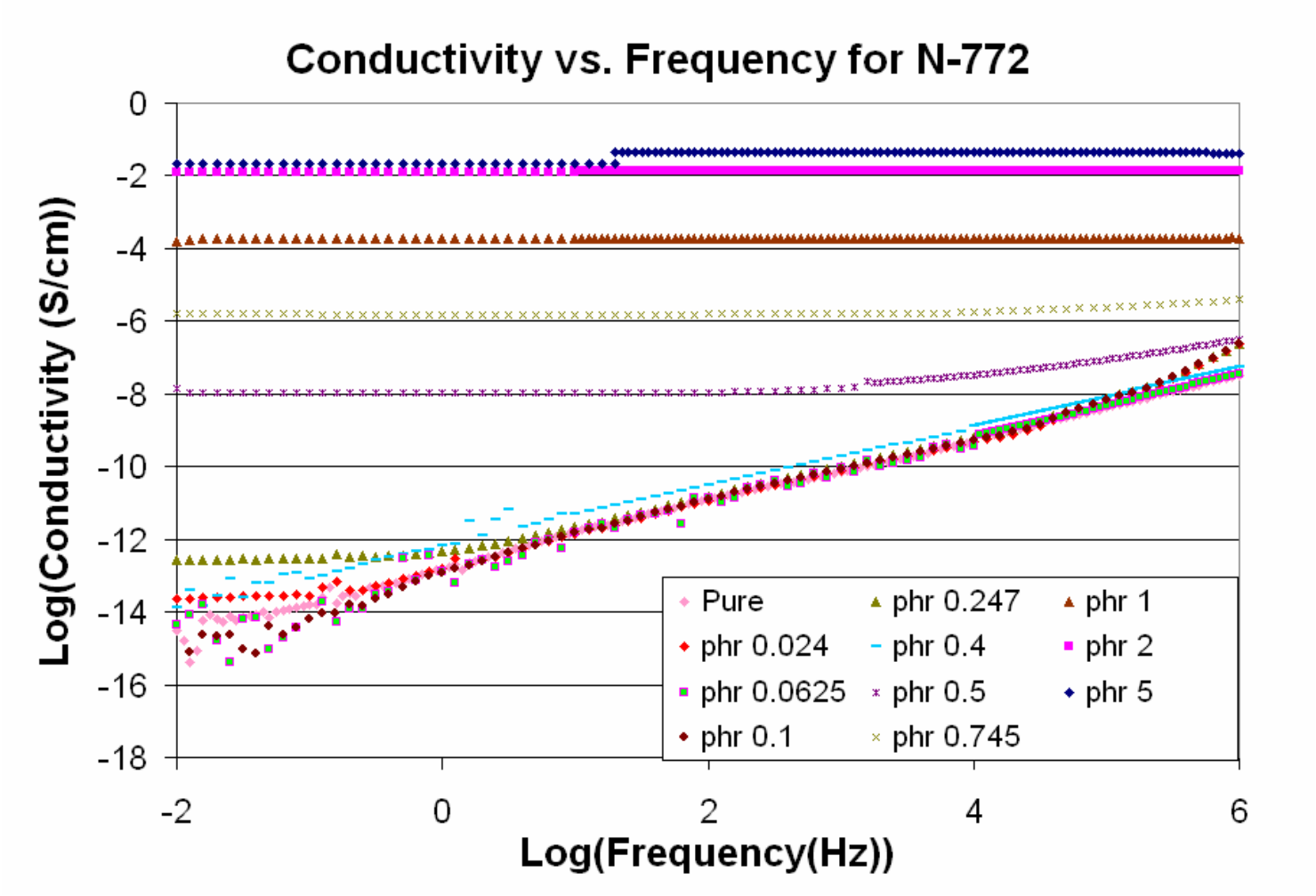

Figure 4.8 Conductivity vs. frequency for PMMA filled with CB N-772

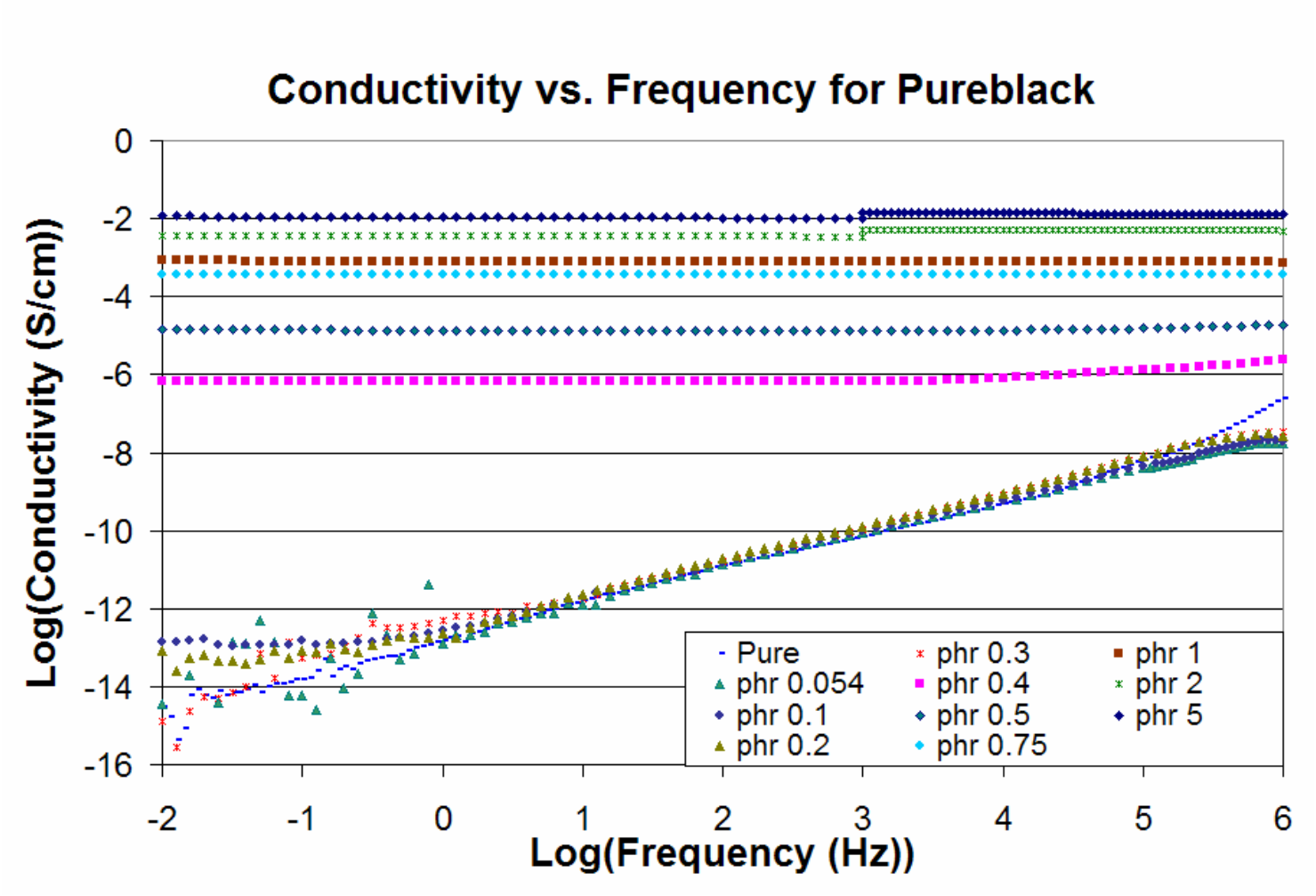

Figure 4.9 Conductivity vs. frequency for PMMA filled with CB PB

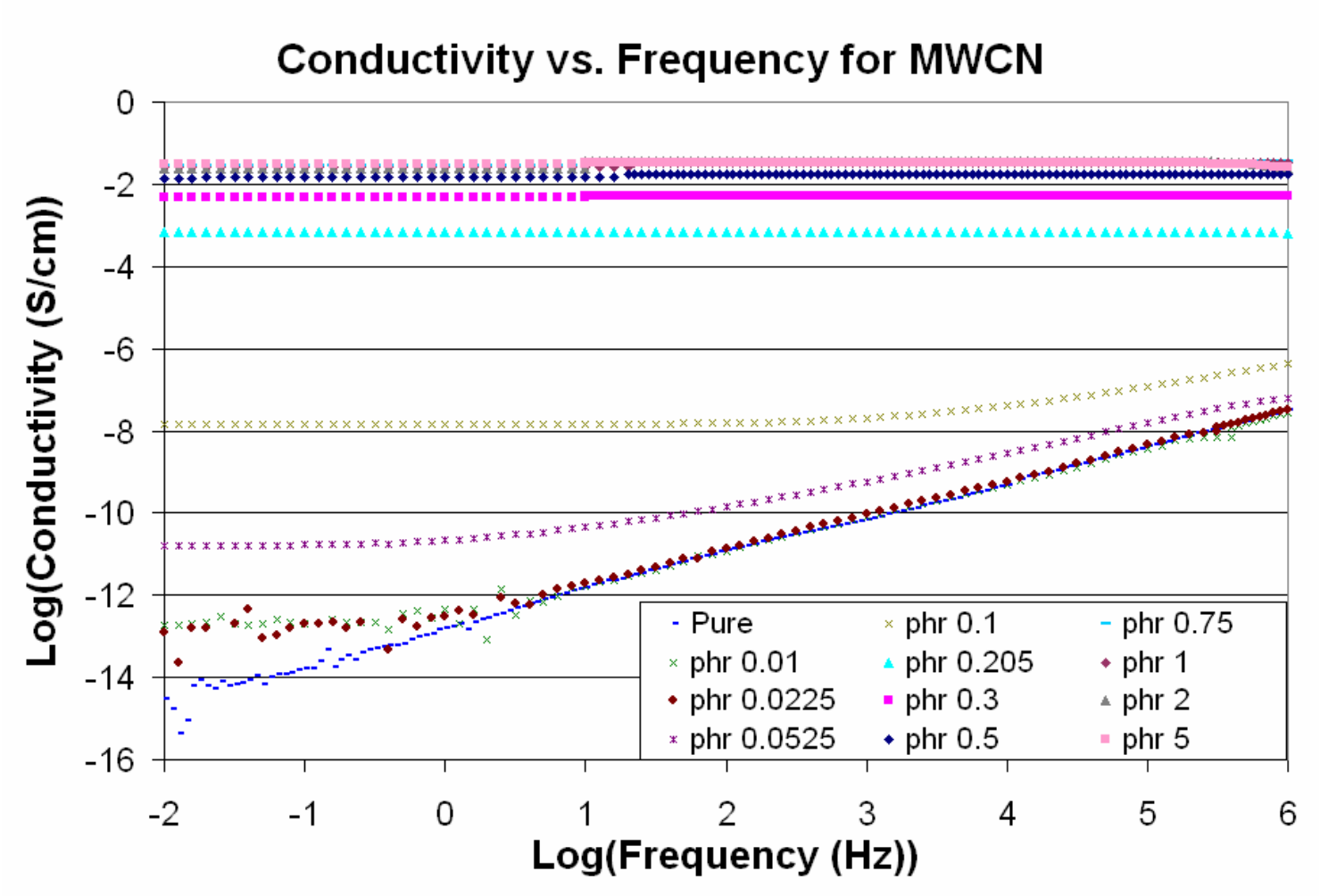

Figure 4.10 Conductivity vs. frequency for PMMA filled with MWCN

4.2.3 Dielectric Properties

The dielectric constant of the composites varies with frequency. The dielectric constant of the material should increase as the filler content increases. This is shown in figure 4.11, which graphs the log (dielectric constant) versus frequency for N-550 composites. At higher phrs, the dielectric constant at high frequencies was negative, and was unable to be graphed on a log scale. This is because the instruments calculated a negative capacitance for the composites, leading to the conclusion that the samples had a resistance lower than the range of the instrument. The same phenomenon has been observed with PMMA/graphite composites [22]. M.A. Seo, J.W. Lett, et al. noted that the real part of the dielectric constant for samples with a graphite content of 35.7% was negative from 0.1 THz to 0.3 THz. They tested their samples in the frequency range of 0.1 THz-1.6 THz [22]. The graph for the real part of the dielectric constant versus frequency for their samples was shown in figure 1.20. When plotting the absolute value of the dielectric, the data lines up, as if it forms a continuous curve; this is shown in figure 4.12 where the log of the absolute value of the dielectric constant versus frequency is plotted. In this graph, the dielectric constant levels off as the frequency increases.

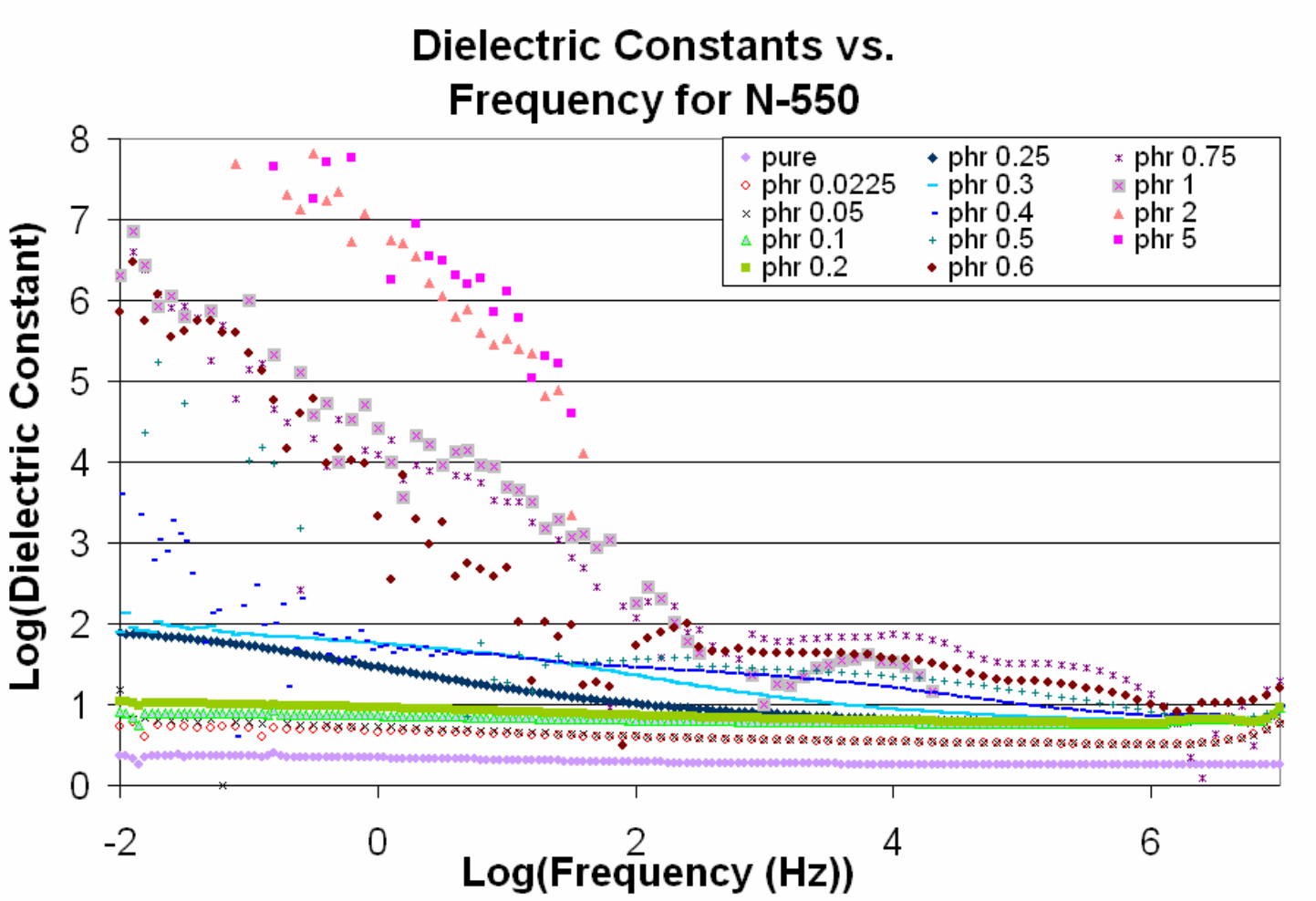

Figure 4.11 Dielectric constant vs. frequency for PMMA filled with CB N-550, showing that at high phrs, the dielectric constant contained negative values

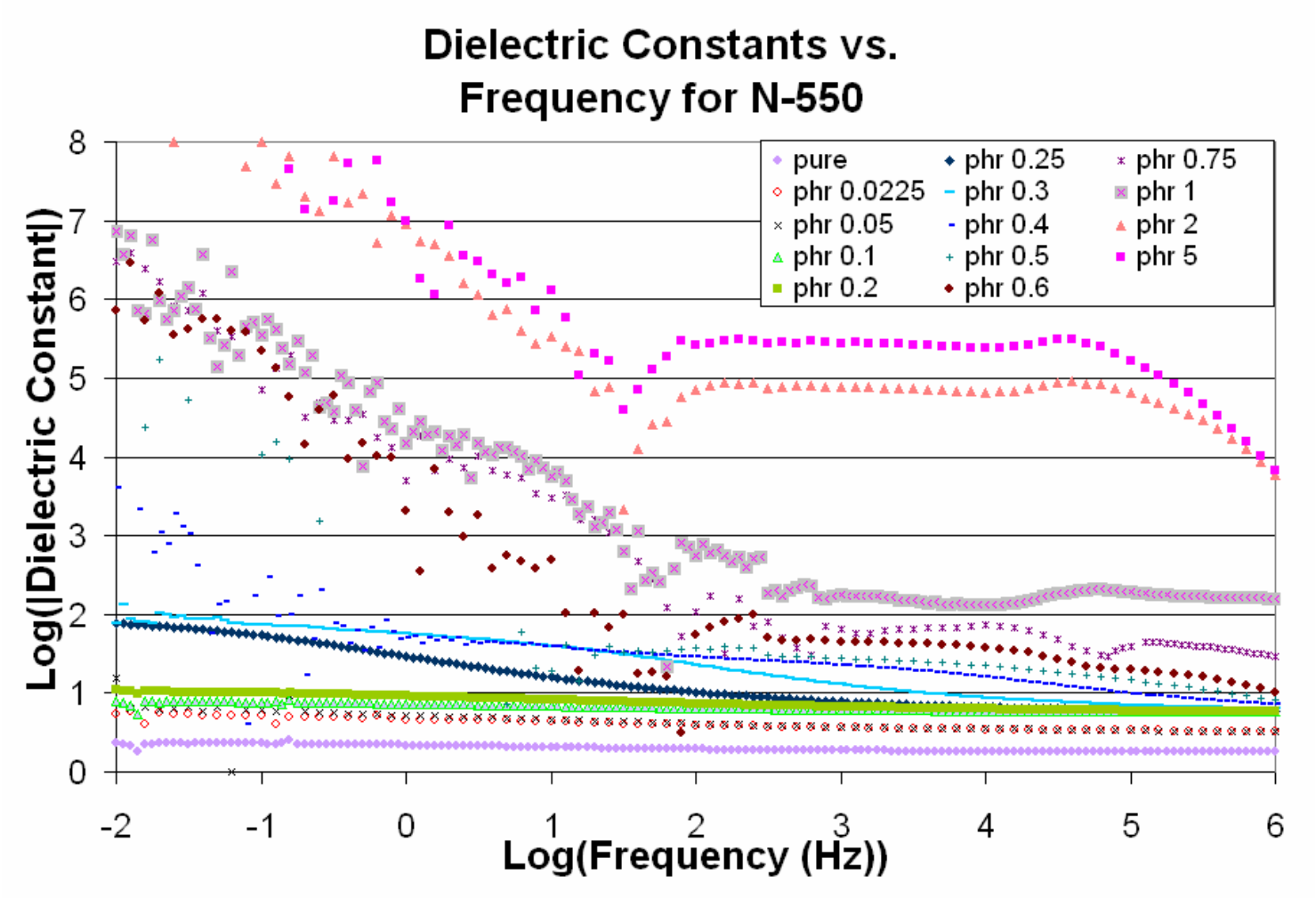

Figure 4.12 Absolute value of dielectric constant vs. frequency for PMMA filled with CB N-550

The log of the absolute values of the dielectric constant vs. frequency for N-772, PB and MWCN are shown in figures 4.13, 4.14 and 4.15 respectively. As the frequency increases, there is a decrease in the dielectric constant, until it levels off. As the phr content decreases, the dielectric constant decreases. Also, the dielectric constant is not as frequency dependent as the phr decreases**.** These behaviors were displayed for all of the composites.

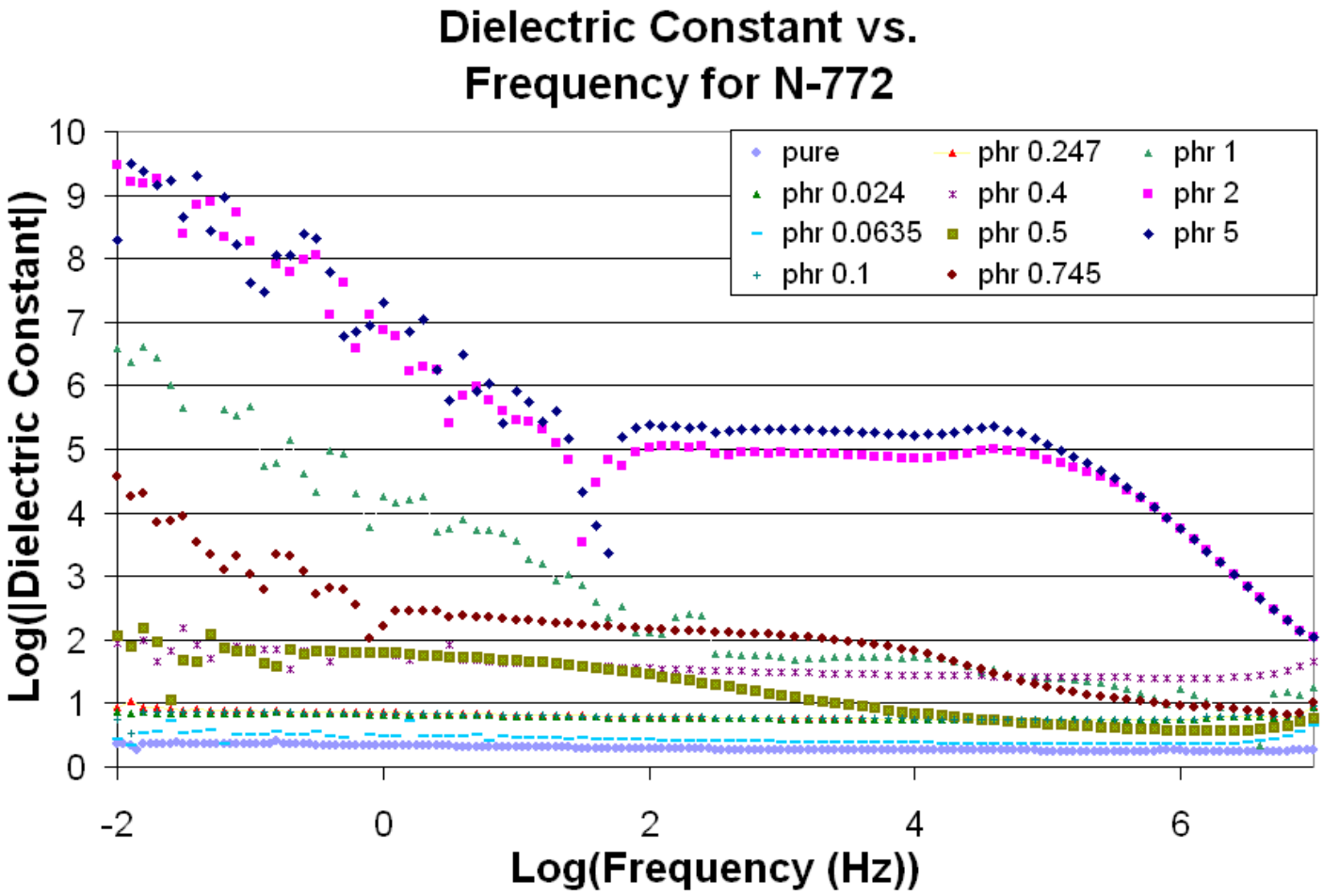

Figure 4.13 Absolute value of dielectric constant vs. frequency for PMMA filled with CB N-772

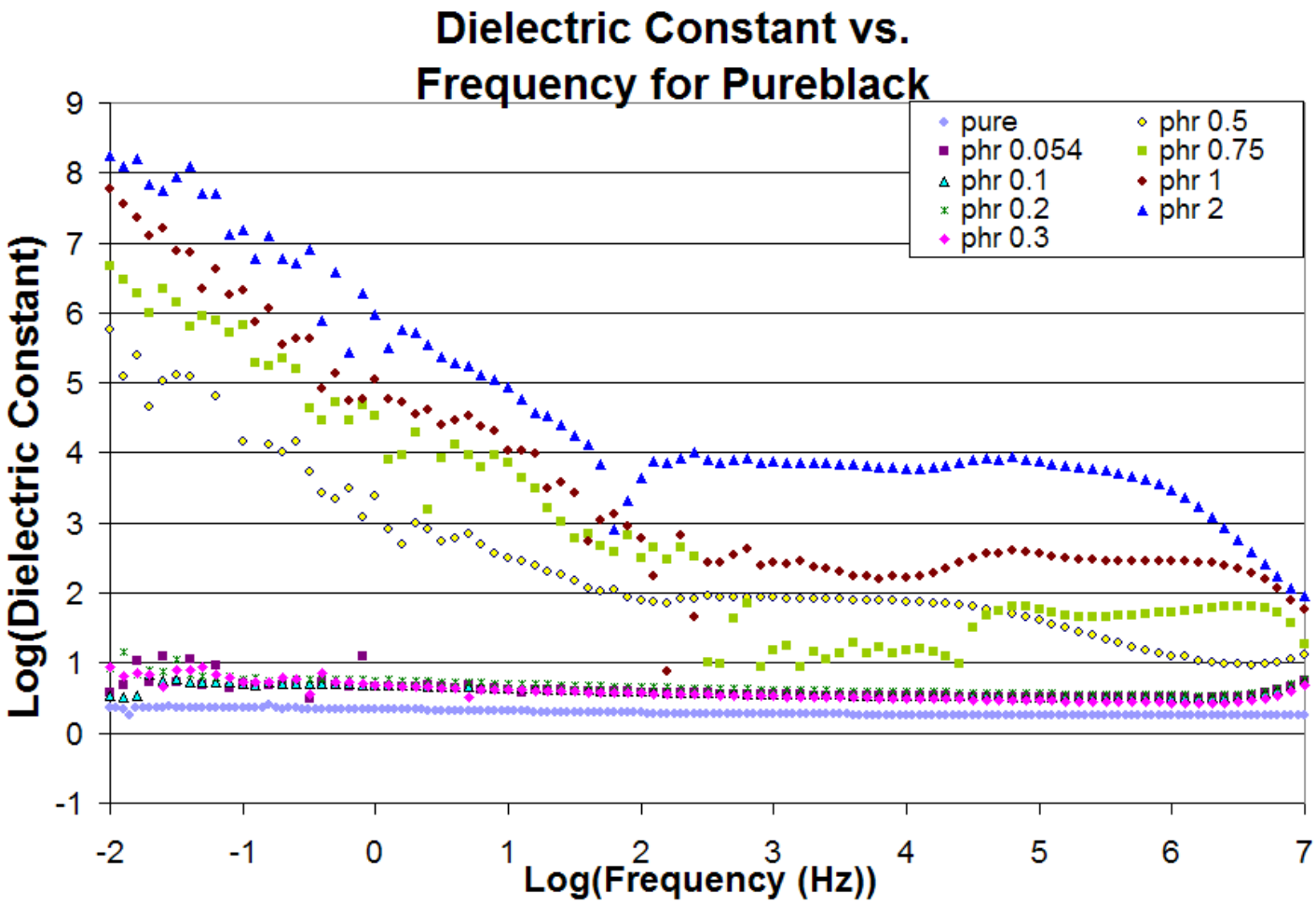

Figure 4.14 Absolute value of dielectric constant vs. frequency for PMMA filled with CB PB

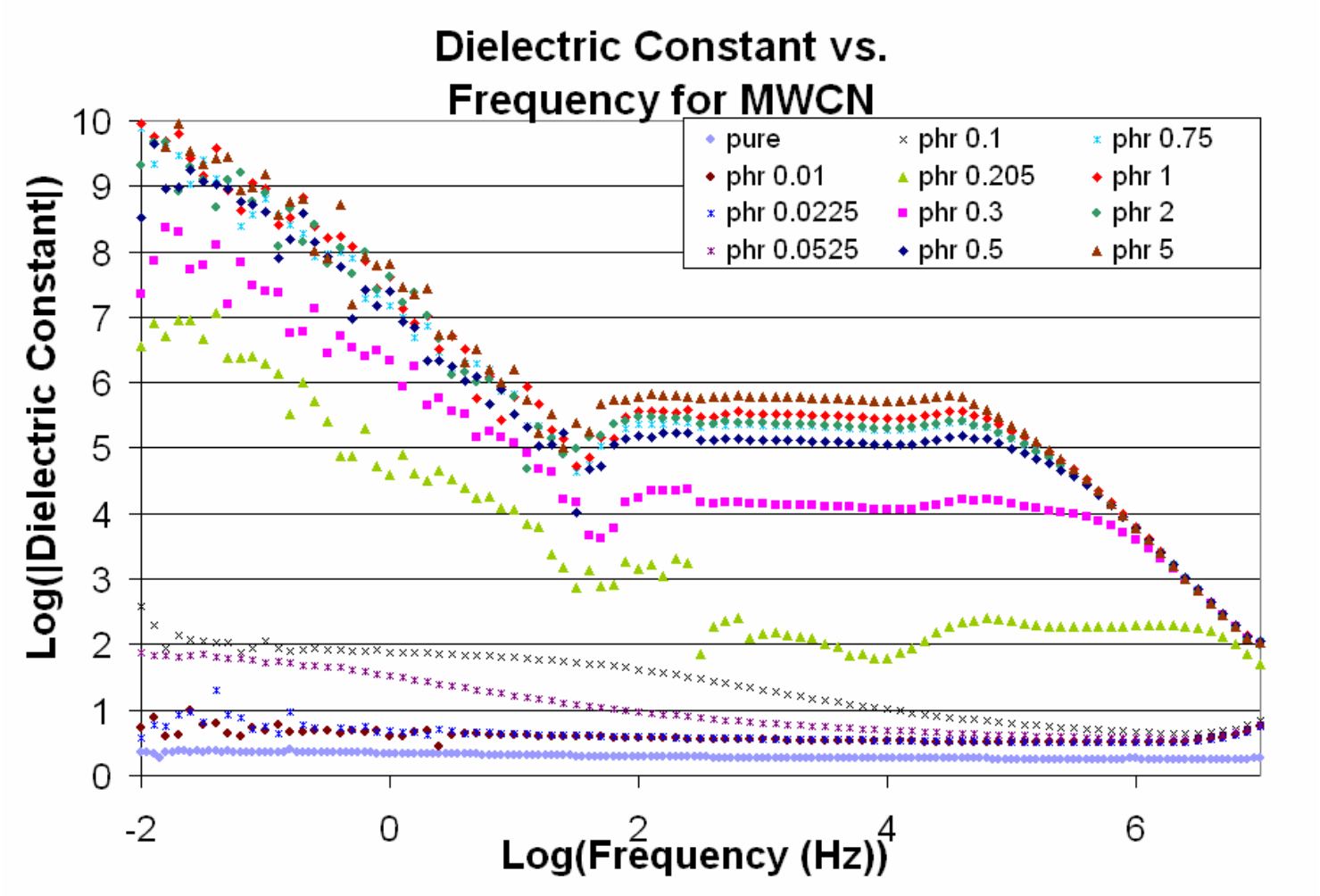

Figure 4.15 Absolute value of dielectric constant vs. frequency for PMMA filled with MWCN

4.3 MICROSTRUCTURE EVALUATION

SEM images were taken to fully understand the microstructure of the composites and the type of fracture that the composite undergoes. Figure 4.16 shows a SEM micrograph of pure PMMA. Note: the sample undergoes intragranular fracture. Figures 4.17 represent SEM micrographs for N-550 samples at phrs of 0.05, 0.2, 0.4 and 0.6 respectively. Figures 4.18 correspond to SEM images for MWCN samples with phrs of 0.05, 0.1, 0.2 and 0.75 respectively.

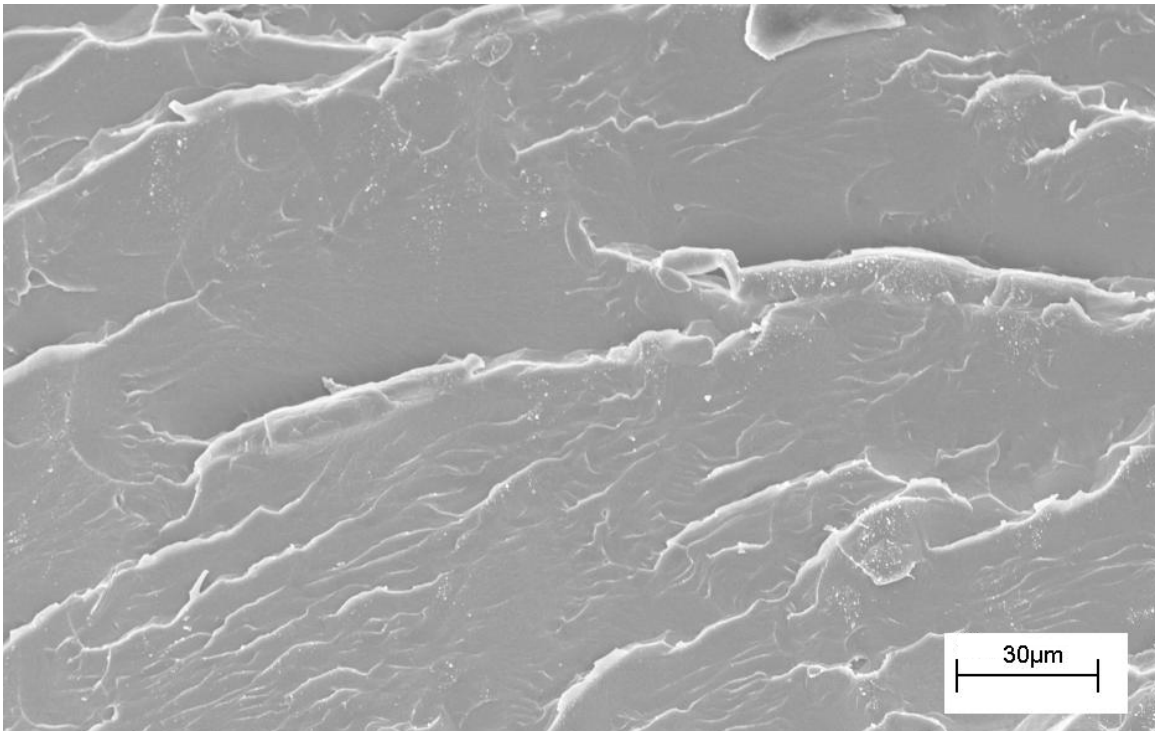

Figure 4.16 SEM image of Pure PMMA the precursor material

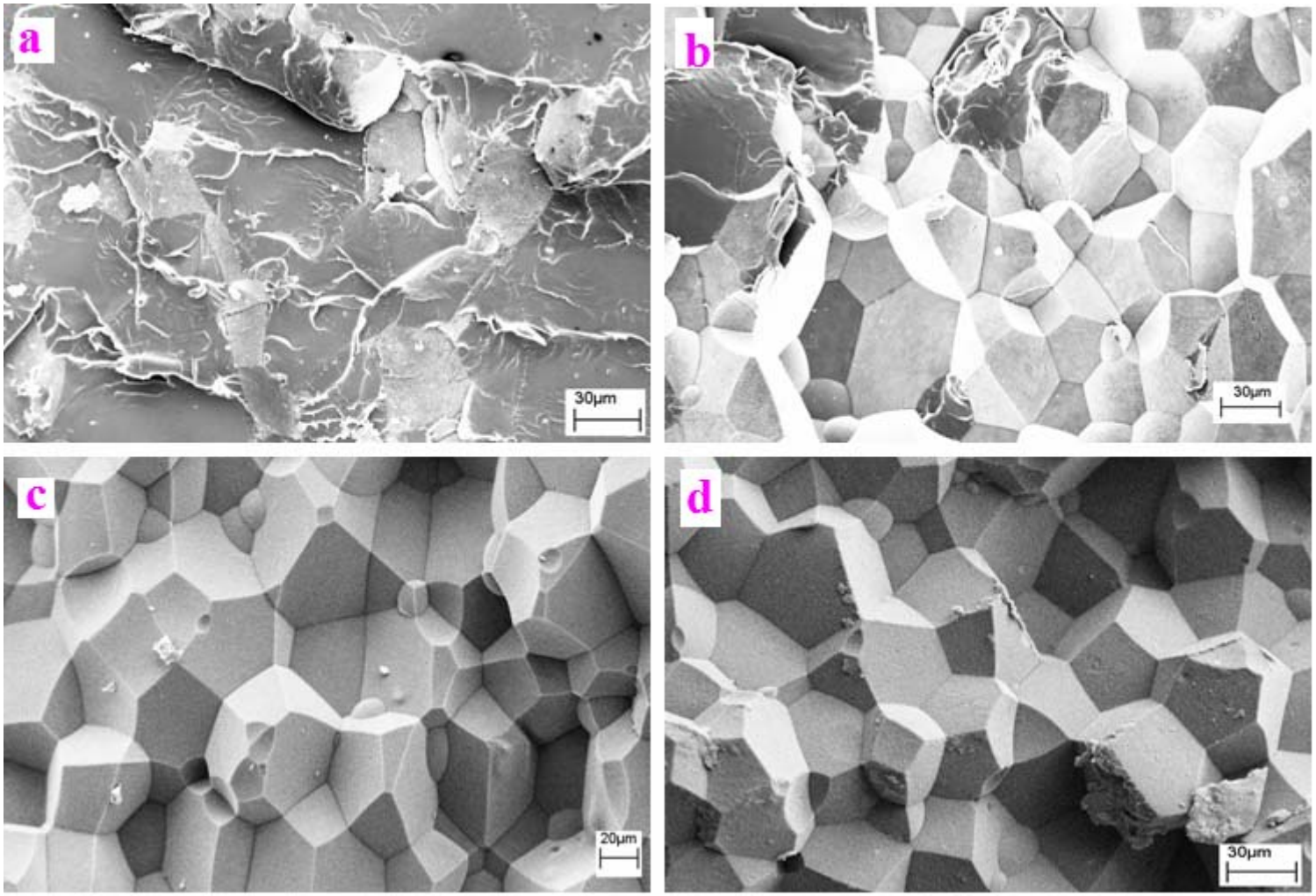

Figure 4.17 SEM images of fractured cross sections of PMMA/N-550 specimens with different phrs: (a) phr 0.05, (b) phr 0.2, (c) phr 0.4, and (d) phr 0.6

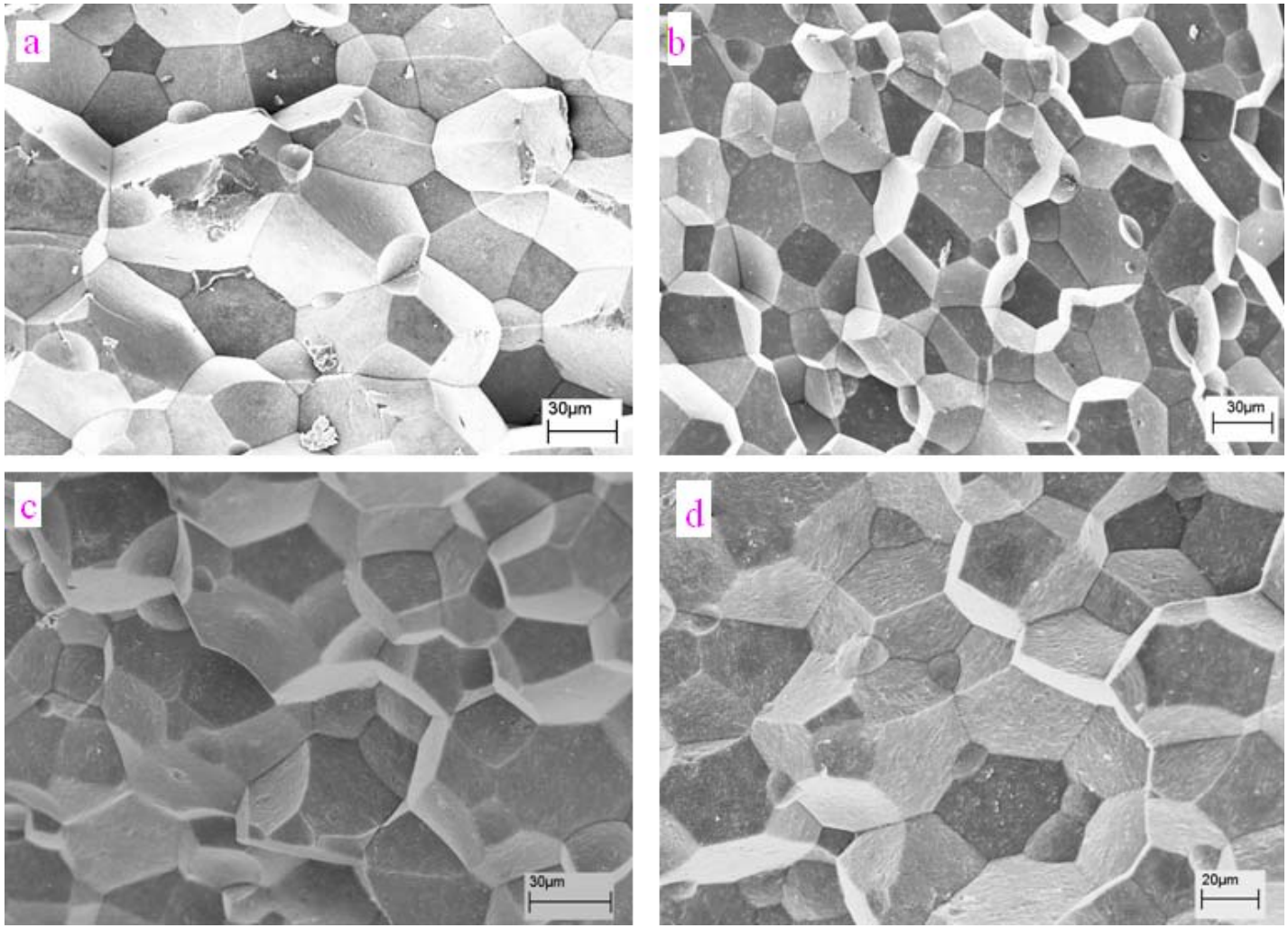

Figure 4.18 SEM images of fractured cross sections of PMMA/MWCN specimens with different phrs: (a) phr 0.05, (b) phr 0.1, (c) phr 0.5, and (d) phr 0.75

Intragranular fracture occurs before percolation for the N-550 samples at a phr of 0.05. As the filler content increases, the segregated network becomes more prevalent and the sample fractures via intergranular fracture. In contrast, in the MWCN samples, a segregated network has already started forming at a phr of 0.05, and all of the images show that intergranular fracture occurred for all of the MWCN samples examined.

4.4 Optical Measurements

Absorbance measurements and optical transmission microscopy were done on both the N-550 and MWCN samples to investigate their optical properties.

Figures 4.19 and 4.20 represent the absorbance measurements taken in the Cary 500 for N-550 and MWCN composites. When the absorbance goes above 4.5%, the data is unreliable. Reliable transmittance did not occur above a phr of 0.3 for the N-550 samples; while with the MWCN samples, reliable transmittance did not occur above a phr of 0.5.

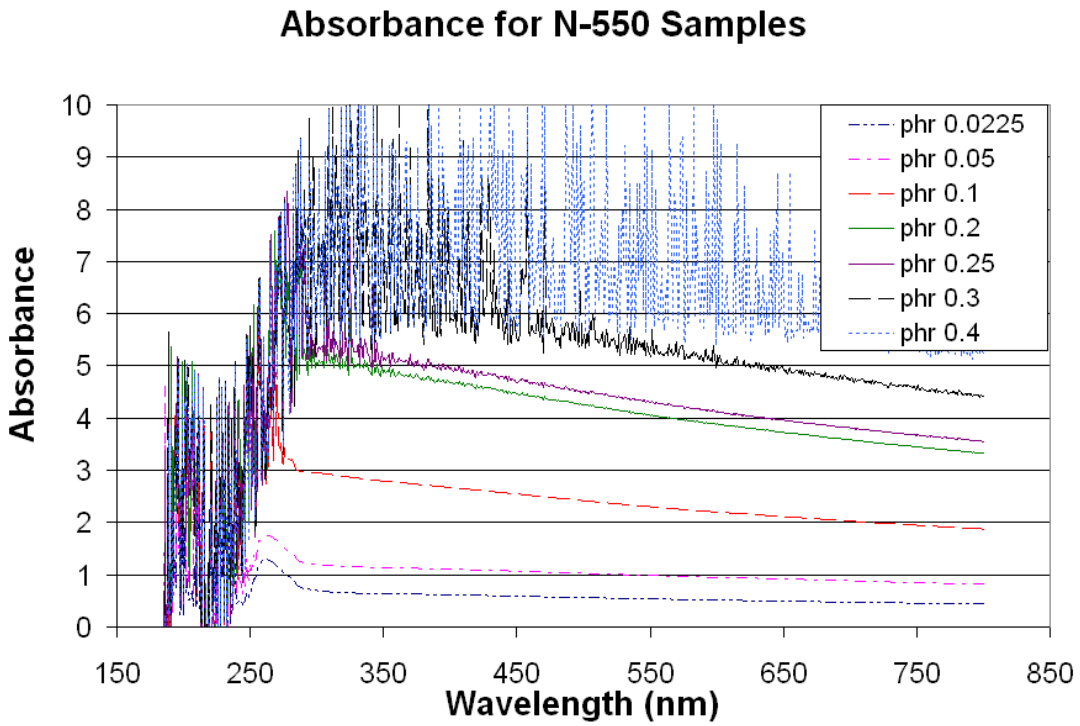

Figure 4.19 Absorbance vs. wavelength graph for 0.5 gram samples of PMMA filled with CB N-550 at various phrs

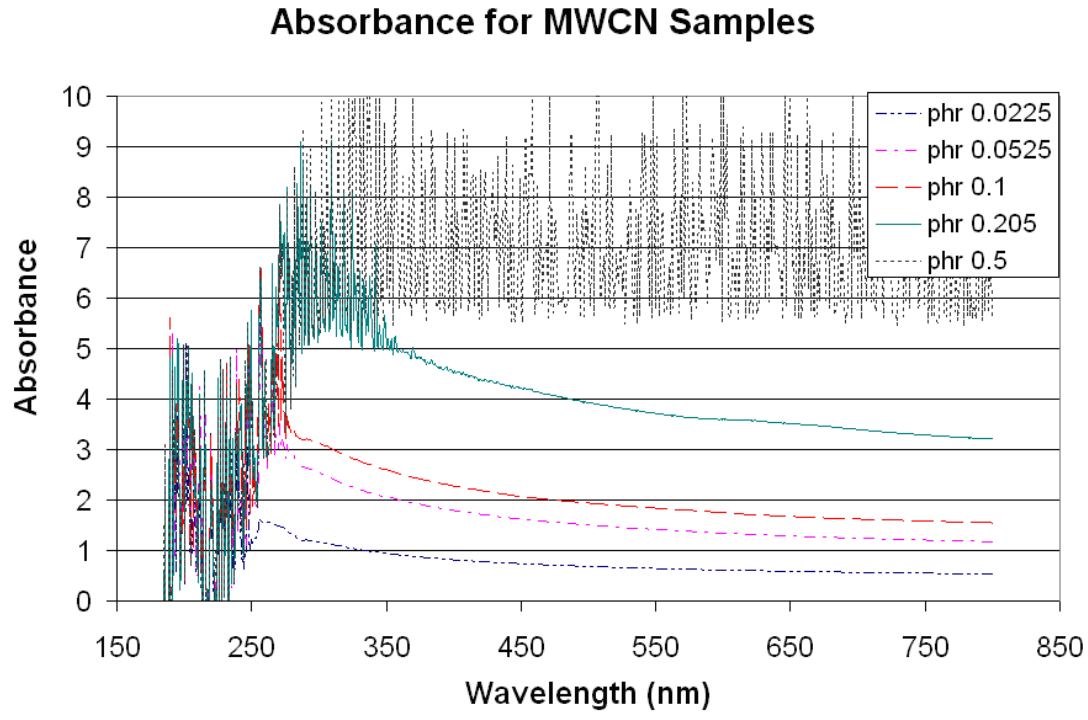

Figure 4.20 Absorbance vs. wavelength graph for 0.5 gram samples of PMMA filled with MWCN at various phrs

Figure 4.21 compares the absorbance measurements for N-550 to MWCN in the form of absorbance versus filler content. The absorbance for the N-550 samples was lower than that of the MWCN for samples containing a phr of less than 0.1. Figure 4.22 displays optical transmission images taken for both N-550 and MWCN samples at phrs of 0.0225 and 0.1. As the filler content increases, the grain boundaries of the PMMA become more defined.

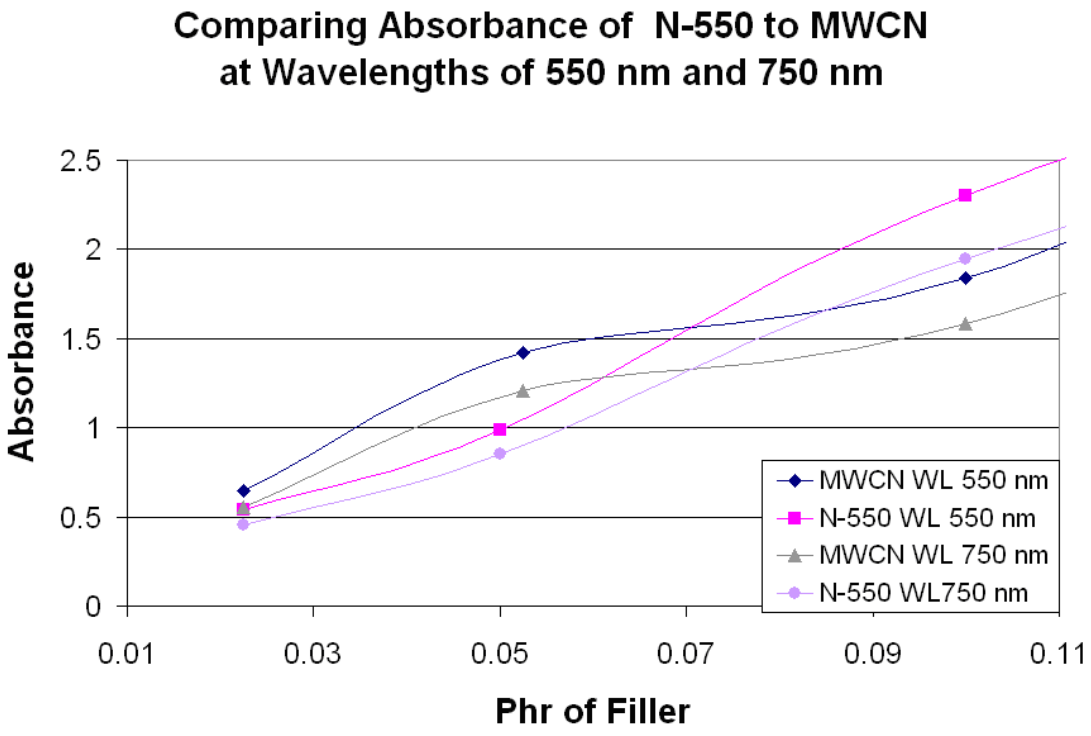

Figure 4.21 Compares the absorbance of PMMA filled with CB N-550 and PMMA filled with MWCN composites at wavelengths of 500nm and 750nm

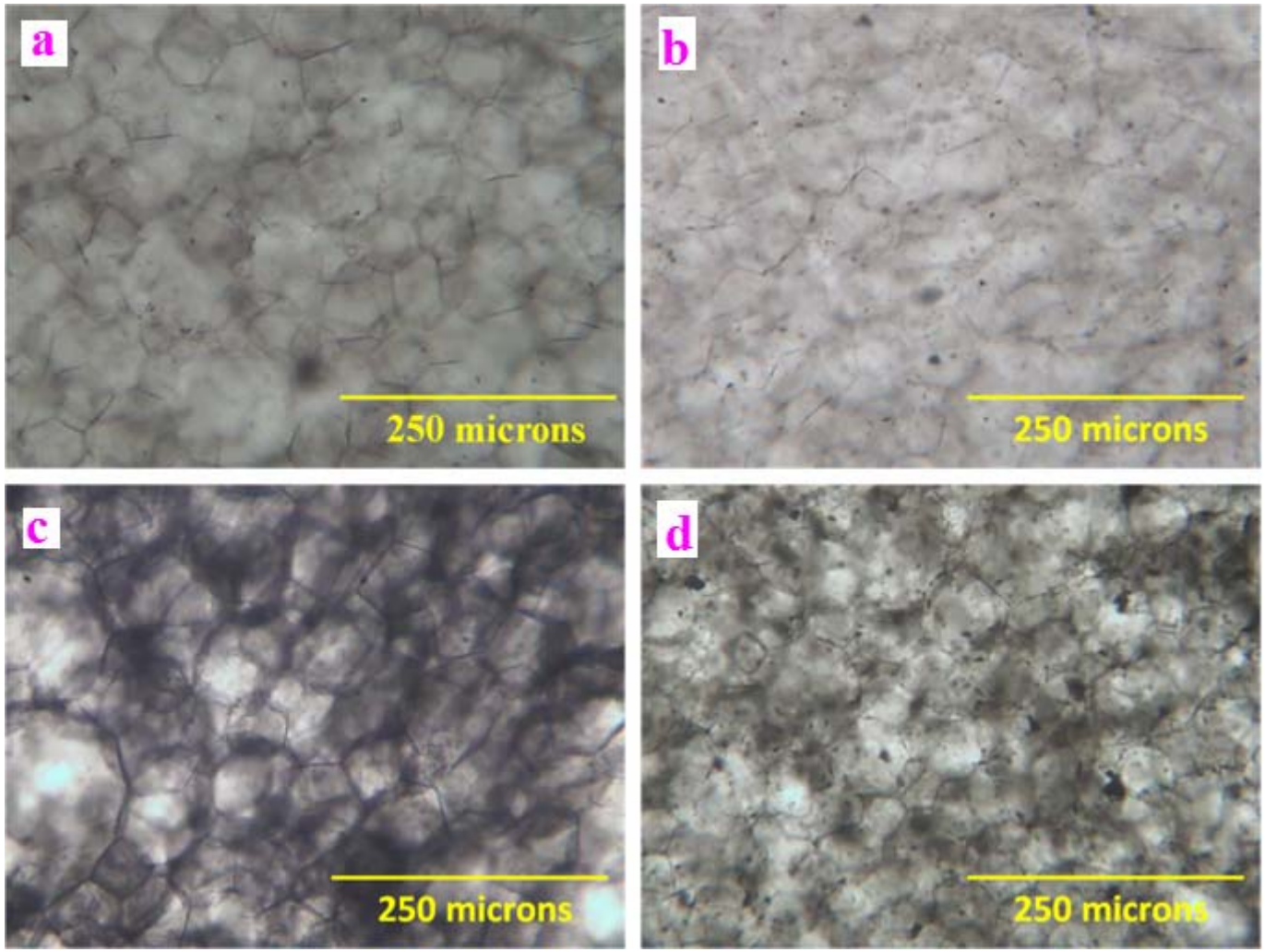

Figure 4.22 Optical transmission micrographs for PMMA filled with (a) CB N-550 with a phr of 0.0225, MWCN with a phr of 0.0225, (c) CB N-550 with a phr of 0.1, and (d) MWCN with a phr of 0.1.

CHAPTER 5

DISCUSSION

5.1 COMPARING ALL CARBON FILLERS

5.1.1 Percolation Threshold

All of the fillers displayed the expected trend; they showed a decrease in the resistivity of the sample with an increase of filler content. The CB fillers all displayed a C_v with a large decrease in the resistivity of the composites. Table 5-1 shows an estimated value for the percolation threshold of PMMA/MWCN, PMMA/CB N-550, PMMA/CB PB and PMMA/CB N-772 composites

Table 5-1 Displays the percolation threshold in phr, for the various fillers that were examined in a PMMA matrix.

Filler	MWCN	N-550	PB	N-772
C_v (in phr form)	0.0225	0.2	0.3	0.4

The behavior for the CB and MWCN samples showed different trends at the percolation threshold; the MWCN showed a gradual decrease in the resistivity of the sample. As a result of the sharp drop with CB, this critical region does not provide a consistent resistivity since a small change in the concentration of filler can lead to a drastic change in the resistivity. Since the percolation slope is not as steep with MWCN, it can be concluded that the conductivity of the MWCN composites is more controllable [59]. There is an increase in the consistency of the surface resistivity and a decrease in the fluctuation between various phr levels with reduced steepness. This is discussed in a paper concerning the examination of in-situ deposition of intrinsically conducting polymers [59]. On the other hand, a large change in resistivity is desired for applications that require fast switching, such as electromagnetic interference shields, and the CB filled specimens would be more desirable.

N-550 had the lowest percolation threshold when evaluating the various CB fillers. N-550 and N-772 have similar characteristics, but the oil absorption of N-550 was 121 cc/100g, almost double what it was for N-772. The oil absorption is directly related to the amount of branching present in the filler. Figure 5.1 (a) is a cartoon representing a CB filler that has a low oil absorption, or branching. Figure 5.1 (b) is a cartoon that represents a CB that would have a higher oil absorption or branching. Therefore, when the oil absorption was higher, there was an increase in the amount of branching which is directly related to an increase in the surface area of the filler, allowing for a network to form more readily throughout the system [4, 19]. This holds true for CB CDX-975 when it was examined. Figure 5.2, shows that the onset of percolation occurred first for the CDX-975 when it was graphed against the other CB. The oil absorption for CDX-975

was 169 cc/100g; therefore, its aggregates had more branching than the other CB fillers. In Turner's paper, he states that as the surface area of the filler increases, there is a decrease in the percolation threshold [5]. N-550 has a greater surface area than N-772 which results in N-550 having a lower percolation threshold.

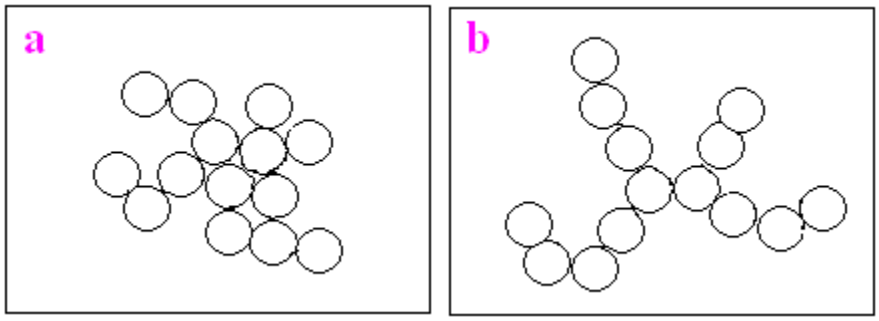

Figure 5.1 Shows that difference in the structure for (a) a CB containing a lower oil absorption and (b) a CB containing a higher oil absorption

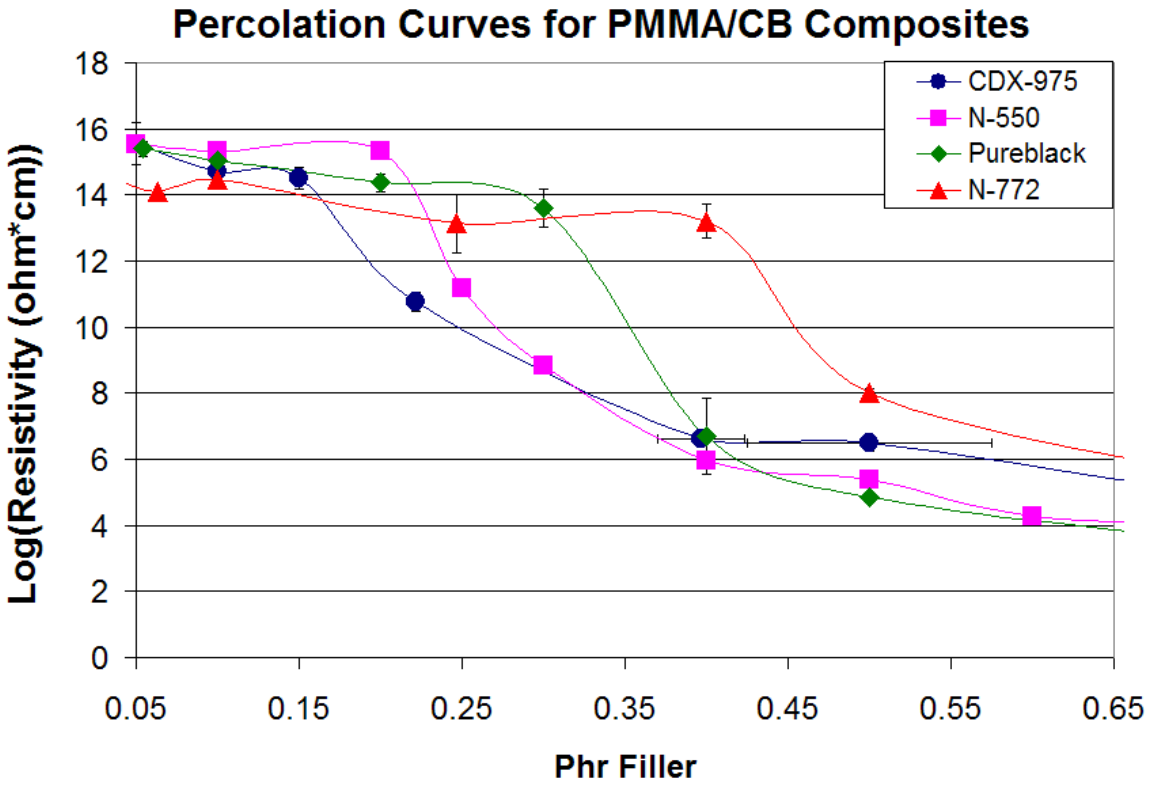

Figure 5.2 Percolation threshold curve showing the trend for all CB fillers investigated including CDX-975

D. He and his group [45] did an in-depth study on applying the Monte Carlo simulation to investigate the percolation threshold of granular composites of conductive and insulating powders. They verified studies that showed that the higher the ratio between the insulating and conducting particulates, the lower the percolation threshold [5, 42, 45]. The simulation showed that if the ratio was roughly one, the packing density of the filler lies between that of a simple cubic and a body centered cubic structure which would lead to a random microstructure [45].

PB had the highest surface area, but N-550 still had a lower percolation threshold. This was due to the pore density; PB had a porosity of 70 kg/cm, about five times less than N-550. With a lower pore density, the particles were more likely to agglomerate and this caused the coordination number to be higher, leading to an increased amount of filler needed in the system before the conductive path was formed. The percolation threshold of various graphite fillers is proportional to 1/ (z-1), where z is the coordination number [60]. As the void volume increased in the graphite filler, the percolation threshold decreased. In fillers with a lower void volume, the surface and structure energy were greater; this led to an increase in the coordination number, resulting in a closer packing of the filler particles [60]. PB has a lower void volume, which helps explain why PMMA/PB has a higher percolation threshold than PMMA/N-550 composites.

As expected, the percolation threshold for the MWCN was lower than any of the CB investigated. This is believed to be due to the larger surface area and anisotropy of the MWCN. Studies have been done, looking at the various shapes of filler particles, and it has been shown that the aspect ratio of the filler particles affects the percolation threshold [42-45]. As the TEM images showed, the CB fillers were roughly spherical in shape, while the MWCN were tubular with an aspect ratio of roughly 100. The classical percolation theory concludes that as the aspect ratio of the filler increases, there will be a decrease in the percolation threshold [43, 61]. It has been shown that in random microstructures, the percolation threshold for hard sphere like particles is around 16%; it has been observed that when the aspect ratio is increased to over 100, the percolation threshold is below 4% [62].

5.1.2 AC Conductivity

The conductivity displayed the same trend for all of the CF. At low phrs, the conductivity increased exponentially with increasing frequency, following the expected behavior for insulating samples. This behavior was related to a fully interconnected network not being present; therefore, the main source of ac conductivity was capacitance coupling, see figures 4.7-4.10. Capacitance coupling is used to describe the transport of electrons through a sample by the means of tunneling across thin insulating gaps governed by $z^*=1/(i\omega C_0\varepsilon^*)$. As the filler concentration increased, the slope of the conductivity versus frequency line decreased until further increase in the concentration of filler had a minimal effect on the conductivity. This is related to infinite clustering where there are multiple dc paths for electrons to travel through the composite and the contribution of ac coupling is minimal [4, 63]. For all of the samples investigated, this infinite clustering occurred at phrs that had a resistivity of less than 10^7 Ω*cm. As the phr increased, there was an increase in the conductivity of the sample, as expected. These same results were present in work done by Ou et al [4].

Figure 5.2 shows the conductivity versus filler content. This is another method of representing the percolation threshold of a sample at a given frequency. The conductivity is inversely related to the resistivity and figure 5.3 has the conductivity calculated for all of the samples at a frequency of 1 Hz. This frequency was chosen since it is at a value where the frequency was not too high that the data may be questionable, but the frequency was not too low that it was too noisy.

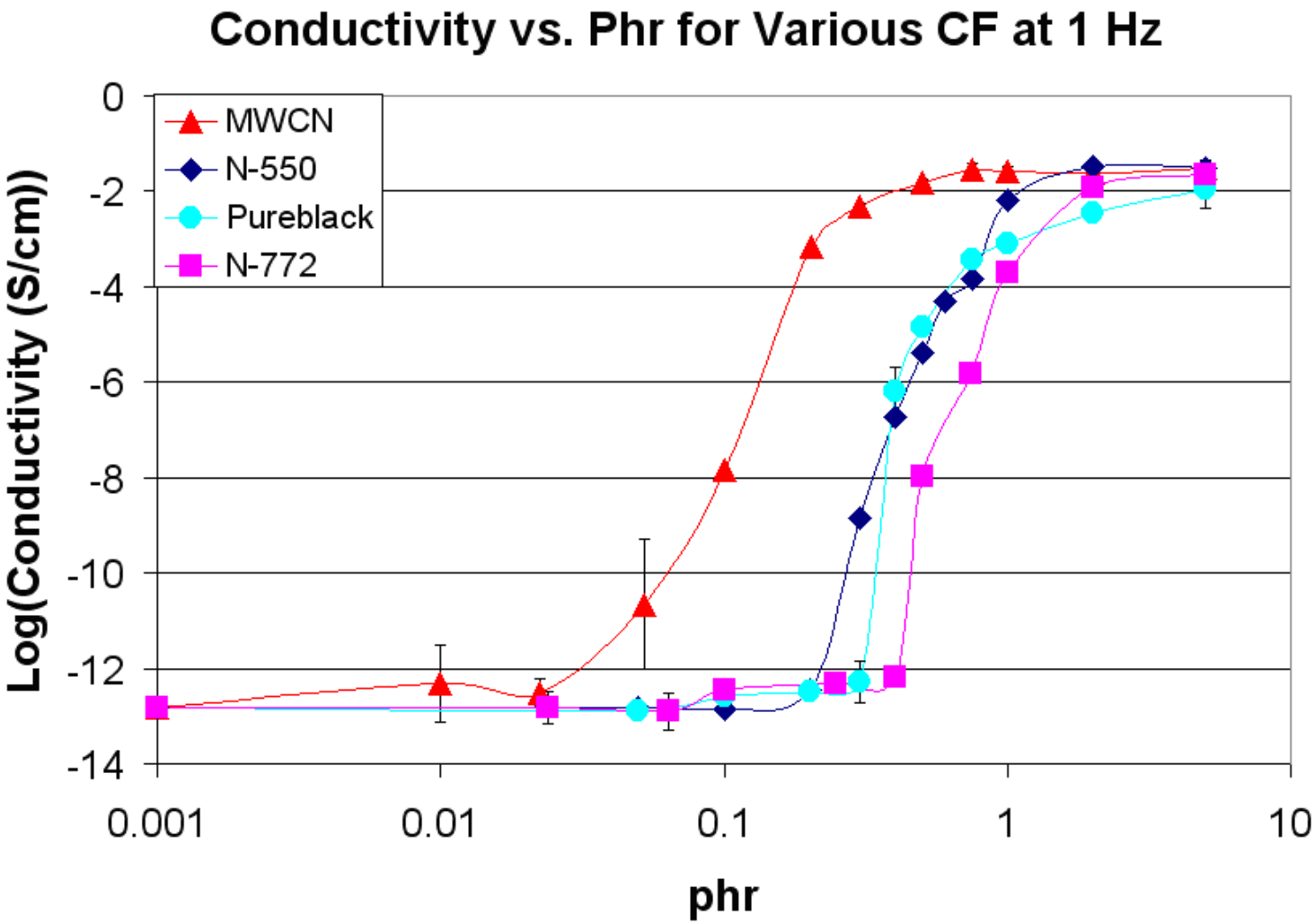

Figure 5.3 Comparison of the conductivity vs. phr graph comparing the conductivities of the various CB fillers and MWCN at 1 Hz

The critical frequency (f_c) of a given composition can be determined, as shown in figure 5.4, for a PMMA/CB N-550 sample with a phr of 0.4. The f_c occurs at the frequency where the sample changes from being frequency independent, where the particles are in direct contact with each other, to frequency dependent, where electrons travel across very thin insulating gaps as a result of capacitance coupling. The f_c is found by drawing tangent lines from the frequency independent region and the frequency dependent region [1, 2, 4, 63].

With determining the critical frequency at various filler contents, a critical exponent (t) can be determined, since $\sigma_{dc} \propto (V_c - C_V)^t$, where V_c is the volume fraction of filler and C_v is the critical volume fraction. Through the use of Monte Carlo simulations for a 3-d microstructure, t has been found to be between 1.6 and 2.0 [64]. Figure 5.5 shows the log (critical frequency) as a function of log (V_c-C_v). In this graph, a linear relationship is found and the slope of the line is 1.6. With this, the t value for the PMMA/CB N-550 samples is 1.6, which leads to $\sigma_{dc} \propto (V_c - C_V)^{1.6}$. This value found agrees with the values found by Ou [4] for PMMA/CB CDX-975 [4] samples, and the value of 1.5 found by Connor's group [64].

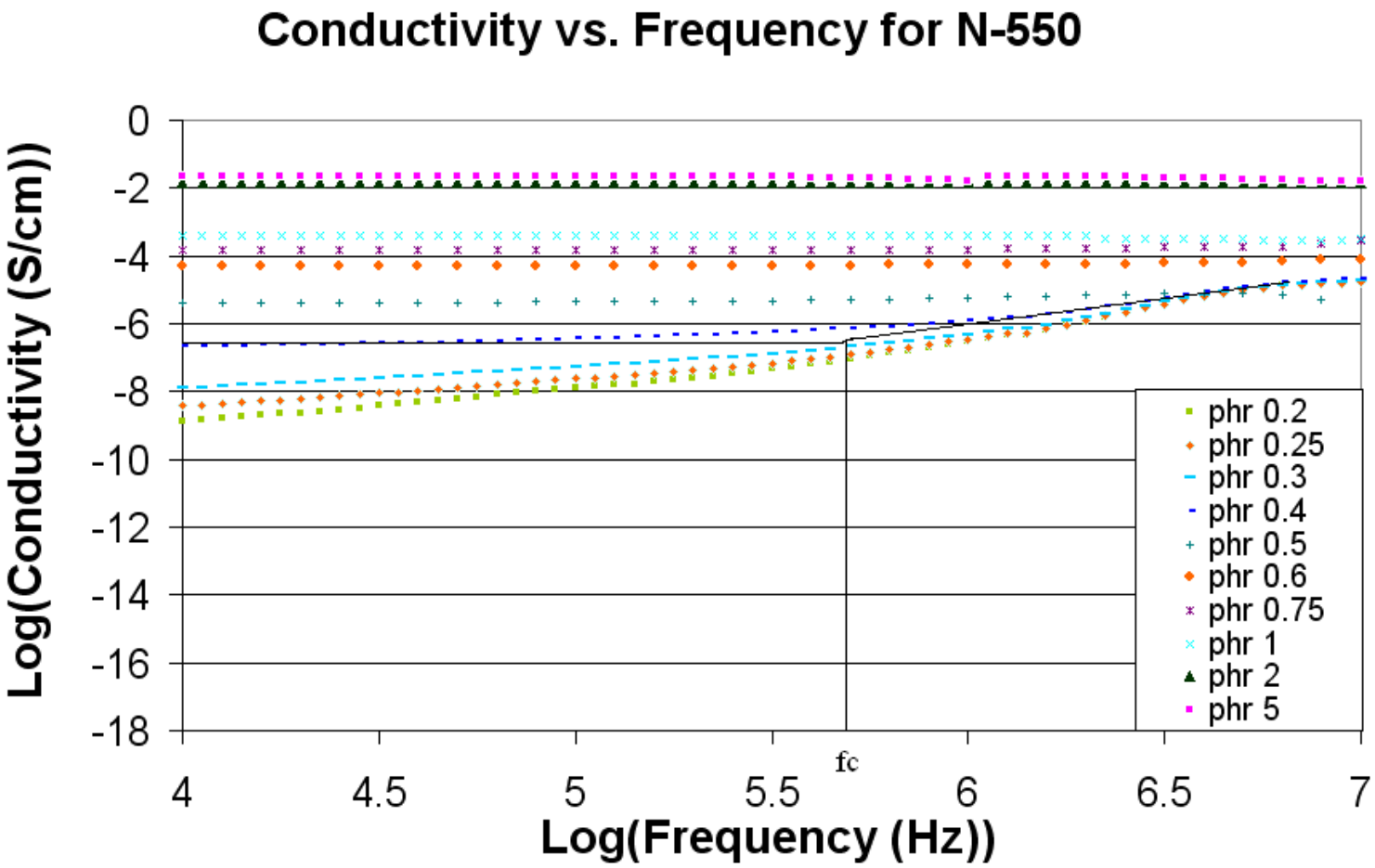

Figure 5.4 Shows the method used to find the critical frequency, displaying the critical frequency for PMMA filled with CB N-550 samples with a phr of 0.4

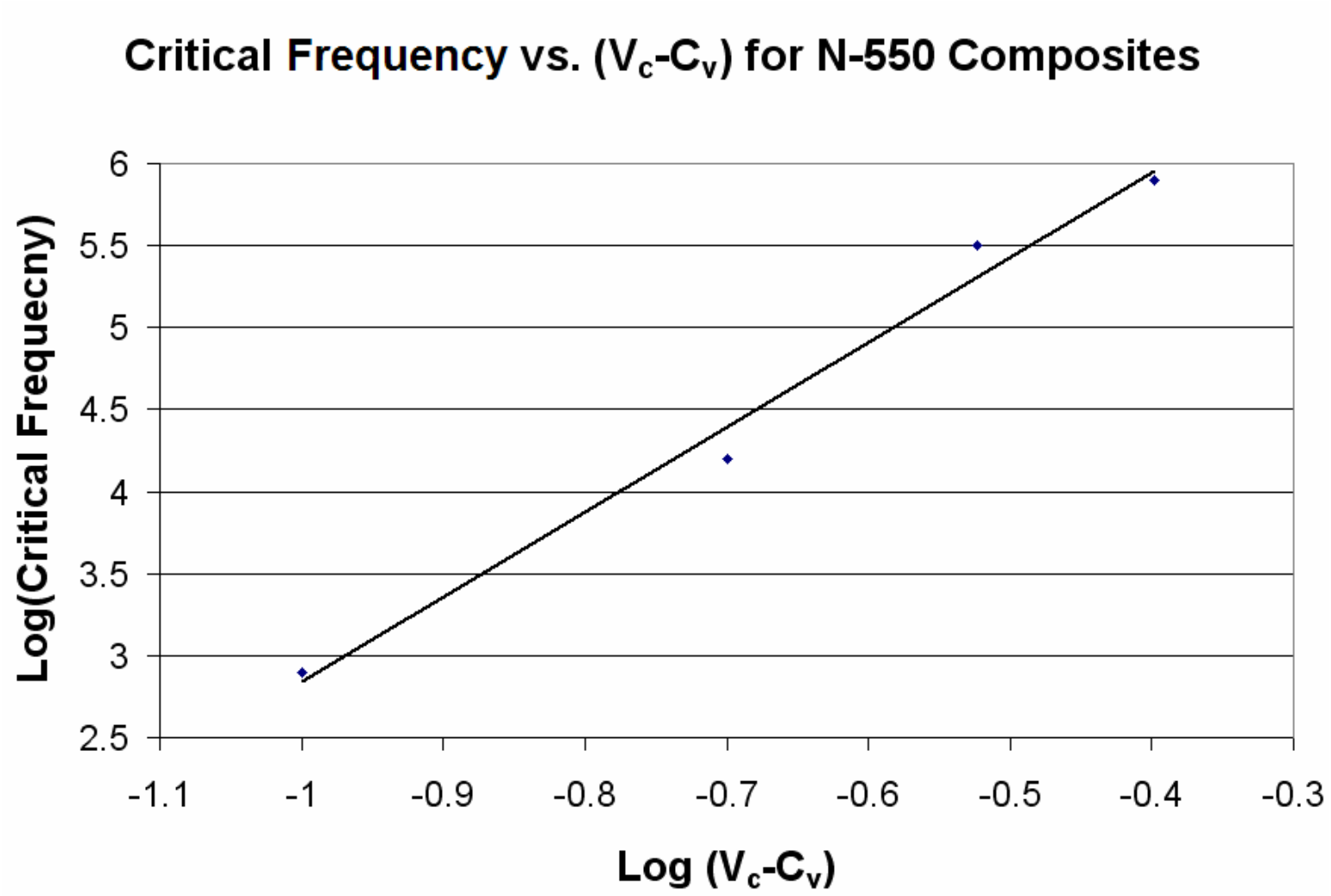

Figure 5.5 Shows the critical frequency vs. (V_c-C_v), to determine the critical exponent t for, PMMA filled with CB N-550 samples

The frequency dependent power law states that conductivity is a function of frequency and concentration is equivalent to the frequency raised to the slope of the frequency dependent region of the curve [1]. M.T. Connor found that the slope was not dependent on the concentration of filler [64]. Connor tested CB composites with a matrix consisting of poly-ethylene-terephthalate (PET). When he graphed the conductivity versus frequency on a log log scale, he noted that at frequencies higher than the critical frequency, the slope of the lines were not all the same. They claimed this was caused by anisotropy in the sample, and this anisotropy also led to error in the calculated f_c [64]. However, results obtained for all CF tested in this thesis and the CDX-975 filled composites tested by Ou [4], all show that the slope of the line on the log (critical frequency) versus log(V_c-C_v) decreases with an increase in the filler concentration.

The critical frequencies for the other PMMA/CF composites were found in the same fashion as the PMMA/CB N-550 composites. The log (critical frequency) as a function of log (V_c-C_v) was graphed for the composites. The t values found for the composites fell in the range of 1.6-2.0. The t values were 1.7, 1.7 and 1.9 for the N-772, the PB and the MWCN composites respectively.

5.1.3 Dielectric Constants

All of the composites displayed similar behaviors in the graphs of the dielectric constants versus the frequency. As the frequency increased, ε' decreased. The slope of the line increased with an increase in the amount of filler. This behavior was expected

and has also been observed for Polyethylene-Graphite composites [65] and acrylonitrile butadiene styrene (ABS)/CB composites [10, 15].

The imaginary and the real part of the dielectric constant were examined to establish whether the filler or the polymer was the key element in determining the behavior of the real and imaginary parts of the dielectric. As more CF was added to the composites and the phr increased, both the imaginary and the real part of the dielectric increased. This behavior is similar to the behavior of the PP/CB composites tested by Zois's group [1].

The more conducting samples also displayed a sharp decrease at roughly 10^5 Hz (figures 4.12-4.15); this decrease has been seen in other conductive polymer composite systems. This same decrease was shown in figure 1.21 in the polyvinylindene fluoride (PVDF)/ acetylene black (AB) composites [47]. For all of the samples, the slope of this line is roughly -1.8, as shown in figure 5.6 which shows the slope of the lines for N-550 samples with phrs of 15, 5 and 2 in the high frequency range. The graph zooms in and focuses on the frequency range from 10^5 Hz to 10^7 Hz [53, 55].

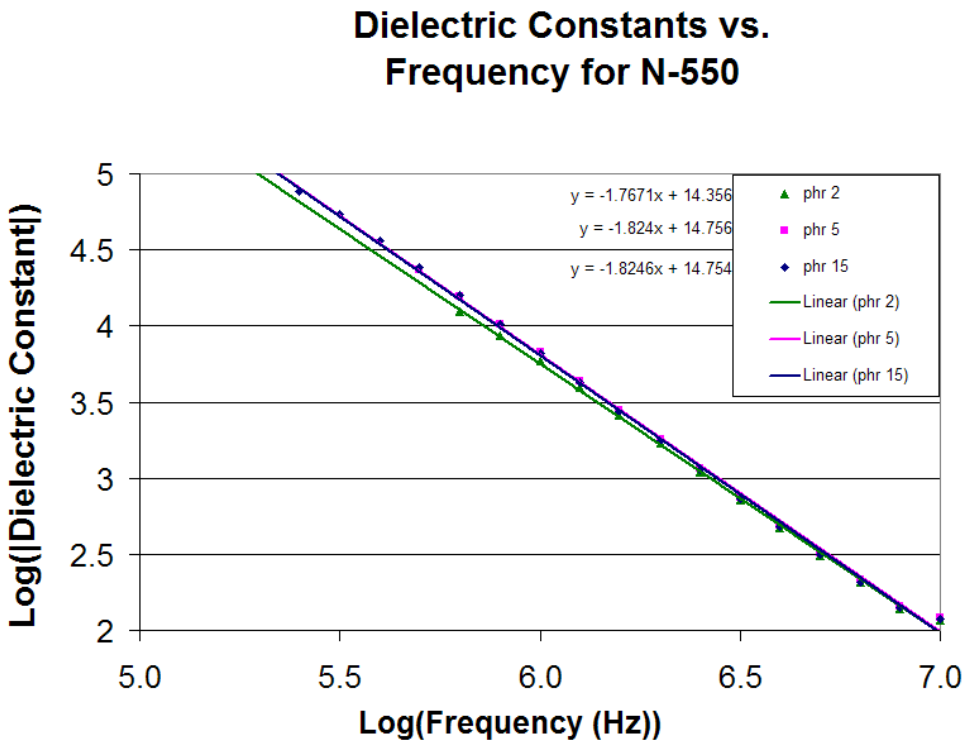

Figure 5.6 Shows the slopes of the dielectric constant vs. frequency in the high frequency region for the conductive samples.

To fully compare the different CF investigated, figure 5.7 shows the dielectric constant versus filler content at a frequency of 1 Hz. At lower concentrations of filler, the dielectric constant was the same, but as the concentration increased, the dielectric constant of the MWCN increased at a faster rate than the CB-filled samples. Once all of the systems were fully percolated, the dielectric constant for the MWCN was greater than any of the CB samples at 1 Hz. The N-550 and N-772 followed the same trend once their systems were fully percolated, and the fully percolated systems have a dielectric constant less than an order of magnitude apart. It is interesting to note that the dielectric constant of a fully percolated PB composite was lower than that of all of the other filler composites, and displayed a more gradual leveling off. In contrast, the other composites had a distinctive leveling off phr value.

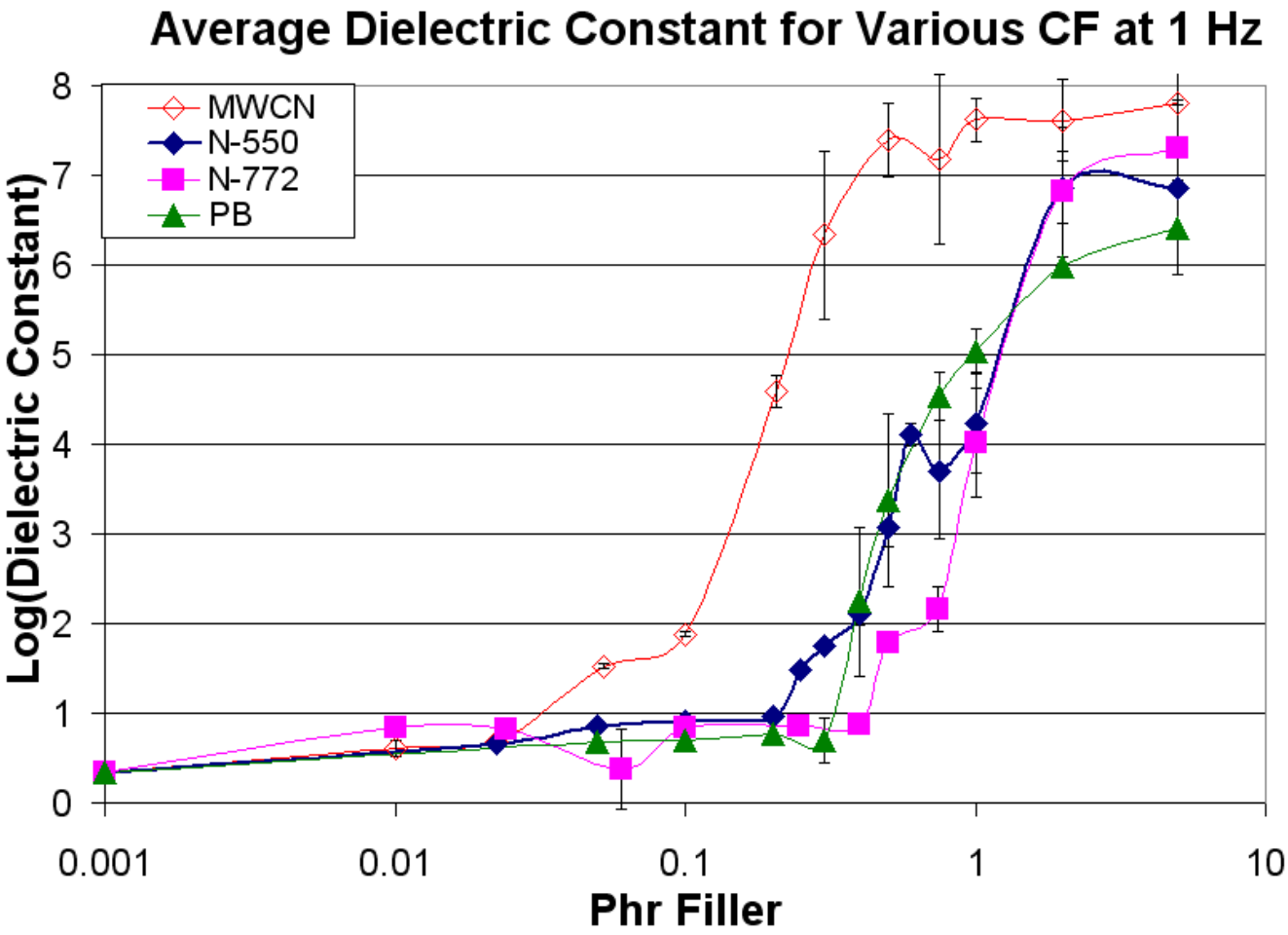

Figure 5.7 Dielectric constant vs. filler content for all samples at a frequency of 1 Hz

Figure 5.8 shows the dielectrics loss of the material for N-550 and MWCN as a function of frequency and concentration. The CB filled composites displayed similar characteristics and had dielectric constants lower than MWCN for the majority of the phrs. N-550 was used to represent all of the CB since it had the highest dielectric constant for the CB filled composites. At a phr of 0.2, the dielectric constant for MWCN was about 3.5 orders of magnitude higher, but the dielectric loss for the material was so substantial that it limits the applications which it can be used for.

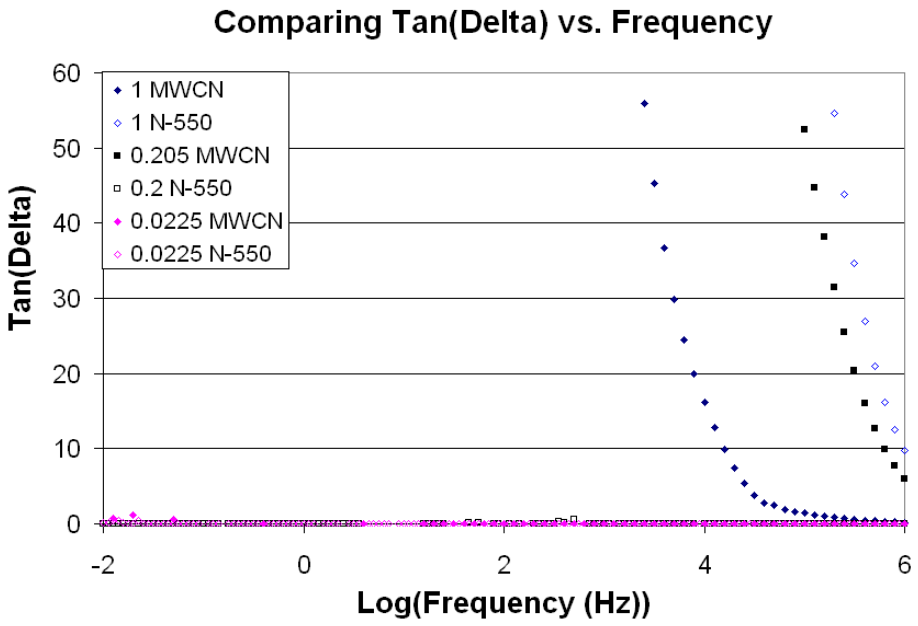

(a)

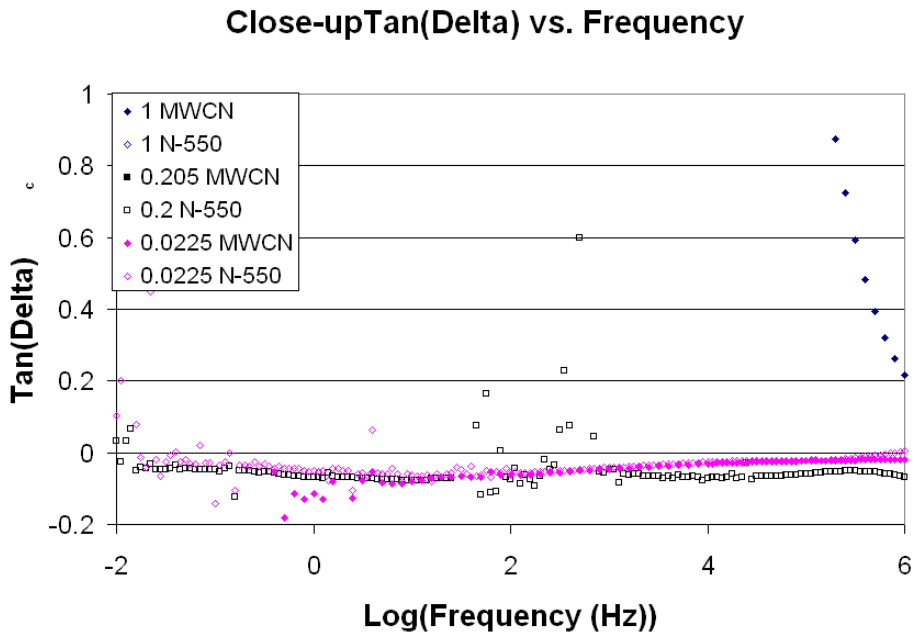

(b)

Figure 5.8 (a) Tan (delta) vs. Frequency graph, (b) Close-up of the tan (delta) vs. frequency used to look at the lower phr samples which display a low dielectric loss

5.2 COMPARING N-550 TO MULTI-WALLED CARBON NANO-TUBES

After evaluating all of the CB fillers, each of the fillers showed the same trend and displayed similar characteristics. Therefore, it can be concluded that the optical and microstructure properties of the CB fillers result in essentially the same behavior, with only some minor differences. A more in-depth study was done on the MWCN and the N-550 (which represents all of the CB filler) composites.

5.2.1 Microstructure Evaluation

The SEM image of the fracture surface of pure PMMA was shown in figure 4.16. The fracture surface displayed the expected behavior for a ductile material, intragranular fracture. The distinction between each grain boundary is not observed. Figure 4.17 shows that initially, for N-550 composites with a phr of 0.05, these composites displayed the same fracture surface as the pure PMMA. As the concentration of filler increased, a segregated network was formed and the composites underwent intergranular fracture. This was observed by the formation of a faceted structure. The CB had coated the PMMA particles and the particles were deformed into polyhedra during pressing [4, 6, 7, 12]. In the SEM images of higher filler content composites, it appears that there is a collection of crystal grains. This structure has been observed in PMMA/indium tin oxide (ITO) composites [6, 8, 11-14], PMMA/CB composites [4, 7, 9, 40] and acrylonitrile butadiene styrene (ABS)/CB composites [10, 15].

The SEM images of the composites containing MWCN show that the formation of the polyhedra occurred at a lower phr content, and a faceted structure was observed at phrs of 0.05. This is due to MWCN having a higher aspect ratio, which allowed the filler particles to form a continuous network and surround the PMMA particles at lower concentrations.

The technique of blending the PMMA and CF resulted in a segregated microstructure. When the CF particles were much smaller than PMMA, CF surrounded the surfaces of the PMMA particles. When the powder was pressed, shearing forces were not introduced; therefore, the particle structure of the PMMA was not ruined since the filler particles did not intrude into the PMMA. The PMMA particles actually deformed into polyhedra when the polymer was pressed at a temperature between the melting temperature and the glass transition temperature and the PMMA particles were coated with CF. When the PMMA was deformed, some of the CF was pushed towards the triple junction [4, 6, 11-14, 40]. This resulted in a highly ordered segregated microstructure, as shown in images 4.17, 4.18, that led to the lower percolation threshold.

In the optical transmittance image, figure 4.22, the polyhedra structure of the PMMA can be seen. This led to the conclusion that a segregated microstructure was formed when the PMMA was coated by the conductive filler.

Ou, et al. [4], further supported the notion that the carbon filler was located between the faces of the PMMA particles. When comparing SEM images of PMMA/CB CDX875 samples of phrs of 1 and 10, the edges of the grains for a phr of 10 were not as rough and pointy as the edges of samples with a phr of 1. This is evidence that the excess carbon filler will preferentially migrate to the triple junction of the PMMA faceted grains

and faces. The excess filler reduces the sharpness of the grain edges of the PMMA since it acts as a cushion, absorbing some of the pressure exerted on the sample during processing [4].

The use of mechanical mixing to produce PMMA/ITO composites has been studied [6, 11-14]. The composites were made in the same fashion as the samples for the PMMA/CB composites, and SEM images have shown that the PMMA also deformed into polyhedra [6, 8, 11-14]. L. E. Levine has done further studies on PMMA/CB composites by performing ultra small-angle x-ray scattering (USAXS) imaging. The samples used for his testing were fabricated at Georgia Institute of Technology, by Dr. Gerhardt's group, by the use of mechanical mixing. He observed how the PMMA particles were deformed into polyhedra. Furthermore, with the USAXS data he saw that the interconnected network had formed throughout the composites, and that there was a formation of triple points where the excess CB filler was located [40].

The MWCN started to surround the PMMA particles and form a continuous network in the composites at lower concentrations than N-550 does. In figure 4.21, at a phr of 0.05, the formation of facets had already occurred in the MWCN. For the N-550 samples, shown in figure 4.20, there were no facets present at a phr of 0.05 and at a phr of 0.2, there were still sections where the PMMA was not totally surrounded and the polyhedra structure was not present. This was further supported by the optical absorbance measurements, which will be discussed in the next section.

5.2.2 Optical Measurements

Optical absorbance measurements were taken for MWCN and N-550 samples to compare the effect of the filler particles on the optical properties of the composites. CF is not the ideal filler to use if the goal was to obtain a transparent polymer since CF absorbs all visible light by an electron band transition. If the goal is to obtain a transparent composite, the filler needs to be transparent and the scattering at the interface between the filler and the matrix needs to be as small as possible to decrease the absorbance. Transparency is defined in equation 35, where I is the intensity transmitted, I_o is the intensity of the incident light, R is the reflection, γ is the extinction coefficient – which includes the scattering and absorbance components - , and t is the thickness [66].

$$(I/I_0) = (1-R)e^{-\gamma t} \qquad \text{Equation 35}$$

However, it is still instructive to measure the optical absorbance of those samples that permitted measurements to be performed. This can lead to a more defined investigation of the characteristics of the composites. It was observed that at phrs below 0.05, the percent of light absorbed by the N-550 sample was lower than the MWCN sample, as was shown in figure 4.22. This can directly be related to the microstructure; when the facets form in the microstructure, the material looks like a collection of crystal grains. In previous work, even through the sample appears to be crystalline, x-ray diffraction have shown that the PMMA/CB CDX-975 was non crystalline [4]. But absorption and internal reflection occurs in the sample, due to the microstructure. When

x-rays are sent through the sample where the formation of the segregated microstructure is not present, the amount of internal reflection that occurs within the sample is less than if the segregated microstructure has formed. When both of the composites have a microstructure consisting of PMMA being deformed into polyhedra, the absorbance of the MWCN is less than that for the N-550.

CHAPTER 6

CONCLUSIONS AND FUTURE WORK

Through the use of mechanically mixing a polymer and a conductive filler together, a conductive polymer composite containing a segregated microstructure can be fabricated. The polymer is deformed into polyhedra and the excess filler is preferentially located at the triple points. The segregated microstructure leads to a decrease in the percolation threshold of the composite and therefore, a lower content of filler is needed to produce a continuous network throughout the composite.

When evaluating the difference between various CB, the onset of percolation was found to be influenced by the oil absorption, which is related to the surface area and porosity of the filler, but the difference was not as drastic as originally expected. On the other hand, the percolation threshold for the MWCN was significantly lower than that of any of the CB. This can be accounted for due to the increase in aspect ratio and anisotropy of the filler.

In the future, PMMA composites containing single-wall carbon nano-tube should be studied. The same electrical and optical experiments should be performed on these composites and they should be compared to PMMA composites containing MWCN and CB N-550.

As the content of filler increases, the dielectric constant of the composite also increases, but this comes with an increase in the dielectric loss of the material. As

expected, this is due to the conductivity increases as the filler content increases. All of the various CB displayed the same characteristics and followed the expected trends.

The composites produced for this thesis showed an increase in the dielectric constant, but this was achieved at the expense of an increase in the dielectric loss of the material. To reduce the dielectric loss of the composite, a coating should be placed on the filler particles to prevent the filler particles to come in direct contact with each other. This covering will act as an interlayer or insulating shell. This coating, will lead to a decrease in the dielectric loss of the material. The effect of various coatings with the same filler and polymer matrix can be examined, as well as various fillers with the same coating and coating thickness can be examined. In addition, the effects of varying the coating thickness for the same filler can be examined [67, 68]. With finding an ideal combination, where the composite contains both a high dielectric constant and a low dielectric loss, this composite will be ideal for super capacitor applications.

I believe that this work has set a foundation to continue research and lead to a better understanding of how fillers affect the conductivity in segregated microstructures through the use of mechanical mixing to produce a segregated microstructure.

REFERENCES

[1] Zois, H., Apekis, L., & Omastova, M. (2001). Electrical Properties of Carbon Black-filled Polymer Composites. *Macromolecular symposia 170*, 249-256.

[2] Zhang, W., Dehghani-Sanij, A.A., & Blackburn, R.S. (2007). Carbon Based Conductive Polymer Composites. *Journal of Materials Science Letters 42*, 3408-3418.

[3] Strumpler, R., & Glatz-Reichenbach, J. (1999). Conducting Polymer Composites. *Journal of Electroceramics 3(4)*, 329-346.

[4] Ou, R., Gupta, S., Parker, C.A., & Gerhardt, R.A. (2006). Fabrication and Electrical Conductivity of PMMA/CB Composites: Comparison Between an Ordered Carbon Black-Nan wire Segregated Structure and a Randomly Dispersed Carbon Black Structure. *Journal of Physical Chemistry B 110 (45)*, 22362-22370.

[5] Milliards, A., & Turner, D.T. (1971). Influence of particle size on the electrical resistivity of compacted mixtures of polymeric and metallic powders. *Journal of Applied Physics 42(2)*, 614-618.

[6] Gerhardt, R.A., Ou, R., Kaposi, C.J., Gupta, S., Shackelford, S., Long, G.G., Levine, L., Li, Z., & Samuels, R.J. Effect of Particle Size and Fabrication Method on the Microstructure and Electromagnetic Properties of Polymer Nan composites. In preparation.

[7] Ou, R., Gupta, S., Parker, C.A., & Gerhardt, R.A. Low Percolation Threshold Composites Consisting of PMMA and Carbon Black. *TMS Letters 2(4)*, 117-118.

[8] Capozzi, C.J., Shackelford, S., Ou, R., & Gerhardt, R.A. (2004). Study of Percolation in PMMA/ Indium Tin Oxide Composites. *Materials Research Symposium* Vol. 819, pp. 303-308.

[9] Gupta, S., Runqing, O.U., & Gerhardt, R.A. (2006). Effect of the Fabrication Method on the Electrical Properties of Poly(acrylonitrile-co-butadiene-co-styrene)/Carbon Black Composites. *Journal of Electronic Materials 35*, 224-229.

[10] Talapatra, S., & Gerhardt, R.A. (2006). Optimization of the Electrical Conductivity of ABS Nanocomposites Filled with Carbon Black and Carbon Nanotubes. *Materials Research Society Symposium Proceedings 977(Processing-Structure-Mechanical Property Relations in Composite Materials)*, 126-131.

[11] Capozzi, C.J., & Gerhardt, R.A. (2006). Effect of Processing on the Microstructure and Electrical Conductivity of Hot Pressed PMMA/ITO Bulk Nanocomposites. *Materials Research Society Symposium Proceedings 977(Processing-Structure-Mechanical Property Relations in Composite Materials)*, 41-43.

[12] Capozzi, C.J., & Gerhardt, R.A. (2007). Novel Percolation Mechanism in PMMA Matrix Composites Containing Segregated ITO Nanowire Networks. *Advanced Functional Materials (17)*, 2515-2521.

[13] Capozzi, C.J., & Gerhardt, R.A. AC Conductivity of Locally Confined ITO in Hot Pressed PMMA Compacts. Submitted to *Journal of Physical Chemistry B.*

[14] Capozzi, C.J., Li, Zhi, Samuels, Robert J. & Gerhardt, R.A. Impedance Spectroscopy and Optical Characterization of ITO-filled PMMA Composites. Submitted to *Journal of Applied Physics* .

[15] Talapatra, S., & Gerhardt, R.A. Effect of Processing Parameters on the Electrical Conductivity and Mechanical Strength of ABS Segregated Network Composites. In preparation.

[16] Wu, Kenter, Ou , Runqing, Ivanov , Ilia, N. & Gerhardt, R.A. Optical and Electrical Characterization of Segregated Network Polystyrene composites filled with Carbon Black, MWNT and SWNT. In preparation.

[17] Bouchet, J., Carrot, C., & Guillet, J. (2000). Conductive Composites of UHMWPE and Ceramics Based on the Segregated Network Concept. *Polymer Engineering and Science 40*, 36-45.

[18] Dang, Z., Zhang, Y., & Tjong, S.-C. (2004). Dependence of Dielectric Behavior on the Physical Property of Fillers in the Polymer-Matrix Composites. *Synthetic Metals 146*, 79-84.

[19] Ponomarenko, A.T., Shevchenko, V.G., & Enikolopyan, N.S. (1990). Filled Polymers I Science and Technology Springer Berlin / Heidelberg.

[20] Tang, H., Chen, X., & Luo, Y. (1995). Electrical and Dynamic Mechanical Behavior of Carbon Black Filled Polymer Composites. *European Polymer Journal 32*, 936-966.

[21] Lu, G., Li, X., Jiang, H., & Mao, X. (1996). Electrical Conductivity of Carbon Fibers/ABA Resin Composites Mixed with Carbon Blacks. *Journal of Applied Polymer Science 62*, 2193-2199.

[22] Seo, M.A., Lee, J.W., & Kim, D.S. (2006). Dielectric constant engineering with polymethylmethacrylate-graphite metastate composites in the terahertz region. *Journal of Applied Physics 99(6)*, 066103-066101-066103-066103.

[23] Barba, A.A., Geatano, L., Matteo, D.A., & Domenico, A. (2006). Carbon Black/Silicone Rubber Blends as Absorbing Materials to Reduce Electro Magnetic Interferences (EMI). *Polymer Bulletin (Berlin) 57*, 587.

[24] Strumpler, R. (1996). Polymer Composite Thermistor for Temperature and Current Sensors. *Journal of Applied Physics 80(11)*, 6091-6096.

[25] Heaney, M.B. (1996). Resistance-expansion-temperature behavior of a disordered conductor-insulator composite. *Applied Physics Letters 69(17)*, 2602-2604.

[26] Chen, J., & Tsubokawa, N. (2001). A novel gas sensor from polymer-grafted carbon black: Effects of polymer, crystalline organic compound, and carbon black on electric response to tetrahydrofuran vapor. *Journal of Macromolecular Science - Pure and Applied Chemistry 38(4)*, 383-398.

[27] Dang, Z.-M., Wang, L., Yin, T., Zhang, Q., & Lei, Q.-Q. (2007). Giant Dielectric Permittivities in Fuctionalized Carbon-Nanotube/Electroactive-Polymer Nanocomposites. *Advanced Materials 19*, 852-857.

[28] Gerhardt, R.A. (2005). Impedance Spectroscopy and Mobility Spectra. In *Encyclopedia of Condensed Matter Physics*, (Bassani, G., et al., Eds.). Academic Press.

[29] Macdonald, J.R. (1987). Impedance Spectroscopy Emphasizing Solid Materials and Systems. John Wiley & Sons, Inc.

[30] Jonscher, A.K. (1996). Dielectric Relaxation in Solids. Chelsea Dielectric Press Ltd., London, UK.

[31] Hsu, C.S., & Mansfeld, F. (2001). Technical Note: Concerning the Conversion of the Constant Phase Element Parameter Y_0 into a Capacitance. *Corrosion 57(9)*, 747-748.

[32] Brug, G.J., Eeden, A.L.G.V.D., Sluyters-Rehbach, M., & Sluyters, J.H. (1984). The Analysis of Electrode Impedances Complicated by the Presence of a Constant Phase Element. *Journal of Electro - analytical Chemistry 176*, 275-295.

[33] Sahimi, M. (1994). Applications of Percolation Theory. CRC Press, Routledge, UK.

[34] Dahman, S.J., & Avlyanov, J. (1999). The Use of Conducting Polymer Composites in Thermoplastics for Tuning Surface Resistivity. In *Conductive*

Polymers and Plastics in Industrial Applications, (Rupprecht, L., Ed.), p. 225-230. William Andrew Inc.

[35] Elimat, Z.M. (2006). AC Electrical Conductivity of Poly(methylmethacrylate)/Carbon Black Composites. *Journal of Physics D: Applied Physics 39*, 2824-2828.

[36] Carmona, F. (1989). Conducting Filled Polymers. *Physica A 157(1)*, 461-469.

[37] Grunlan, J.C., Gerberich, W.W., & Francis, L.F. (2000). Lowering the Percolation Threshold of Conductive Composites Using Particulate Microstructure. *Journal of Applied Polymer Science 80*, 692-705.

[38] Dong, X.M., Fu, R.W., Zhang, M.Q., Qin, Z.P., Zhang, B., & Rong, M.Z. (2003). Effects of Processing on Electric Response of Carbon Black Filled Poly(methyl methacrylate) Composites against Organic Solvent Vapors. *Polymer Journal (35)*, 1003-1008.

[39] Hubbard, A.T. (2002). Encyclopedia of Surface and Colloid Science. Marcel Dekker

[40] Levine, L.E., Long, G.G., Ilavsky, J., Gerhardt, R.A., Ou, R., & Parker, C.A. (2007). Self-assembly of carbon black into nanowires that form a conductive three dimensional micro-network. *Applied Physics Letter 90(1)* 014101.

[41] Yu, G., & Zhang, M.Q. (1999). Conductive Polymer Blends with Carbon Black: Positive Temperature Coefficient Behavior. *Polymer Engineering and Science 39*, 1678-1688.

[42] Kusy, R.P. (1977). Influence of Particle Size Ratio on the Continuity of Aggregates. *Journal of Applied Physics D: Applied Physics 48*, 5301-5306.

[43] Li, J., Ma, P.C., Chow, W.S., To, C.K., Tang, B.Z., & Kim, J.-K. (2007). Correlation between Percolation Threshold, Dispersion State, and Aspect Ratio of Carbon Nanotubes. *Advanced Functional Materials 17*, 3207-3215.

[44] Rajagopal, C., & Satyam, M. (1978). Studies on Electrical conductivity of Insulator-Conductor Composites. *Journal of Applied Physics 49(11)*, 5536-5542.

[45] He, D., & Ekere, N.N. (2004). Effect of Particle Size Ratio on the Conducting Percolation Threshold of Granular Conductive -Insulating Composites. *Journal of Applied Physics D: Applied Physics 37*, 1848-1852.

[46] Lebovka, N., Lisunova, M., Mamunya, Y.P., & Vygornitskii, N. (2006). Scaling in Percolation Behaviour in Conductive-Insulating Composites with Particles of Different Size *Journal of Physics D: Applied Physics 39*, 2264-2271.

[47] Kasap, S.O. (1997). Principle of Electronic Materials and Devices. McGraw-Hill Campanies, Inc., New York, N.Y.

[48] Seeger, K. (1997). Semiconductor Physics An Introduction. Springer-Verlag, Heidelberg, Germany.

[49] Hench, L.L., & West, J.K. (1990). Principles of Electronic Ceramics. John Wiley & Sons, Inc., New York, N.Y.

[50] Sorensen, T.S., Diaz-Calleja, R., Riande, E., Guzman, J., & Andriod, A. (1997). Contributions from Interfacial Polarization, Conductivity and Polymer Relaxations to the Complex Permittivity of a Film of Poly [(5-ethyl-1,3-dioxan-5-yl)methyl acrylate] Containing Ionic Impurities. *Journal of the Chemical Society, Faraday Transactions (93)*, 2399-2411.

[51] Mauritz, K.A., & Lambert, B. *Dielectric Spectroscopy* (2008). http://www.psrc.usm.edu/mauritz/dilect.html.

[52] Brosseau, C., Boulic, F., Queffelec, P., Bourbigot, C., Mest, Y.L., Loaec, J., & Beroual, A. (1997). Dielectric and Microstructure Properties of Polymer Carbon Black Composites. *Journal of Applied Physics 81(2)*, 882-891.

[53] Chen, Q., Du, P., Jin, L., Weng, W., & Han, G. (2007). Percolative conductor/polymer Composite Films with Significant dielectric Properties. *Applied Physics Letters 91*, 022912-022911-022912-022913.

[54] Meier, J.G., Mani, J.W., & Kluppel, M. (2007). Analysis of Carbon Black Networking in Elastomers by Dielectric Spectroscopy. *Physics Review 75*, 054202-054201-054202-054210.

[55] Jäger, K.-M., McQueen, D.H., Tchmutin, I.A., Ryvkina, N.G., & M.Klüppel. (2001). Electron transport and ac electrical properties of carbon black polymer composites. *Journal of physics. D, applied physics 34*, 2699-2707.

[56] CCC Columbian Chemicals Company, 2006. http://www.columbianchemicals.com/.

[57] Superior Graphite Co. , 2008 http://www.superiorgraphite.com/products/index.php?id_ctg=113.

[58] Cheap Tubes Inc., 2007. http://www.cheaptubesinc.com/MWNTs.htm.

[59] Dahman, S.J., & Avlyanov, J. (1999). The Use of Conducting Polymer Composites in Thermoplastics for Tuning Surface Resistivity. In *Conductive*

Polymers and Plastics in Industrial Applications, (Rupprecht, L., Ed.), p. 302. William Andrew Inc.

[60] Zou, J.-F., Yu, Z.-Z., Pan, Y.-X., Fang, X.-P., & Ou, Y.-C. (2002). Conductive Mechanism of Polymer/Graphite Conducting Composites with Low Percolation Threshold. *Journal of Polymer Science: Part B: Polymer Physics 40* 954–963.

[61] Sandler, J.K.W., Windle, A.H., Martin, C.A., Schwarz, M.-K., Bauhofer, W., Schulte, K., & Shaffer, M.S.P. (2003). Percolation in Multi-wall Carbon Nanotube-Epoxy Composites Influence of Processing Parameters, Nanotube Aspect Ratio and Electric Fields on the Bulk Conductivity. *Materials Research Society Symposium - Proceedings 788*, 221-226.

[62] Martin, C.A., Sandler, J.K.W., Shaffer, M.S.P., Schwarz, M.-K., Bauhofer, W., Schulte, M., & Windle, A.H. (2004). Formation of Percolating Networks in Multi-Wall Carbon-Nanotube-Epoxy Composites. *Composites Science and Technology 64*, 2309-2316.

[63] Balberg, I., D. Azulay, Toker, D., & Milloy, O. (2004). Percolation and Tunneling in Composite Materials. *International Journal of Modern Physics B 18*, 2091-2121.

[64] Connor, M.T., Roy, S., Ezquerra, T.A., & Balta Calleja, F.J. (1998). Broadband Ac Conductivity of Conductor-polymer Composites. *Physical Review B: Condensed Matter 57(4)*, 2286.

[65] Panwar, V., Sachdev, V.K., & Mehra, R.M. (2007). Insulator Conductor Transition in Low-Density Polyethylene-Graphite Composites. *European Polymer Journal 43(2)*, 573-585.

[66] Sun, J., Gerberich, W.W., & Francis, L.F. (2003). Electrical and Optical Properties of Ceramic–Polymer Nanocomposite Coatings. *Journal of Polymer Science: Part B: Polymer Physics 41*, 1744–1761.

[67] Shen, Y., Lin, Y., & Nan, C.-W. (2007). Interfacial Effect on Dielectric Properties of Polymer Nanocomposites Filled with Core/Shell-Structured Particles. *Advanced Functional Materials*, 1-6.

[68] Shen, Y., Lin, Y., Li, M., & Nan, C.-W. (2007). High Dielectric Performance of Polymer Composite Films Induced by a Percolating Interparticle Barrier Layer. *Advanced Materials 19*, 1418-1422.